Margarida Lourenço Ferreira

Licenciatura em Biologia Humana

New Artificial Blood Substitutes using Fluorinated Ionic Liquids

Dissertação para obtenção do Grau de Mestre em
Bioquímica para a Saúde

Orientador: Doutora Ana Belén Pereiro Estévez,
Investigadora Auxiliar, ITQB/FCT-UNL

Co-orientador: Doutora Karina Shimizu,
Pós-Doc, IST-UL

Setembro 2016

Margarida Lourenço Ferreira

Licenciatura em Biologia Humana

New Artificial Blood Substitutes using Fluorinated Ionic Liquids

Dissertação para obtenção do Grau de Mestre em
Bioquímica para a Saúde

Orientador: Doutora Ana Belén Pereiro Estévez,
Investigadora Auxiliar, ITQB/FCT-UNL

Co-orientador: Doutora Karina Shimizu,
Pós-Doc, IST-UL

Setembro 2016

New Artificial Blood Substitutes using Fluorinated Ionic Liquids

COPYRIGHT

Margarida Lourenço Ferreira

Instituto de Tecnologia Química e Biológica António Xavier
Universidade Nova de Lisboa

Aos meus pais e irmã que sempre me apoiaram na realização dos meus sonhos

Agradecimentos

Ter chegado aqui foi uma das maiores vitórias que consegui alcançar até hoje. No longo caminho que percorri muitas pessoas estiveram lá sem hesitar para me ajudar a conquistar esta etapa da minha vida.

Quero agradecer em primeiro lugar à minha orientadora Doutora Ana Pereiro que desde o início confiou e acreditou em mim e nas minhas capacidades, dando-me a oportunidade para crescer cientificamente, liberdade para aceitar novos desafios, sem nunca me deixar desistir, estando sempre lá para me apoiar e ajudar a chegar aqui. Também agradecer ao Doutor João Araújo pela constante disponibilidade e paciência para me ajudar ao longo deste ano. À minha coorientadora Doutora Karina Shimizu por toda a aprendizagem e disponibilidade. Um especial agradecimento à Professora Doutora Lourdes Vega e ao Professor Doutor Fèlix Llovell pela confiança e oportunidade que me deram para colaborar no seu trabalho, recebendo-me em Barcelona para poder realizar parte da minha tese.

Agradeço à Joana Bastos e Nicole Vieira, que para além de me darem sempre ânimo e me ajudarem no meu trabalho, foram amigas imprescindíveis para ultrapassar todos os obstáculos diários ao longo deste ano, estando sempre lá para mim. Agradeço a todos os meus colegas do laboratório Fluídos Alternativos para a Química Verde, por todos os momentos felizes que passamos.

Agradeço às minhas amigas, que tive a felicidade de encontrar na minha vida académica e que vou levar comigo para a vida, Catarina Lopes, Filipa Gonçalves e Catarina Lourenço, que sempre acreditaram em mim. Agradeço aos meus amigos de sempre, Miriam Antunes e Diogo Ribeiro, que me apoiaram em tudo e tiveram paciência para longas horas de cafés e desabafos. À Daniela Francisco, pelas palavras reconfortantes na hora certa que me incentivaram a ir mais longe. Agradeço ao José Medeiro, que sempre me deu uma força constante para continuar em frente, nos momentos mais complicados, ao longo destes dois anos.

Por último e em especial, agradeço do fundo do coração aos meus pais, Luís e Raquel, pois foram eles que sempre me deram a oportunidade de correr atrás dos meus sonhos, sem nunca questionar as minhas decisões, mas sempre estando lá a apoiar me sem limites ou exceções. Agradeço à minha irmã, Daniela, que sempre foi a minha ouvinte, a minha melhor amiga e me disse aquilo que queria e não queria ouvir para enfrentar todos os meus limites.

Palavras-chave

Líquidos Iónicos Fluorados, Transportadores Artificiais de Oxigénio, Solubilidade de Gases Respiratórios, Transição de Fases, Nanosegregação.

Resumo

Nos anos 80, as preocupações subjacentes à segurança e qualidade do sangue humano para fins biomédicos estimularam o desenvolvimento de transportadores artificiais de oxigénio (TAOs), também designados de substitutos artificiais do sangue. Posteriormente, surgiram as emulsões baseadas em perfluorocarbonetos (PFCs), que embora ainda hoje não sejam comercializadas, são considerados uns dos TAOs mais eficazes e fiáveis no transporte de gases respiratórios.

O trabalho desenvolvido nesta tese visa a substituição total ou parcial dos PFCs existentes nas emulsões por líquidos iónicos fluorados (LIFs), com o objetivo de desenvolver TAOs mais eficazes e seguros.

Inicialmente, foi realizada a caracterização termodinâmica de diversos LIFs, de modo a obter informações acerca do comportamento de fases dos mesmos. Posteriormente, foram analisadas as características nanoestruturais destes compostos através de simulação de dinâmica molecular. Para finalizar, a solubilidade dos gases respiratórios em LIFs foi estudada utilizando uma abordagem teórico-experimental, através de uma equação de estado baseada na teoria estatística de fluído associante (soft-SAFT EoS).

Por fim, podemos concluir que os resultados obtidos neste projeto são de extrema importância para a seleção do melhor líquido iónico fluorado a ser utilizado no desenvolvimento de transportadores artificiais de oxigénio.

Este trabalho foi financiado através dos projetos PTDC/EQU-FTT/118800/2010 e PTDC/QEQ-EPR/5841/2014

Keywords

Fluorinated Ionic Liquids, Artificial Oxygen Carriers, Respiratory Gases Solubility, Phase Behaviour, Nanosegregation.

Abstract

Intensive efforts to develop artificial oxygen carriers (AOCs), the so-called artificial blood substitutes, started in 1980s due to concerns about blood safety. Emulsions based on perfluorocarbons (PFCs) arose as one of the most reliable and effective candidate blood substitute. However, beyond the several approaches to commercialize these products, there are still no commercially available PFC-emulsions in the market.

This work is part of an ongoing project where fluorinated ionic liquids (FILs) were studied in order to evaluate their capacity to replace partially or totally the PFCs, opening doors to design and develop new suitable and effective AOC.

The thermodynamic characterization of several FILs was accomplished in order to obtain insights on their phase behaviour. Nanostructural features of these pure compounds were also characterized using Molecular Dynamics (MD) simulations. Finally, the solubility of respiratory gases in FILs was analysed using a theoretical-experimental combined approach, soft statistical associating fluid theory equation of state (soft-SAFT EoS).

The results achieved in this thesis are an outstanding, helpful contribution to find out the best promising FIL that can be selected as an appropriate candidate for artificial gas carriers.

This work was supported through project PTDC/EQU-FTT/118800/2010 and PTDC/QEQ-EPR/5841/2014

Contents

List of Figures

List of Tables

List of Abbreviations

AOC	Artificial oxygen carrier
HIV	Human immunodeficiency virus
HBOC	Haemoglobin-based oxygen carrier
PFCOC	Perfluorocarbon-based oxygen carrier
PFC	Perfluorocarbon
IL	Ionic liquid
FIL	Fluorinated ionic liquid
Hb	Haemoglobin
FDA	American food and drug administration
DSC	Differential scanning calorimetry
TGA	Thermogravimetric analysis
SAFT	Statistical associating fluid theory
EoS	Equation of state
MD	Molecular dynamics
$[C_2C_1py][C_4F_9SO_3]$	1-Ethyl-3-methylpyridinium perfluorobutanesulfonate
$[C_4C_1pyr][N(C_4F_9SO_2)_2]$	1-Butyl-1-methylpyrrolidinium bis(nonafluorobutylsulfonyl)imide
$[C_4C_1pyr][C_4F_9SO_3]$	1-Butyl-1-methylpyrrolidinium perfluorobutanesulfonate
$[C_8C_1Im][C_4F_9SO_3]$	1-Methyl-3-octylimidazolium perfluorobutanesulfonate
$[C_6C_1Im][C_4F_9SO_3]$	1-Hexyl-3-methylimidazolium perfluorobutanesulfonate
$[N_{4444}][C_4F_9SO_3]$	Tetrabutylammonium perfluorobutanesulfonate
NMR	Nuclear Magnetic Resonance
CL&P	Canongia Lopes & Pádua
OPLS	Optimized potentials for liquid simulations
CPD	Conformer distributions profiles
DFT	Density functional theory
PNPP	Pre-peak or polar-nonpolar peak
COP	Charge-ordering peak
CP	Contact peak
PES	Potential energy surface
$[C_2C_1Im][N(FSO_2)_2]$	1-Ethyl-3-methylimidazolium bis(fluorosulfonyl)imide
$[C_4C_1Im][N(CF_3SO_2)_2]$	1-Butyl-3-methylimidazolium bis(trifluoromethanesulfonyl)imide
LJ	Lennard-Jones
TPT1	First order thermodynamic perturbation theory
DGT	Density gradient theory

FVT	Free-volume theory
[C_nC_1Im][$C_4F_9SO_3$]	1-*n*-3-methylimidazolium perfluorobutanesulfonate
[C_2C_1Im][$C_4F_9SO_3$]	1-ethyl-3-methylimidazolium perfluorobutanesulfonate
[C_2C_1Im][$C_4F_9CO_2$]	1-ethyl-3-methylimidazolium perfluoropentanoate
[C_2C_1py][$C_4F_9CO_2$]	1-ethyl-3-methylpyridinium perfluoropentanoate
AAD	Absolute average deviation
VLE	Vapour-liquid equilibria/equilibrium

List of Symbols

T	Temperature
$T_{s\text{-}s}$	Solid-solid transition temperature
T_m	Melting temperature
T_{onset}	Onset temperature
T_{start}	Start temperature
T_{dec}	Decomposition temperature
N	Nosé-Hoover
P or p	Pressure
$S(q)$	Total static structure factors
$S_{ij}(q)$	Partial static structure factor
i	Atom type i
j	Atom type j
$g_{ij}(r)$	Partial radial distribution function
q	Scattering vector
ρ_o	Average atom number density
R or r	Cutoff
x_i	Atomic fractions i
x_j	Atomic fractions j
$b_i(q)$	Bound neutron scattering lengths of i
$b_j(q)$	Bound neutron scattering lengths of j
$sin(\pi R)/(\pi r/R)$	Lorch-type window function
$P(n_a)$,	Probability distribution function
n_a	Aggregate size
a^{res}	Residual Helmholtz free energy
a^{id}	Ideal contribution
a^{ref}	Reference term
a^{chain}	Chain term
a^{assoc}	Association term
a^{polar}	Polar term
σ_{ii} or σ	Segment diameter
ε_{ii}/k_B or ε/k_B or ε	Dispersive energy
η_{ij}	Size binary parameter
ξ_{ij} or ξ	Energy binary parameter
ρ	Molecular density

k_B	Boltzmann constant
m_i or m	Chain length
$g_{LJ}^{ii}(\sigma_{ii})$	Function of density and temperature
X_i^{α}	Fraction of pure component *i* not bonded at sites of type α
M_i	Number of association sites of type α on component i
N_{avog}	Avogrado's constant
X_j^{β}	Fraction of pure component *j* not bonded at sites of type β
$\Delta_{\alpha\beta,ij}$,	Specific site-site function
$K_{\alpha\beta,ij}$ or K^{HB}	Association volume parameter
$f_{\alpha\beta,ij}$	Mayer f-function
$\varepsilon_{\alpha\beta,ij}^{HB}/k_B$ or ε^{HB}/k_B	Association energy parameter
α^{qq}	Padé approximation
a_2^{qq}	Second-order term in the perturbation expansion
a_3^{qq}	Third-order term in the perturbation expansion
J	Integral for the reference fluid
Q_i or Q	Quadrupole moment
x_{pi} or x_p	Fraction of the molecule affected by the quadrupole
$a_0(\rho)$	Helmholtz free energy density
ρ_i	Molar density of component *i*
c_{ij} or c	Influence parameter
μ_{0i}	Equilibrium chemical potential
p_0	Equilibrium chemical pressure
z	Direction perpendicular to interface
η	Viscosity
η_0	Dilute gas term
$\Delta\eta$	Dense-state term
M_w	Molecular weight
v_c	Critical volume
Ω^*	Reduced collision integral
F_c	Empirical factor
ω	Non-sphericity factor
μ_r	Polarity factor
κ	Hydrogen bonding
α	Proportionality between the energy barrier and the density
B	Free-volume overlap

L_v	Length parameter
A	Associating site, A
B	Associating site, B
e	Associating site, *e*
H	Associating site, *H*
x_{H_2O}	Water composition
H_c	Henry constant
x_{CO_2}	Carbon dioxide composition
x_{N_2}	Nitrogen composition
x_{O_2}	Oxygen composition

1. General Introduction

1.1 General Context

In the past decades, safe and effective artificial oxygen carriers (AOC), also named as "blood substitutes", have been proposed and extensively studied in chemistry and medical science. The constant necessity of donor blood is crucial for diverse medical situations, such as accidents and casualties which result in acute blood loss and the need to restore oxygen transport to the tissues. The inherent complications associated to the traditional blood transfusion make urgent the formulation of new suitable alternatives.(1–4)

The major interest to find out new products to replace the blood transfusion arises after the human immunodeficiency virus (HIV) appears, where cross-infections occurred. This fact brought into question the safety and community trust in the blood supply.(2,5) Nowadays, several screening tests are done to make sure that virus cross-infection is prevented, but they are expensive and time-consuming.(6) However, the emergence of new infectious agents requires the constant implementation of additional tests, increasing the cost even more. Even so, donated blood may contain infectious agents yet to be identified.(5,6) Furthermore, the non-viral complications that were usually neglected, such as blood bacterial contamination and transfusion-induced immunosuppressive effects, have been now the focus of intense efforts toward development of donor screening and prevention strategies.(5) The problems associated to blood banking (such as the limited shelf-life and severe shortages, and the increased demands of blood) have also been an obstacle.(7,8)

In the past several decades, an ideal AOC has been searched, but this goal is not yet achieved because there are no approved or commercially available products.(4) There are two principal types of AOCs that have been studied, which are current in clinical trials: haemoglobin-based oxygen carriers (HBOCs) and perfluorocarbon-based oxygen carriers (PFCOCs). Taking into account its reliability, emulsions based on perfluorocarbons (PFCs) are currently among the preferred AOC candidates.(9)

The extensive understanding of the unique physical and chemical properties of ionic liquids (ILs) has opening doors to design new biocompatible compounds, allowing their application in biomedical research.(10,11) However, there are still ILs families that are quite unexplored which is the case of fluorinated ionic liquids (FILs).

The main goal of the project where this work is included is the development of a new and improved generation of oxygen therapeutics using FILs. In this thesis, an effort to contribute to the design and development of FILs capable to partially or totally replace the PFCs currently used in the emulsions for oxygen therapeutics, is under investigation. The several advantages (such as enhancement

of respiratory gas solubility, emulsion stability due the outstanding chemical and biological inertness and lowering vapour pressure) (12) make these compounds feasible candidates to be used as oxygen carriers.

Towards that goal, combined experimental-theoretical approaches were used to obtain insights in to phase behaviour, nanostructure and capacity of the FILs to solubilize respiratory gases. This study was carried out in order to understand physicochemical and structural properties of FILs in order to select the most reliable compound to replace PFCs in the emulsions used as oxygen therapeutics. The results obtained in this thesis are expected to represent a big step in ionic liquid community, due to the great possibilities emerging in biomedical research using ILs.

1.2 Artificial Oxygen Carriers

The artificial oxygen carriers are usually known as “blood substitutes”. However the use of this term has decreased because these products only transport the respiratory gases for a limited period of time, and do not replace the other vital functions of blood such as transport of nutrients, immune response, and coagulation.(2,13)

The underlying goal inherent to AOCs is the formulation of an effective and safe product, due to the problems of traditional blood transfusion and the enormous demand in clinical use. Some of the clinical indications where AOCs can be advantageous are: pre-hospital administration in the field or during them route care; on administrations in remote environments in the case of disaster or combat situations; in situations of blood transfusion refusal; and for transplant organ preservation.(14)

In recent years, several efforts were done in order to obtain an ideal AOC characterized by the following characteristics: bulk supply availability, inexpensive, nontoxic, effective for the transport and delivery of oxygen without tissue damage, non-pathogenic, compatible with all blood types, rapid metabolization and elimination *in vivo*, without immune system interactions, easy to handle and store, long shelf-life and stability, and prolonged circulation time with effective function.(8,15)

There are two types of AOCs that are distinguished by the transport mechanism of respiratory gases: perfluorocarbon-based oxygen carriers (PFCOCs, where the oxygen is dissolved in perfluorocarbon (PFC) emulsions) and the haemoglobin-based oxygen carriers (HBOCs, in which oxygen is covalently bound to the haemoglobin (Hb)).(2,8) The main differences between the two classes are the molecular structures, uptake and release profiles of respiratory gases, transport mechanisms, nature of the materials, manufacture process, and cost.(2)

HBOCs, as the name indicates, are composed by a chemical modified Hb which is structurally similarly to the *in vivo* human Hb. They can be derived from human, animal or genetic recombination sources.(13) An impressive diversity of structural modifications and formulations of HBOCs have been developed and some of them are currently in clinical trials.(14) The final products are usually formulated as solutions, capsules or suspensions of liposomes, and more recently, as micro and nanoparticles.(7) Each formulation has its own distinct mechanisms for oxygen delivery with different physiological responses. However, there are many of clinical implications in the use of these substitutes, such as neurovascular, immunologic, gastrointestinal and infectious.(15)

PFCOCs are formulated as emulsions for intravenous administration because the PFCs are highly hydrophobic leading to a lower solubility in water. Consequently, to reduce the large tension at the interface between fluorocarbon and aqueous phase, surfactants are normally used to stabilize the PFC-emulsions.(2,8,16,17) There are two surfactants that have been used in the formulation of fluorocarbon emulsions: poloxamers and egg-yolk phospholipids (which is that most utilized nowadays).(2)

The preparation of PFC-emulsions involves the coating of the fluorocarbons with the surfactant compound in a saline phase leading to droplet formation. The gas molecules are dissolved in these droplets occupying the spaces between the fluorocarbons. Afterwards, these droplets, when administered into the blood circulation, can fill the gaps between the red blood cells that are still in the plasma on ischemic microcirculation. This enables the diffusion of the oxygen molecules into the tissues, supplying oxygenation and restoring aerobic metabolism.(2)

The first commercial injectable PFC-emulsion approved by the American Food and Drug Administration (FDA) was Fluosol, which uses perfluorodecalin (PFD), a purely cyclical PFC that is rapidly excreted from the body. The interest of this product was its use in percutaneous transluminal coronary angioplasty. However the cardiologists did not adopt Fluosol because improvements in angioplasty technology made its use redundant. The principal limitation associated with this product was the storage method. It was necessary to defrost the compound and re-constitute it before using. Furthermore, its poor efficacy as an oxygen carrier was later demonstrated. Other PFC-emulsions of the first generation, such as Perftotran and Oxypherol, were produced. However, these formulations were withdrawn from clinical trials or never reached this phase due to their toxicity effects.(3,8,16)

The development of second generation PFC emulsions happened with the aim to: (i) formulate products with higher efficacy by increasing the total PFC content and, in turn, the oxygen-carrying capacity; (ii) eliminate side effects, by utilizing phospholipids as surfactants rather than poloxamers; and (iii) improve stability regarding storage and hence shelf-life. However, the concentration increment of PFCs to enhance their oxygen carrier potential, leads an increment of their viscosity hindering their use in blood circulation. Additionally, the lower sensitivity to manufacturing process and storage was a

problem encountered in these new products. They were essentially based on perflubron or perfluorodecalin and some of the examples are Oxigent, Oxyfluor, TherOx, among others. Sustained efforts have subsequently led to more advanced second generation products that are nowadays in clinical trials.(2,8,15,16) The composition and characteristics of some injectable PFC emulsions are shown in **Table 1.1.**

Fluorocarbon emulsions offer a simple, elegant and cost-effective vehicle for delivering oxygen to tissues. Nowadays, efforts are focused in extending the range of therapeutic indications of such products to apply them in other biomedical applications.(18,19)

Table 1.1. Composition and applications of injectable PFC emulsion oxygen carriers.

Emulsion	Perfluorocarbons	Application
	"First generation" emulsions	
Fluosol	Perfluorodecalin or perfluorotripropylamine in albumin emulsion	Patients with severe blood loss, religious objections to transfusions and high-risk coronary balloon angioplasty
Perftotran	Perfluorodecalin or perfluoromethylcyclopiperidine in nonionic surfactant	Cardiac valvuloplasty surgery
	"Second generation" emulsions	
Oxygent	Perfluorobron in lectin with perfluorodecyl bromide	Cardiopulmonary bypass
Oxyfluor	Perfluorodichlorooctane in egg yolk phospholipid and safflower oil	Surgery

Adapted from reference (20)

1.3 Perfluorocarbons

Perfluorocarbons (PFCs) are chemically and biologically inert, heat stable, fluorine-substituted hydrocarbons (linear, cyclic or polycyclic) that can dissolve large amounts of oxygen, carbon dioxide and other gases. In addition, the ability to produce small particle sizes and low-viscosity suspensions turns the PFCs into a great AOCs.(21) These compounds are essentially composed of fluorine-carbon bonds, which contribute to their high chemical and thermal stability, because it is the strongest single bound in organic chemistry. The fluorine atoms are large in size, and compared to hydrogen have a high electron density resulting in a compact shield, thus providing protection to backbone C-C, and making this structure even more stable.(3)

Their unique gas-dissolving ability are a consequence of the weakness of intermolecular cohesion forces characteristic of liquid fluorocarbons, enabling the formation of spaces to accommodate gas molecules within the liquid.(22) No chemical bonding, coordination, or charge-transfer complexes between the PFCs and the dissolved gas molecules seem to occur. These compounds are apolar and non-associated liquids. Then, the gas dissolving ability is determined by the shape of the molecules. The fluorocarbons are considered metabolically inert.(22) The most investigated fluorocarbons for oxygen delivering are illustrated in **Figure 1.1.**

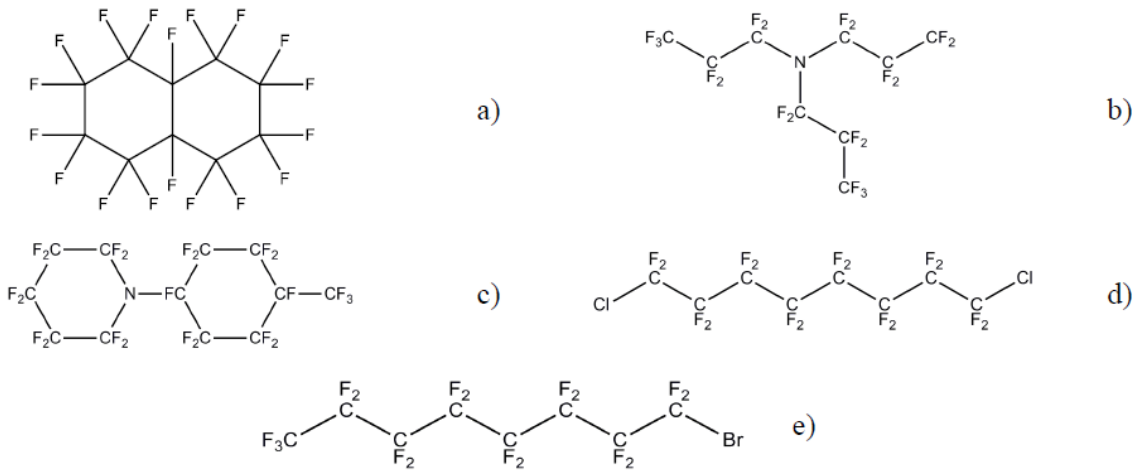

Figure 1.1. PFCs most investigated as AOCs: a) perfluorodecalin, b) perfluorotripropylamine, c) perfluoromethylcyclohexypiperidine, d) *α*,*ω*-dicholoroperfluorooctane, e) perfluorooctyl bromide (perfluorobron).

Perfluorocarbons have numerous biomedical applications, such as using them pure as liquids for liquid ventilation or in the emulsified form for respiratory failure treatment.(18) They are also used as high-density intraoperative fluids for eye surgery,(23) as red blood cell substitutes including all the situations of: surgical anaemia, haemolytic anaemia, ischemic disease, angioplasty, extracorporeal organ perfusion, cardioplegia (24) and radiotherapy of tumours.(3) Furthermore, they have been used as an ultrasound imaging contrast agent,(25) as a marker during magnetic resonance imaging (MRI) and other approaches concerning this technique.(25) Other applications of fluorocarbons in medicine are being explored, such as drug delivery, gene therapy, brain cooling, and organ and cell preservation.(26)

There are a large number of other relevant industrial applications of PFCs such as co-solvents in supercritical extraction;(27) as medium in two-phase reaction mixture;(28) as refrigerants, aerosol propellants and foam blowing agents (29) and in cell culture aeration.(30) Moreover, due to the exceptional solubility of carbon dioxide in perfluoroalkanes, they are attractive for carbon removal from gaseous effluents in industrial processes.(31)

However, the perfluorocarbons present clear limitations such as high vapour pressures and poor solvating capacity for organic compounds, which might compromise their use as artificial oxygen carriers.

1.4 Fluorinated Ionic Liquids

Ionic liquids (ILs) are a subset of molten salts, thus composed by ionic compounds, with melting points below 373 K. ILs are liquids because the anions and cations are chosen precisely to destabilize the solid-phase crystal. Then, these compounds present low symmetry, higher distribution charge and low intermolecular interactions.(32) The most common studied ILs are nitrogen-based and in **Figure 1.2.** and **Figure 1.3**, are depicted the most common cations and anions reported in the literature.

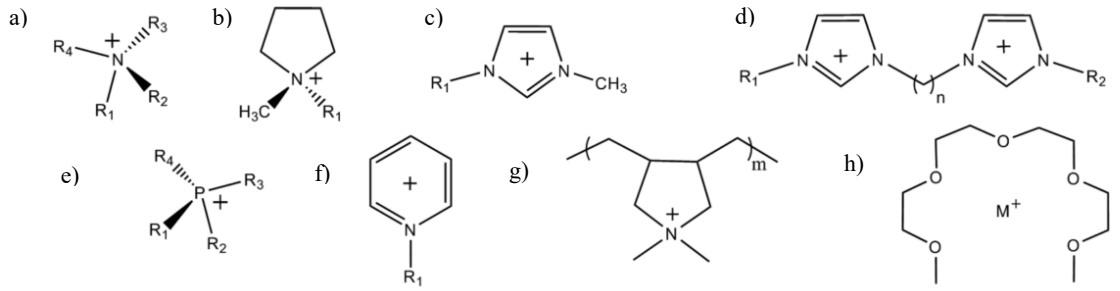

Figure 1.2. Most common cation structures of ILs: a) ammonium, b) pyrrolidinium, c) 1-methyl-3-alkylimidazolium, d) 1,3-bis[3-methylimidazolium-1-yl]alkane, e) phosphonium, f) pyridinium, g) poly(diallyldimethylammonium) and h) metal (M^+) tetraglyme. (Adapted from reference (32))

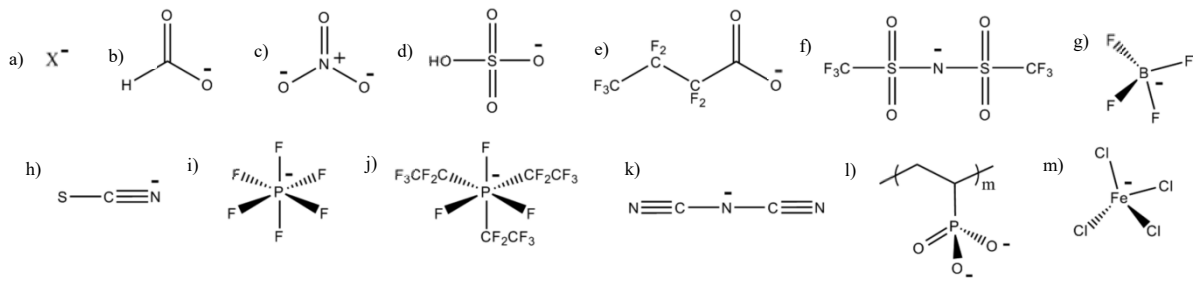

Figure 1.3. Most common anion structures of ILs: a) halides (F^-, Cl^-, Br^-, I^-), b) formate, c) nitrate, d) hydrogen sulfate, e) heptafluorobutyrate, f) bis(perfluoromethylsulfonyl)imide, g) tetrafluoroborate, h) thiocyanate, i) hexafluorophosphate, j) tris(pentafluoroethyl)trifluorophosphate, k) dicyanamide, l) poly(phosphonate), m) and tetrachloroferrate. (Adapted from reference (32))

Nowadays, ILs has been investigated as green solvents (33) due to their exceptional properties such as negligible vapour pressure, large liquid range, high thermal stability, high ionic conductivity, large electrochemical window and ability to solvate compounds of widely varying polarity.(34) They

create cleaner and more sustainable chemistry, increasing their interest as an environmental friendly solvents.(35)

The most outstanding feature of ILs is the possible manipulation of their properties, due to the enormous range of possible cation-anion combinations. Thus, ILs are recognized as "designer solvents" enabling the modification of hydrophobicity, solution behaviour, thermophysical properties, biocompatibility, or toxicological behaviour.(32) The ionic liquids can be applied in the most diverse fields, such as solvents and catalysts, analytics, in engineering, electrochemistry, physical chemistry, biological and pharmaceutical uses.(11,36-39)

Although the IL field has been largely investigated, there are still unexplored families such as the fluorinated ionic liquids (FILs) family (12). The molecular structure of FILs is characterized by the additional carbon-fluorine bonds which increase their rigidity and decrease their polarity.(40) They are of a particular interest in areas where PFCs are relevant such as biomedical applications and *in vivo* AOCs.

In this work, FILs are defined as ionic liquids with fluorinated chain lengths equal or longer than four carbon atoms, distinguishing them from mere fluoro-containing FILs, such as bis(trifluoromethylsulfonyl)imide, hexafluorophosphate and tetrafluoroborate anions.(12,40) These ILs can present advantageous and different properties due to the addition of a new nanosegregated fluorinated domain, which can modify their mesomorphic properties and molecular geometry, increasing the tuneability power of conventional ionic liquids.(41,42)

The impact of these compounds in biomedical applications has been pointed out due to their potential as gas carriers, artificial blood substitutes, liquid ventilation media, imaging agents and intravenous formulations.(9,41,43-45) They combine the best properties of ionic liquids (ILs) with those of perfluorocarbons, namely: high gas solubility, low surface tension, relatively low vapour pressure, generally high thermal and chemical stabilities, weak interactions with organic compounds, remarkable chemical and biological inertness, tuneable toxicity and easy recovery and recyclability.(12,45) These exceptional properties also enable their application as new alternative cleaner compounds, substituting the usually harmful perfluorinated surfactants used in a wide range of industrial applications.(9,46,47) Several FILs have been explored for other applications such as electrochemistry, mostly used as electrolyte components in the production of energy storage devices, metal batteries such as lithium, fuel and solar cells. These compounds can be also useful in the catalysis of several reactions.(48-55)

The unique properties of FILs lead to high gas solubility and low energies required for expelling the gas molecules due to the repulsive tendency of fluorine atoms. The high solubility of gases, especially carbon dioxide in FILs has already been demonstrated.(44,56) A comparison between values for the CO_2 solubility in a fluorinated ionic liquid (56) and in perfluoro-n-octane (57) at similar

conditions indicates that the new FILs have greater solubilisation capacities for CO_2 than the traditional PFCs. On the other hand, FILs have also shown an improved behaviour as surfactants which is conferred by the highly nanostructured nature,(41,46,58) remarkably facilitating the formation and stabilization of dispersions of perfluorocarbons in a conventional IL.(59) All the mentioned properties of the FILs are significant to allow their application in the PFC- emulsions as oxygen carriers. The FILs could be used as a surfactant in order to enhance the emulsion stability and increase the solubility of respiratory gas, or could totally replace the PFCs. The FILs research has been emerge but the information is still very scarce. Deep studies about structuration, solubility of gases, biocompatibility, and other physicochemical properties are necessary in order to use these compounds as AOCs.

In this thesis, the structural and thermal characterization of these FILs was performed using differential scanning calorimetry (DSC) and thermogravimetric analysis (TGA). These techniques allow the identification of the solid-fluid transitions, decomposition temperatures and thermodynamic behaviour of these compounds. Additionally, molecular dynamics (MD) simulations have been carried out in order to study and understand the complex nanostructure and properties at atomistic level. Finally, the Soft Statistical Associating Fluid Theory Equation of State (soft-SAFT EoS) was used in order to give insights into vapour-liquid equilibria of the binary mixtures FILs + gases in order to study the solubility of respiratory gases in the FILs.

1.5 References

(1) Chang, T. M. S. Red Blood Cell Substitutes: Past, Present, and Future. *Artificial Oxygen Carrier*. Springer Tokyo, **2005**, 22-33.

(2) Riess, J. G. Oxygen Carriers ("Blood Substitutes") – Raison d'Etre, Chemistry, and Some Physiology. *Chem Rev.* **2001**, 101, 2797-2919

(3) Winslow, R. M. Blood Substitutes. *Academic Press*. **2005**.

(4) Palmer, A. F.; Intaglietta, M. Blood Substitutes. *Annu Rev Biomed Eng.* **2014**, 16, 77-101.

(5) Busch, M. P.; Kleinman, S. H., Nemo, G. J. Current and Emerging Infectious Risks of Blood Transfusions. *J Am Med Assoc.* **2003**, 289, 959-962.

(6) Cabrales, P.; Intaglietta, M. Blood Substitutes: Evolution from Noncarrying to Oxygen- and Gas-Carrying Fluids. *ASAIO Journal*. **2013**, 59, 337-354.

(7) Jia, Y.; Duan, L.; Li, J. Hemoglobin-Based Nanoarchitectonic Assemblies as Oxygen Carriers. *Adv Mater.* **2016**, 28, 1312-1318.

(8) Castro, C. I.; Briceno, J. C. Perfluorocarbon-Based Oxygen Carriers: Review of Products and Trials. *Artif Organs*. **2010,** 34, 622-634.

(9) Martinho, S.; Araújo, J. M. M.; Rebelo, L. P. N.; Pereiro, A. B.; Marrucho, I. M. (Liquid + Liquid) Equilibria of Perfluorocarbons with Fluorinated Ionic Liquids. *J. Chem. Thermodynamics*. **2013**, 64, 71-79.

(10) Elliott, G. D.; Kemp, R.; MacFarlane, D. R. The Development of Ionic Liquids for Biomedical Applications – Prospects and Challenges *ACS symposium series*, Oxford University Press. **2009**, 1030, 95-105.

(11) Marrucho, I. M.; Branco, L. C.; Rebelo, L. P. N. Ionic Liquids in Pharmaceutical Applications *Annu Rev Chem Biomol. Eng.* **2014**, 5, 527-546.

(12) Pereiro, A. B.; Araújo, J. M. M.; Martinho, S.; Alves, F.; Nunes, S.; Matias, A.; Duarte, C. M. M.; Rebelo, L. P. N.; Marrucho, I. M. Fluorinated Ionic Liquids: Properties and Applications. *ACS Sustainable Chem. Eng.* **2013**, 1, 427-439.

(13) Alayash, A. I. Blood substitutes: why haven't we been more successful? *Trends in Biotechnol*. **2014**, 32, 177-185.

(14) Njoku, M.; St Peter, D.; Mackenzie, C. F. Haemoglobin-based oxygen carriers: indications and future applications. *Br J Hosp Med*. **2015**,76, 78-83.

(15) Cohn, C. S.; Cushing, M. M. Oxygen Therapeutics: Perfluorocarbons and Blood Substitute Safety. *Crit Care Clin.* **2009**, 25, 399-414.

(16) Vorob'ev, S. I. First- and Second-Generation Perfluorocarbon Emulsions. *Pharm Chem J.* **2009**, 43, 209-218.

(17) Riess, J. G. Perfluorocarbon-based Oxygen Delivery. *Artif Cells, Blood Substitutes, and Biotechnol.* **2006**, 34, 567-580.

(18) Krafft, M. P. Fluorocarbons and Fluorinated Amphiphiles in Drug Delivery and Biomedical Research. *Adv Drug Deliver Rev.* **2001**, 47, 209-228.

(19) Riess, J. G. Fluorous Micro- and Nanophases with a Biomedical Perspective. *Tetrahedron*. **2002**, 58, 4113-4131.

(20) Modery-Pawlowski, C. L.; Tian, L. L.; Pan, V.; Sen Gupta, A. Synthetic Approaches to RBC Mimicry and Oxygen Carrier Systems. *Biomacromolecules*. **2013**, 14, 939-948.

(21) Lowe, K. C. Fluorinated Blood Substitutes and Oxygen Carriers. *J Fluor Chem*. **2001**, 109, 59-65.

(22) Centis, V.; Vermette, P. Enhancing Oxygen Solubility Using Hemoglobin- and Perfluorocarbon-based Carriers. *Front Biosci*. **2009**, 14, 665-688.

(23) Miller, J. H.; Googe, J. M.; Hoskins, J. C. Combined Macular Hole and Cataract Surgery. *Am J Ophthalmol*. **1997**, 123, 705-707.

(24) Cohn, S. M. Blood Substitutes in Surgery. *Surgery*. **2000**, 127, 599-602.

(25) Díaz-López, R.; Tsapis, N.; Fattal, E. Liquid Perfluorocarbons as Contrast Agents for Ultrasonography and ^{19}F-MRI. *Pharm Res*. **2010**, 27, 1-16.

(26) Lehmler, H-J. Perfluorocarbon Compounds as Vehicles for Pulmonary Drug Delivery. *Expert Opin. Drug Deliv*. **2007**, 4, 247-262.

(27) Horváth, I. T.; Rabai, J. Facile Catalyst Separation Without Water - Fluorous Biphase Hydroformylation of Olefins. *Science*, **1994**, 266, 72-75.

(28) Wallington, T. J.; Schneider, W. F.; Worsnop, D. R.; Nielsen, O. J.; Sehested, J.; Debruyn, W. J.; Shorter, J. A. The Environmental Impact of CFC Replacements HFCs and HCFCs. *Environ Sci Technol.* **1994**, 28, 320A-326A.

(29) Elibol, M.; Mavituna, F. A Remedy to Oxygen Limitation Problem in Antibiotic Production: Addition of Perfluorocarbon. *Biocheml Eng J.* **1999**, 3, 1-7.

(30) Wasanasathian, A.; Peng, C.-A. Enhancement of Microalgal Growth by Using Perfluorocarbon as Oxygen Carrier. *Art. Cells, Blood Subs., Immob. Biotech.* 2001, 29, 47-55.

(31) Walden, P. Molecular Weights and Electrical Conductivity of Several Fused Salts. *Bull de l'Académie Impérial des Sci St.-Pétersbog*. **1914**, 8, 405-422.

(32) Hayes, R.; Warr, G. G.; Atkin, R. Structure and Nanostructure in Ionic Liquids. *Chem Rev*. **2015**, 115, 6357-6426.

(33) Earle, M. J.; Seddon, K. R. Ionic liquids. Green Solvents for the Future. *Pure Appl Chem.* **2000**, 72, 1391-1398.

(34) Zhang, S.; Sun, N.; He, X.; Lu, X.; Zhang, X. Physical Properties of Ionic Liquids: Database and Evaluation. *J Phys Chem Ref Data*. **2006**, 35, 1475-1517.

(35) Petkovic, M.; Seddon, K. R.; Rebelo, L. P. N.; Pereira, C. S. Ionic liquids: a Pathway to Environmental Acceptability. *Chem Soc Rev*. **2011**, 40, 1383-403.

(36) Patel, D. D.; Lee, J.-M. Applications of Ionic Liquids. *Chem Rec*. **2012**, 12, 329-55.

(37) Werner, S.; Haumann, M.; Wasserscheid, P. Ionic Liquids in Chemical Engineering. *Annu Rev Chem Biomol Eng*. **2010**, 1, 203-30.

(38) Patel, R.; Kumari, M.; Khan, A. B. Recent Advances in the Applications of Ionic Liquids in Protein Stability and Activity: A Review. *Appl Biochem Biotechnol*. **2014**, 172, 3701-20.

(39) Shamsi, S. A.; Danielson, N. D. Utility of Ionic Liquids in Analytical Separations. *J Sep Sci*. **2007**, 30, 1729-50.

(40) Shen, Y.; Kennedy, D. F.; Greaves, T. L.; Weerawardena, A.; Mulder, R. J.; Kirby, N.; Song, G.; Drummond, C. J. Protic Ionic Liquids with Fluorous Anions: Physicochemical Properties and Self-Assembly Nanostructure. *Phys Chem Chem Phys*. **2012**,14, 7981-7992

(41) Pereiro, A. B.; Pastoriza-Gallego, M. J.; Shimizu, K.; Marrucho, I. M.; Lopes, J. N. C.; Piñeiro, M. M.; Rebelo, L. P. N. On the Formation of a Third, Nanostructured Domain in Ionic Liquids. *J Phys Chem B*. **2013**, 117, 10826-10833.

(42) Shimizu, K.; Freitas A. A.; Canongia Lopes, J. N. Structural Characterization of the $[C_nC_1im][C_4F_9SO_3]$ Ionic Liquid Series: Alkyl versus Perfluoroalkyl Side Chains. *J Mol Liq*. **2016**, http://dx.doi.org/10.1016/j.molliq.2016.08.014.

(43) Vieira, N. S. M.; Reis, P. M.; Shimizu, K.; Cortes, O. A.; Marrucho, I. M.; Araújo, J. M. M.; Esperança, J. M. S. S.; Canongia Lopes, J. N.; Pereiro, A. B.; Rebelo, L. P. N. A Thermophysical and Structural Characterization of Ionic Liquids with Alkyl and Perfluoroalkyl Side Chains. *RSC Adv*. **2015**, 5, 65337-65350.

(44) Almantariotis, D.; Gefflaut, T.; Pádua, A. A. H.; Coxam J.-Y., Gomes M. F. C. Effect of Fluorination and Size of the Alkyl Side-Chain on the Solubility of Carbon Dioxide in 1-Alkyl-3-methylimidazolium Bis(trifluoromethylsulfonyl)amide Ionic Liquids. *J Phys Chem B*. **2010**, 114, 3608-3617.

(45) Zhou, L.; Fan, J.; Shang, X. CO_2 Capture and Separation Properties in the Ionic Liquid 1-n-Butyl-3-Methylimidazolium Nonafluorobutylsulfonate. *Materials*. **2014**, 7, 3867-3880.

(46) Pereiro, A. B.; Araújo, J. M. M.; Teixeira, F. S.; Marrucho, I. M.; Piñeiro, M. M.; Rebelo, L. P. N. Aggregation Behavior and Total Miscibility of Fluorinated Ionic Liquids in Water. *Langmuir*. **2015**, 31, 1283-1295.

(47) Teixeira, F. S.; Vieira, N. S. M.; Cortes, O. A.; Araújo, J. M. M.; Marrucho, I. M.; Rebelo, L. P. N. Phase Equilibria and Surfactant Behavior of Fluorinated Ionic Liquids with Water. *J Chem Thermodyn*. **2015**, 99-107.

(48) Zhou, Z.-B.; Matsumoto, H.; Tatsumi, K. Cyclic Quaternary Ammonium Ionic Liquids with Perfluoroalkyltrifluoroborates: Synthesis, Characterization, and Properties. *Chem Eur J*. **2006**, 12, 2196-2212.

(49) Arvai, R.; Toulgoat, F.; Médebielle, M.; Langlois, B.; Alloin, F.; Iojoiu, C.; Sanchez, J. Y. New Aryl-Containing Fluorinated Sulfonic Acids and their Ammonium Salts, useful as Electrolytes for Fuel Cells or Ionic Liquids. *J Fluor Chem*. **2008**, 129, 1029-1035.

(50) Appetecchi, G. B.; Montanino, M.; Carewska, M.; Moreno, M.; Alessandrini, F.; Passerini, S. Chemical–Physical Properties of Bis(perfluoroalkylsulfonyl)imide-based Ionic Liquids. *Electrochim Acta*. **2011**, 56, 1300-1307.

(51) Tsuzuki, S.; Umecky, T.; Matsumoto, H.; Shinoda, W.; Mikami, M. Interactions of Perfluoroalkyltrifluoroborate Anions with Li Ion and Imidazolium Cation: Effects of Perfluoroalkyl Chain on Motion of Ions in Ionic Liquids. *J Phys Chem B*. **2010**, 114, 11390-11396.

(52) Luo, J.; Jensen, A. H.; Brooks, N. R.; Sniekers, J.; Knipper, M.; Aili, D.; Li, Q.; Vanroy, B.; Wübbenhorst, M.; Yan, F.; Meervelt, L. V.; Shao, Z.; Fang, S.; Luo, Z.-H.; De Vos, D. E.; Binnemans, K.; Fransaer, J. 1,2,4-Triazolium Perfluorobutanesulfonate as an Archetypal Pure Protic Organic Ionic Plastic Crystal Electrolyte for All-Solid-State Fuel Cells. *Energy Environ Sci*, **2015**, 8, 1276-1291.

(53) Abate, A.; Petrozza, A.; Roiati, V.; Guarnera, S.; Snaith, H.; Matteucci, F.; Lanzani, G.; Metrangolo, P.; Resnati, G. A Polyfluoroalkyl Imidazolium Ionic Liquid as Iodide Ion Source in Dye Sensitized Solar Cells. *Org Electron* **2012**, 13, 2474-2478.

(54) Pozzi, G.; Mihali, V.; Foschi, F.; Penso, M.; Quici, S.; Fish, R. H. 3,5-Bis(n-perfluorooctyl)benzyltriethylammonium Bromide (F-TEBA): An Efficient, Easily Recoverable Fluorous Catalyst for Solid-Liquid PTC Reactions. *Adv Synth Catal*. **2009**, 351, 3072-3076.

(55) Tsukada, Y.; Iwamoto, K.; Furutani, H.; Matsushita, Y.; Abe, Y.; Matsumoto, K.; Monda, K.; Hayase, S.; Kawatsuraa, M.; Itoha, T. Preparation of Novel Hydrophobic Fluorine-Substituted-Alkyl Sulfate Ionic Liquids and Application as an Efficient Reaction Medium for Lipase-Catalyzed Reaction. *Tetrahedron Lett*. **2006**, 47, 1801-1804.

(56) Muldoon, M. J.; Aki, S. N. V. K.; Anderson, J. L.; Dixon, J. K.; Brennecke, J. F. Improving Carbon Dioxide Solubility in Ionic Liquids. *J Phys Chem B.* **2007,** 111, 9001-9009.

(57) Dias, A. M. A.; Carrier, H.; Daridon, J. L.; Pàmies, J. C.; Vega, L. F.; Coutinho, J. A. P.; Marrucho, I. M. Vapor-Liquid Equilibrium of Carbon Dioxide-Perfluoroalkane Mixtures: Experimental Data and SAFT Modeling. *Ind Eng Chem Res*. **2006**, 45, 2341-2350.

(58) Luís, A.; Shimizu, K.; Araújo, J. M. M.; Carvalho, P. J.; Lopes-da-Silva, J. A.; Canongia Lopes, J. N.; Rebelo, L. P. N.; Coutinho, J. A. P.; Freire, M. G., Pereiro, A. B. Influence of Nanosegregation on the Surface Tension of Fluorinated Ionic Liquids. *Langmuir*. **2016**, 32, 6130-6139.

(59) Merrigan, T. L.; Bates, E. D.; Dorman, S. C.; Davis, J. H. New Fluorous Ionic Liquids Function as Surfactants in Conventional Room-Temperature Ionic Liquids. *Chem Commun*. **2000**, 20, 2051-2052.

2. Nanoscale Structuring of the Fluorinated Ionic Liquids

2.1 Introduction

Fluorinated compounds have an increased potential in several biomedical approaches due to their bulky fluorocarbon compositions. Their outstanding gas dissolving capacity, extreme inertness, high surface activity and strong tendency to self-aggregate into stable and well-organized assembler make them great candidates for fluorocarbon emulsions, microemulsions, gels, dispersions, aerosols, etc. used in biomedical applications. In this thesis, general insights in the nanostructure of several FILs have been characterized in order to design and develop the best fluorinated compounds to use in biomedical research.(1)

The nanostructural characterization of ionic liquids (ILs) has been broadly studied. The self-assembled nanostructure of these compounds has been demonstrated due to the polar / apolar nanosegregation.(2–7) Several studies (2–5) have established the interplay between cations and anions and charged/non-charged moieties, which leads to the segregation between the polar and apolar regions in the ILs. This self-aggregation creates high-charge and low-charge electronic density distribution domains in the liquid.(2–5) The contribution of the different ion-ion interactions and other molecular effects, like symmetry and flexibility of the structured features, have also an impact on the properties of ionic liquids.(6)

Nevertheless, the structural organization of the fluorinated ionic liquids (FILs) is still quite unexplored. This organization is more complex due to the addition of a new nanosegregated domain from the contribution of the fluorinated side chains. The molecular structure of the FILs is characterized by the presence of the carbon-fluorine bonds, the most stable and strongest single bond in organic chemistry.(8) These bonds increase the rigidity and decrease the polarity of these compounds.(9) Moreover, the addition of the fluorinated domains might confer advantageous properties to FILs due to modification of the mesomorphic properties and molecular geometry.(8,10–13) The self-assembly nanostructure of FILs have been already reported and strongly supported in previous works.(10,14) In these studies, the formation of one polar and two apolar (fluorinated and hydrogenated) nanosegregated domains was demonstrated. Then, there are evidences in the literature of the tri-continuous nanostructures in ILs with perfluorinated regions added in the cation or anion, leading to the segregation of the polar, hydrocarbon and fluorocarbon moieties. (8,10–13)

This structural behaviour can widely contribute to the thermal behaviour of the selected FILs. The phase transitions and decomposition temperatures are critical properties that provide information about structure (15) and the liquid range of these compounds. These thermal properties are also

important to know the thermal range of application of these FILs.(16,17) Besides, the melting temperature gives structural information due their dependency of the molecular arrangement in the crystal lattice. The structural factors (like intermolecular interactions, molecular symmetry, conformational changes, distribution of charge and size of the ions) can influence the range and number of the phase transitions.(7,18) The presence of linear alkyl side chains is related to the increment of the flexibility of these FILs. This flexibility increases the conformational changes of these compounds yielding more solid-solid polymorphic transitions.(19) Then, the motion of the side chains might provide important information about the behaviour of the ILs structure.(18)

To study the role of the three nanosegregated domains in this complex structural behaviour, FILs with the richest phase behaviour were selected. This study allows us to understand which structural features are the most outstanding, to design and develop the most favourable FIL for artificial oxygen carriers. In order to achieve well-matched compounds that follow the complex biological processes, several structure variations were considered. The effect of the hydrogenated side chain length, the type of cation and the type of anion in the thermodynamic and thermal behaviour of FILs were studied through the complete solid-fluid phase transitions analysis using calorimetric and thermal tools. Moreover, information about the structural modifications at atomic level were obtained by molecular dynamics (MD) simulations. This information extends the knowledge about the complex structuration, sustaining the impressive thermal behaviour of these novel compounds.

2.2 Materials

1-Ethyl-3-methylpyridinium perfluorobutanesulfonate, $[C_2C_1py][C_4F_9SO_3]$, 99% mass fraction purity, 1-butyl-1-methylpyrrolidinium bis(nonafluorobutylsulfonyl)imide, $[C_4C_1pyr][N(C_4F_9SO_2)_2]$, > 98% mass fraction purity, 1-butyl-1-methylpyrrolidinium perfluorobutanesulfonate, $[C_4C_1pyr][C_4F_9SO_3]$, > 98% mass fraction purity, and 1-methyl-3-octylimidazolium perfluorobutanesulfonate $[C_8C_1Im][C_4F_9SO_3]$, > 99% mass fraction purity, were supplied by IoLiTec GmbH. All the chemical structures and acronyms of the FILs are represented in **Table 2.1**.

These FILs were all dried under vacuum ($3 \cdot 10^{-2}$ Torr) and vigorously stirred at 323.15 K for at least 2 days, immediately before the experiments, in order to remove water and volatile substances. The water content was measured by Karl Fischer titration and was lower than 100 ppm in all FILs. The purity of the commercial products was also checked by ^{1}H and ^{19}F NMR.

Furthermore, 1-hexyl-3-methylimidazolium perfluorobutanesulfonate, $[C_6C_1Im][C_4F_9SO_3]$ (10) and tetrabutylammonium perfluorobutanesulfonate, $[N_{4444}][C_4F_9SO_3]$ (10) were used for comparison purposes. Their chemical structures and acronyms are also shown in **Table 2.1**.

Table 2.1 - Chemical structure and respective acronyms of the studied fluorinated ionic liquids.

FIL Designation	Chemical Structure
1-Ethyl-3-methylpyridinium perfluorobutanesulfonate **[C_2C_1py][$C_4F_9SO_3$]**	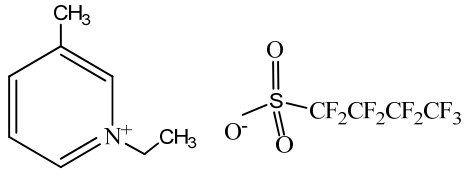
1-Butyl-N-methylpyrrolidinium bis(nonafluorobutylsulfonyl)imide **[C_4C_1pyr][$N(C_4F_9SO_2)_2$]**	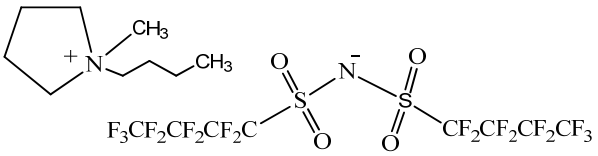
1-Butyl-N-methylpyrrolidinium perfluorobutanesulfonate **[C_4C_1pyr][$C_4F_9SO_3$]**	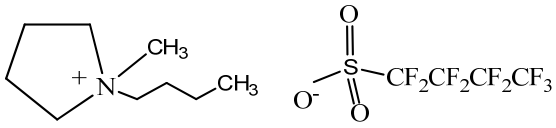
1-Methyl-3-octylimidazolium perfluorobutanesulfonate **[C_8C_1Im][$C_4F_9SO_3$]**	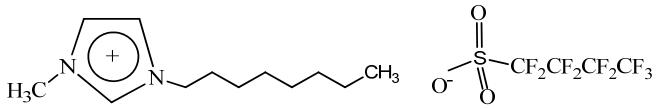
1-Hexyl-3-methylimidazolium perfluorobutanesulfonate **[C_6C_1Im][$C_4F_9SO_3$]**[a]	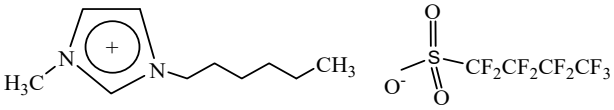
Tetrabutylammonium perfluorobutanesulfonate **[N_{4444}][$C_4F_9SO_3$]**[a]	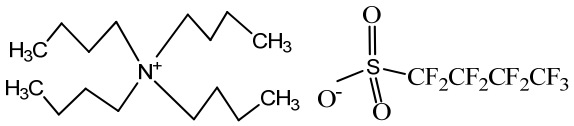

[a] from reference (10)

2.3 Experimental Procedure

2.3.1 Thermodynamic Characterization

Each fluorinated ionic liquid was taken from the respective Schlenk flask with a syringe under nitrogen flow, to avoid contaminations or humidity, and immediately placed in the measuring devices.

2.3.1.1. Differential scanning calorimetry

A Differential Scanning Calorimeter (DSC) from TA Instruments, model Q200 (see **Figure 2.1**), was used to measure the phase transitions of the FILs. The cooling was accomplished by a refrigerator system capable to reach a minimum temperature of 183.15 K. The sample was continuously purged using 50 ml·min^{-1} of dry dinitrogen gas. About 5 to 10 mg of each FIL was sealed in an aluminium standard sample pan. Indium, with a melting point at 429.76 K, was used as standard for the DSC calibration. Samples were all cooled down to 183.15 K and tempered during 30 min. Afterwards, they were heated until different temperatures leaving a range of 20 K between the last transition and the end of the cycle. The cooling–heating cycles were repeated three times at different scan rates (10 K·min^{-1}, 5 K·min^{-1} and 1 K·min^{-1} for [C_4C_1pyr][$N(C_4F_9SO_2)_2$], [C_4C_1pyr][$C_4F_9SO_3$] and [C_8C_1Im][$C_4F_9SO_3$] and 5 K·min^{-1}, 2.5 K·min^{-1} and 1 K·min^{-1} for [C_2C_1py][$C_4F_9SO_3$]). This scan rate selection guarantees the best delineation and characterization of the several solid-fluid phase transitions of each ionic liquid. The standard uncertainty of the apparatus was estimated ± 2 K. All DSC runs with the different scan rates are plotted in **Figures A.1** to **A.4** of the **Appendix**. The DSC runs of [C_6C_1Im][$C_4F_9SO_3$] (10) and [N_{4444}][$C_4F_9SO_3$] (10) were used for comparison and are also shown in **Figures A.5** and **A.6** of the **Appendix**. Universal Analysis 2000 v. 4.5A software (TA instruments) was used to integrate the calorimetric peaks and determine the solid-solid transition ($T_{s\text{-}s}$) and melting temperatures (T_m).

2.3.1.2 Thermogravimetric analysis

A TGA Q50 Thermogravimetric Analysis (TA instruments) equipment (see **Figure 2.2**) was used to measure the weight loss as a function of temperature. These experiments provide useful information concerning the decomposition of the pure FILs, which is crucial to their applications range. The samples were continuously purged using 50 ml·min^{-1} of dry dinitrogen gas. About 10 to 25 mg of fluorinated ionic liquid was crimped in an aluminium standard sample pan. Samples were heated up to 873.15 K at a scan rate of 1 K·min^{-1} until complete thermal degradation. The relative uncertainty of the temperature was ± 4 K. The TGA runs are illustrated in **Figure A.7** of the **Appendix** for all FILs herein studied.

Regarding TGA analysis, the Universal Analysis 2000 v. 4.5A software (TA instruments) was also used to determine the onset (T_{onset}), start (T_{start}) and decomposition (T_{dec}) temperatures (corresponding to the temperatures where the baseline slope changed during heating, the weight loss was less than 1% and the weight loss was 50%, respectively).

Figure 2.1. Differential Scanning Calorimeter (DSC) of TA Instrument, model Q200.

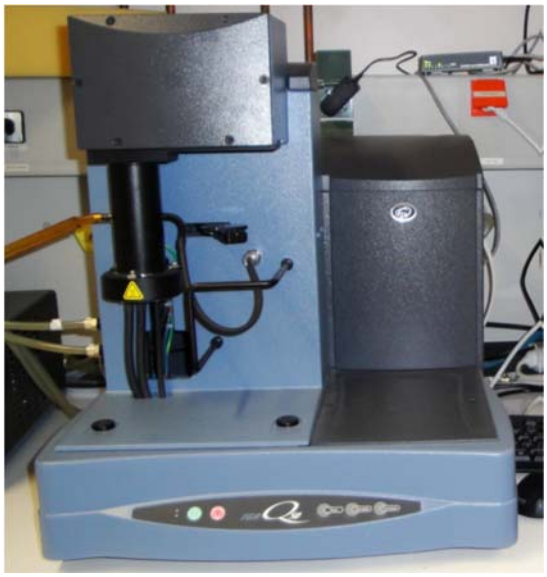

Figure 2.2. TGA Q50 Thermogravimetric Analysis (TA instruments).

2.3.2 Molecular Dynamics (MD) Simulations

The selected FILs for this study were modelled with a previously reported CL&P atomistic force field (20–22) that is an extension of AMBER/OPLS force fields.(23) This approach was applicable to enclose all ionic liquids in a systematic way. Afterwards, the Molecular Dynamics (MD) simulations were carried out by using the DL_POLY 2.20 package.(24)

The $[C_2C_1py][C_4F_9SO_3]$, $[C_4C_1pyr][C_4F_9SO_3]$ and $[C_4C_1pyr][N(C_4F_9SO_2)_2]$ FILs were modelled in simulation boxes with 800 ion pairs for each pure compound, with a time step of 2 fs and a cutoff distance of 1.6 nm (with the Ewald summation approach applied to electrostatic interactions beyond that distance). The simulation runs were started from low-density configurations and therefore equilibrated under isothermal-isobaric ensemble conditions (*N*-*p*-*T*) at $T = 343$ K and $p = 0.1$ MPa, with Nosé-Hoover thermostats and barostats with relaxation time constants of 0.5 and 2.0 ps, respectively. In order to reach the equilibrium, constant and consistent density values were obtained through consecutive runs at the studied temperature. In the case of $[C_6C_1Im][C_4F_9SO_3]$, $[C_8C_1Im][C_4F_9SO_3]$ and $[N_{4444}][C_4F_9SO_3]$, the MD simulations were already available from a previous work.(10,17) The MD results were used to characterize the FILs structure, aggregates formation and dihedral analysis.

2.3.2.1 Structural Analysis

The total static structure factors, $S(q)$, were calculated using a previously described methodology,(25) and briefly obtained from:

$$S(q) = \sum_i \sum_j S_{ij}(q) \qquad \textbf{(1)}$$

$$S_{ij}(q) = \frac{\rho_o x_i x_j b_i(q) b_j(q) \int_0^R 4\pi r^2 \left[g_{ij}(r) - 1 \right] \frac{\sin(qr)}{qr} \frac{\sin(\pi R)}{\pi r / R} dr}{\left(\sum_i x_i b_i(q) \right)^2} \qquad \textbf{(2)}$$

where $S_{ij}(q)$ is the partial static structure factor between atoms of type *i* and *j* (e.g. carbon, hydrogen or nitrogen) calculated from the corresponding Fourier transform of the partial radial distribution function $g_{ij}(r)$; q is the scattering vector; ρ_o is the average atom number density; R is the cutoff used in the calculation of $g_{ij}(r)$, i.e. half the side of the simulation box (in this case $r = 3.5$ nm); x_i and x_j are the atomic fractions of *i* and *j*; and $b_i(q)$ and $b_j(q)$ are the coherent bound neutron scattering lengths of the corresponding atom type, interpolated from recommended values in the International Tables for

Crystallography.(26) The term $\sin(\pi R)/(\pi r/R)$ of the equation 2 is a Lorch-type window function used to reduce the effect of using a finite cutoff in the radial distribution function calculation.(27)

2.3.2.2 Aggregation Analysis

The aggregation analysis was accomplished for $[C_4C_1pyr][C_4F_9SO_3]$ and $[C_4C_1pyr][N(C_4F_9SO_2)_2]$ FILs with the aim to point out the assessment of the association between the alkyl side chains of the apolar domains (hydrogenated and fluorinated domains). The connectivity analysis of the alkyl chains (apolar aggregates) is based on previously described algorithms (28,29) that generate neighbour lists of the given type interaction centres, in a three-stage sequential processes.

Firstly, the definition of the interactions was done considering all the carbon atoms of the alkyl (cations) and/or perfluoroalkyl (anions) side chains (except the ones that are directly connected to the charged moieties of the ions). The apolar aggregates obtained in this study are the ones under investigation. Secondly, an interatomic distance for each interaction defined above was established considering the $g_{ij}(r)$ data.(29) The distance between the carbons atoms of the cation hydrogenated alkyl side chains was defined as 0.5 nm; the distance between the carbon atoms of the anion perfluoroalkyl side chains was set to 0.6 nm. Thirdly, the use of the threshold criteria allowed the computation of closest-neighbour lists for each interaction centre for all recorded configurations in the production runs, thus ascertaining the connectivity within the apolar domains. In the case of the apolar domains, two chains were considered to belong to the same aggregate if the distance between any two carbon atoms of the two chains was lower than the threshold value. Finally, the probability distribution function, $P(n_a)$, of finding an alkyl side chain in an aggregate of a given size (with n_a alkyl side chains) was computed from the generated connectivity lists.(28)

2.3.2.3 Dihedral Analysis

The MD simulations were also used to obtain specific data that were analysed with the purpose of carefully describe the conformational and intermolecular behaviour of the $[N(C_4F_9SO_2)_2]^-$ anion. In order to achieve this goal, conformer distribution profiles (CDP, population histograms as a function of the C1-S1-S2-C2 dihedral angle of $[N(C_4F_9SO_2)_2]^-$) were obtained at 343 K for the pure $[C_4C_1pyr][N(C_4F_9SO_2)_2]$. The geometry for the isolated single $[N(C_4F_9SO_2)_2]^-$ anion was fully optimized at the density functional theory level according to Becke's three-parameter hybrid method with LYP correlation (B3LYP) (30) in vacuum using the 6-31G(d) basis set. DFT calculations were carried out using the Gaussian 03 program package.(31)

2.4 Results and Discussion

The results obtained through the combined experimental and theoretical approaches were discussed in order to understand the thermal and dynamic properties at molecular and structural level of these compounds. The results were analysed in order to infer the nature of the outstanding crystallization processes that describe the selected FILs as highly nanostructured compounds. In this work, the influence of the hydrogenated alkyl side chain length and the effect of different cations and anions types were analysed. Firstly, the influence of the hydrogenated side chain length was examined by comparing two FILs based in imidazolium cations conjugated with perfluorobutanesulfonate anion. Secondly, the effect of the cation was studied through a comparison between four FILs based on perfluorobutanesulfonate anion with ammonium, pyridinium, pyrrolidinium and imidazolium cations. Finally, the influence of the anion type was investigated in FILs based on pyrrolidinium cation conjugated with perfluorobutanesulfonate and bis(nonafluorobutylsulfonyl)imide anions.

Regarding the thermal properties, the melting (T_m), glass transition (T_g) and solid-solid transition (T_{s-s}) temperatures for the six studied FILs are summarized in **Table 2.2**, with their corresponding enthalpies. Their onset (T_{onset}), start (T_{start}) and decomposition (T_{dec}) temperatures are shown in **Table 2.3**.

The project where this thesis was integrated, has a collaboration with the University of Vigo where the rheological behaviour of these pure FILs was determined. These experimental data support the calorimetric study of the pure FILs carried out in this work. In the rheological study (see **Figure A.8** of **Appendix)**, the viscoelastic properties were determined because they are directly correlated with the internal molecular structure, reflecting the phase and structural changes. The previous studies are in agreement with the phase transitions determined by DSC analysis, as shown in the **Figure A.8** of **Appendix**. However, for some isolated cases, the solid-solid transitions were not all identified in the rheological analysis due to the specifications of the rheometer used. Furthermore, the sensitivity of the both techniques is different, underlying the complementary of the two experimental approaches.

Table 2.2 Solid-solid transitions, $T_{s\text{-}s}$; melting temperature, T_m; enthalpy, ΔH and glass transitions, T_g of selected fluorinated ionic liquids.

	Scan rate / K·m^{-1}	$T_{s\text{-}s}$ / K	T_m / K	ΔH / J·g^{-1}	T_g / K
[C_2C_1py][$C_4F_9SO_3$]	5	249 -	- 278[b]	2.17 33.4	- -
[C_4C_1pyr][$N(C_4F_9SO_2)_2$]	5	256 275 285 -	- - - 375	4.01 3.62 2.15 7.30	- - - -
[C_4C_1pyr][$C_4F_9SO_3$]	1	274 323 -	- - 364	18.9 5.19 19.9	- - -
[C_8C_1Im][$C_4F_9SO_3$]	1	279 -	- 308[c]	9.51 38.9	- -
[C_6C_1Im][$C_4F_9SO_3$][a]	1	265 290 294 -	- - - 297	0.789 18.7 17.8 8.48	- - - -
[N_{4444}][$C_4F_9SO_3$][a]	5	-	327	25.2	235

[a] from reference (10)
[b] from reference (32)
[c] from reference (16)

Table 2.3. Thermal properties of selected fluorinated ionic liquids acquired by TGA: start temperature, T_{start}, onset temperature, T_{onset} and decomposition temperature, T_{dec}.

	T_{start}[a] / K	T_{onset}[a] / K	T_{dec}[a] / K
[C_2C_1py][$C_4F_9SO_3$][b]	574	629	652
[C_4C_1pyr][$N(C_4F_9SO_2)_2$][b]	587	639	656
[C_4C_1pyr][$C_4F_9SO_3$]	589	632	651
[C_8C_1Im][$C_4F_9SO_3$][c]	582	623	656
[C_6C_1Im][$C_4F_9SO_3$][c]	566	627	666
[N_{4444}][$C_4F_9SO_3$][c]	545	587	619

[a] Note that these values are from scanning TGA at 1 K·min^{-1}, and do not represent isothermal stabilities.
[b] from reference (32)
[c] from reference (16)

The onset temperatures versus melting temperatures are plotted in **Figure 2.3**. To explore the application of the FILs as gas carriers, the most relevant temperature is 310.15 K, the human body average temperature. In the **Figure 2.3**, $[C_2C_1py][C_4F_9SO_3]$ shows the highest thermal stability for FILs with a melting temperature below 310.15 K. This FIL is the most promising to be used in the biomedical application studied in this work. **Figure 2.3** also includes FILs with higher melting points that are solid and insoluble / immiscible in biological fluids at the target temperature, 310.15 K. This fact makes them non-viable candidates for artificial oxygen carriers. However, it is important to note that the most important goal of this study is to characterize and understand the crystallization processes of several FILs in order to design and develop the most promising compounds for biomedical applications. With this goal in mind, the FILs with the richest phase scenario were selected. Then, this work may provide an overall study not only of the thermal properties as a tool to determine the liquid range of the fluids, but also yield information about the exceptional crystalline structures that characterize the FILs as highly nanostructured species.

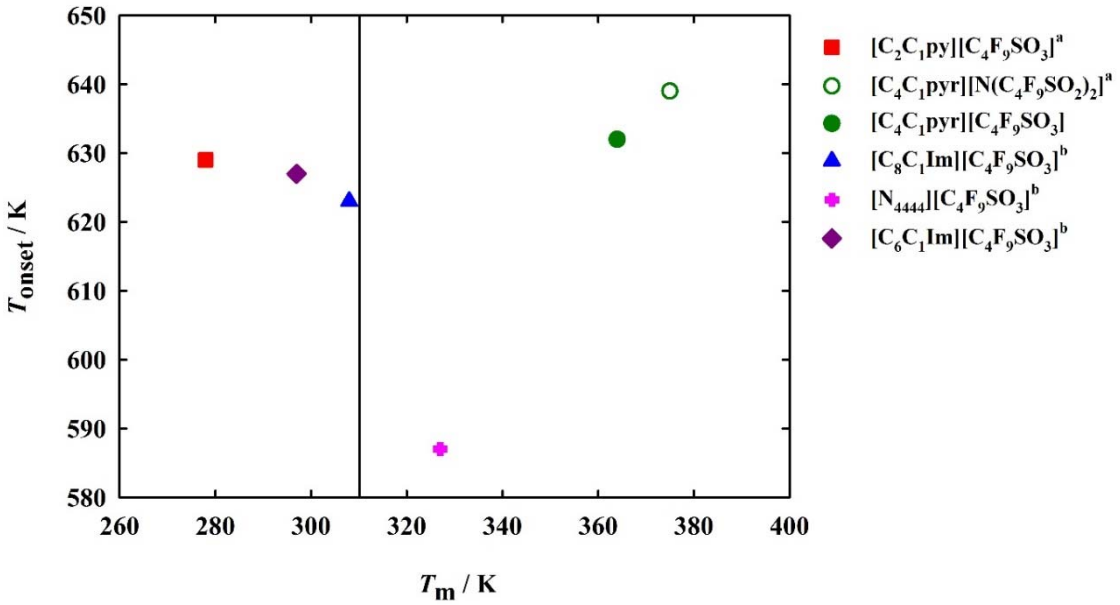

Figure 2.3. Onset temperature versus melting temperature of the studied FILs and comparison with previous experimental data ([a] from reference (32) and [b]from reference (16)), where full symbols represent FILs with perfluorobutanesulfonate anion and empty symbols represent FILs based on bis(nonafluorobutylsulfonyl)imide anion.

2.4.1 Influence of the hydrogenated side chain in the nanostructure of Fluorinated Ionic Liquids

As a first approach, the $[C_6C_1Im]^+$ and $[C_8C_1Im]^+$ cations conjugated with perfluorobutanesulfonate $[C_4F_9SO_3]^-$ anion were compared to infer the influence of the hydrogenated alkyl side chain in the thermodynamic characterization of FILs. In **Table 2.2** are depicted the melting temperatures where a slight increase in the case of $[C_8C_1Im]^+$ is revealed. However, the opposite behaviour was noticed for onset temperatures which are illustrated in **Table 2.3**. This result suggests a slight increase in the melting point and a decrease in the decomposition temperature when the hydrogenated alkyl chain is longer.

It has been described (33) that the ionic liquids with imidazolium cations conjugated with traditional fluoro-containing anions, like bis(trifluoromethylsulfonyl)imide anion, usually exhibit lower melting temperatures when the hydrocarbon side chain length increases. This does not agree with the present results. However, the same cations combined with chloride anion were reported, and the same tendency was showed.(34) In another study, imidazolium cations combined with perfluorobutanesulfonate anion showed an increment in melting temperatures when the hydrogenated alkyl chain length is longer,(35) supporting our results. Regarding the decomposition temperatures of these FILs, a decrease in the thermal stability was visible when the alkyl side chain length is longer. This behaviour was also reported with imidazolium ILs based on chloride, hexafluorophosphate, tetrafluoroborate and bis(trifluoromethylsulfonyl)imide anions,(36) supporting the onset temperatures obtained in this work.

Also, the number of solid-solid transitions were taken into consideration, since each phase transition in the heating ramp may correspond to a possible conformation of the ionic liquid structure. **Figure 2.4** illustrates the comparison between $[C_6C_1Im]^+$ and $[C_8C_1Im]^+$ cations, where the phase transitions were determined in a heating cycle of 1 K min^{-1}. In the case of the $[C_6C_1Im]^+$ cation represented in **Figure 2.4.a** and in **Table 2.2**, three successive peaks corresponding to solid-solid transitions at 265, 290 and 294 K were observed, while the last peak is the melting temperature at 297 K. The $[C_8C_1Im]^+$ cation (see **Figure 2.4.b** and **Table 2.2**) only showed a single solid-solid transition at 279 K and the melting point at 308 K. These results suggest: (i) the decreasing number of solid-solid transitions when the hydrogenated side chain is longer; and (ii) the melting temperature has the opposite behaviour, increasing when the hydrocarbon side chain length increases.

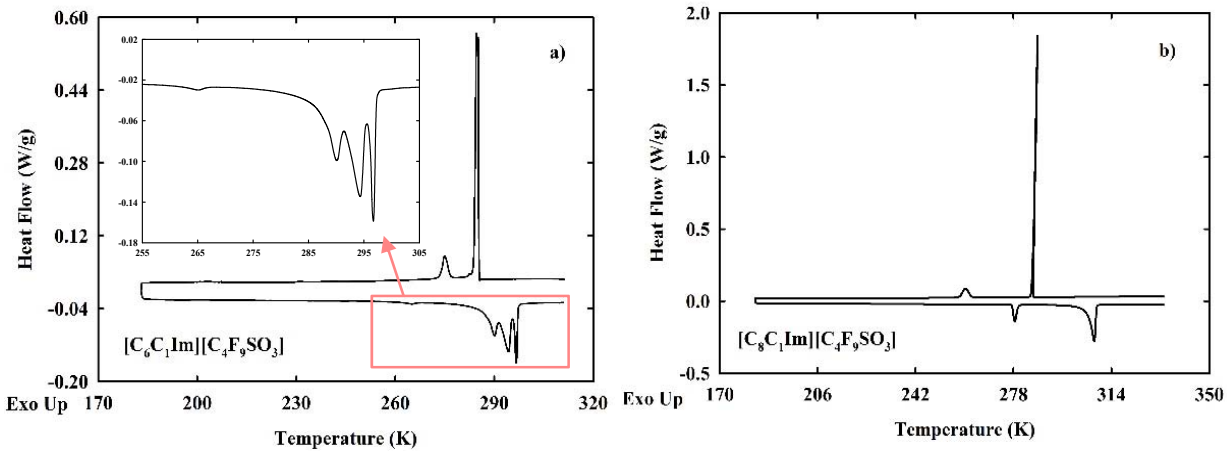

Figure 2.4. Comparison of DSC runs for imidazolium FILs with different hydrogenated side chains: (a) $[C_6C_1Im][C_4F_9SO_3]$ and (b) $[C_8C_1Im][C_4F_9SO_3]$ at a scan rate of 1 K·min^{-1}.

It was already established (17) that when the hydrogenated alkyl side chain is longer than six carbon atoms some degree of nanosegregation between fluorinated and hydrogenated domains is found. In **Figure 2.5** the global structure factors functions, $S(q)$, are plotted calculated with the appropriate Fourier transforms of the pair correlation functions obtained from the MD trajectories from $[C_6C_1Im][C_4F_9SO_3]$ and $[C_8C_1Im][C_4F_9SO_3]$ FILs. The q-value range used for all FILs studied in this thesis is $2.0 < q / nm^{-1} < 18.0$ since the low-q range of $S(q)$ corresponds to the structural features at intermolecular level of the systems. In this range, the $S(q)$ functions of ionic liquids usually show three successive peaks at low, intermediate and high q-values. The low q-value peak is the so-called pre-peak or polar-apolar peak (PNPP) that usually occurs due to the nanosegregation between the polar and apolar moieties formed by the alkyl chain segments of the ionic liquid constituents. The intermediate peak is the charge-ordering peak (COP), which is exclusive to ionic liquids or molten salts and is related to the neighbouring conditions each ion is experiencing when surrounded by its ion counterparts, in order to establish a local electroneutrality. The higher q-value peak is named as contact peak (CP) concerning the distances between the atoms from different ions and defines the limits between intra- and intermolecular structural features being characteristic of ionic liquids and molecular fluids.(17) However, the CP results from multiple contributions from different distances correlations, making difficult to define specific structural features from the q-value shifts and will be not discussed in this thesis.

In the $S(q)$ function represented in the **Figure 2.5**, the $[C_6C_1Im][C_4F_9SO_3]$ (blue line) shows three well-defined peaks at q-values of 3.90, 9.55, 13.37 nm^{-1} while in the case of $[C_8C_1Im][C_4F_9SO_3]$ (orange line) three peaks occurs at q-values of 3.90, 9.40, 13.60 nm^{-1}. In both cases, the presence of a well-defined PNPP, suggests an effective segregation between the polar/apolar moieties. The COP q-

values define the space occupied by the polar network, which will be influenced by the apolar moieties. In this case, the *q*-value of COP in $[C_8C_1Im][C_4F_9SO_3]$ decreases, meaning that the polar network is larger to accommodate the apolar domains from the hydrogenated side chain that is longer than $[C_6C_1Im][C_4F_9SO_3]$.

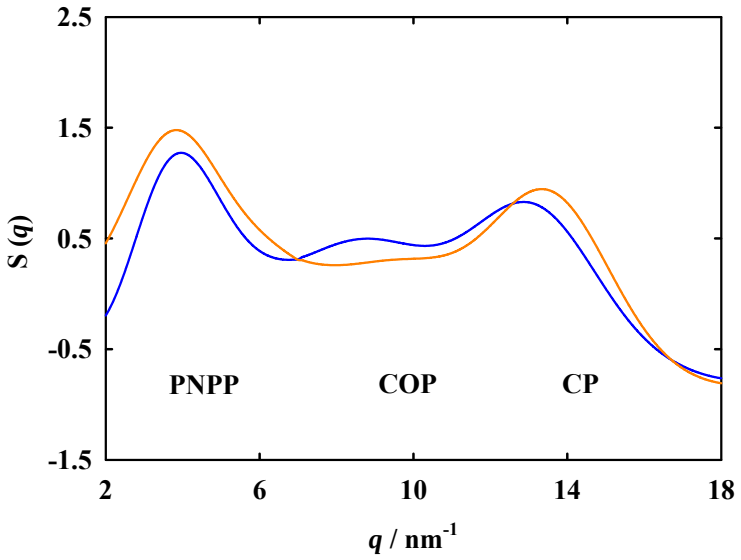

Figure 2.5. Structure factor functions, $S(q)$, of $[C_6C_1Im][C_4F_9SO_3]$ (blue line) and $[C_8C_1Im][C_4F_9SO_3]$ (orange line), corresponding to FILs with different hydrogenated side chain lengths. The low-q spectra at the range of $2.0 < q / nm^{-1} < 18.0$ is depicted.

In order to extend the knowledge about the nanosegregation of these two ionic liquids, in **Figure 2.6** are plotted the snapshots from the simulation boxes for $[C_6C_1Im][C_4F_9SO_3]$ and $[C_8C_1Im][C_4F_9SO_3]$, respectively. In the snapshot of $[C_6C_1Im][C_4F_9SO_3]$ (**Figure 2.6.a**) is clearly illustrated the nanosegregation between the three regions since three distinct domains are formed: one from the polar network represented by the blue (positive charges) and red (negative charges) segments and two from apolar moieties represented by the space filled areas (grey for hydrocarbon chains and green for fluorocarbon chain). Since the fluorinated counterparts of the anion are long enough, they can intrude into the hydrogenated clusters and arrange into three domains. They may act as self-counterparts assuming different spatial positions and increasing the possibility of rearrangement in different conformations when the ionic liquid crystalizes. This fact happens due to the similar size between the several domains, supporting the increased number of solid-solid transitions that occur in the thermal analysis of $[C_6C_1Im][C_4F_9SO_3]$ (see **Figure 2.4.a** and **Table 2.2**). This ionic liquid presents one of the richest phase transitions scenario.

Regarding $[C_8C_1Im][C_4F_9SO_3]$ FIL (**Figure 2.6.b**) the same nanosegregation is occurring. However, the perfluorobutyl chains are not bulky enough to overcome the continuous cluster that is

formed by the increased hydrogenated side chain. This fact happens because $[C_8C_1Im][C_4F_9SO_3]$ presents a large and continuous hydrogenated domain when is compared with the fluorinated domain. This hydrogenated domain starts to percolate the simulation box, diminishing the space for the three domains co-exist as uniform systems. This structural behaviour may explain the increment of the temperature necessary to enable the disruption of the continuous domain built by the hydrogenated counterparts. On the other hand, this disproportion between the two apolar domains behaviour may affect the balance enclosed by the three types of domains (polar, hydrogenated apolar and fluorinated apolar), as is depicted in the case of $[C_6C_1Im][C_4F_9SO_3]$ FIL. It can diminish the possibility of the $[C_8C_1Im][C_4F_9SO_3]$ adopting different conformations in a crystal, decreasing the number of solid-solid transitions (see **Figure 2.4.b** and **Table 2.2**).

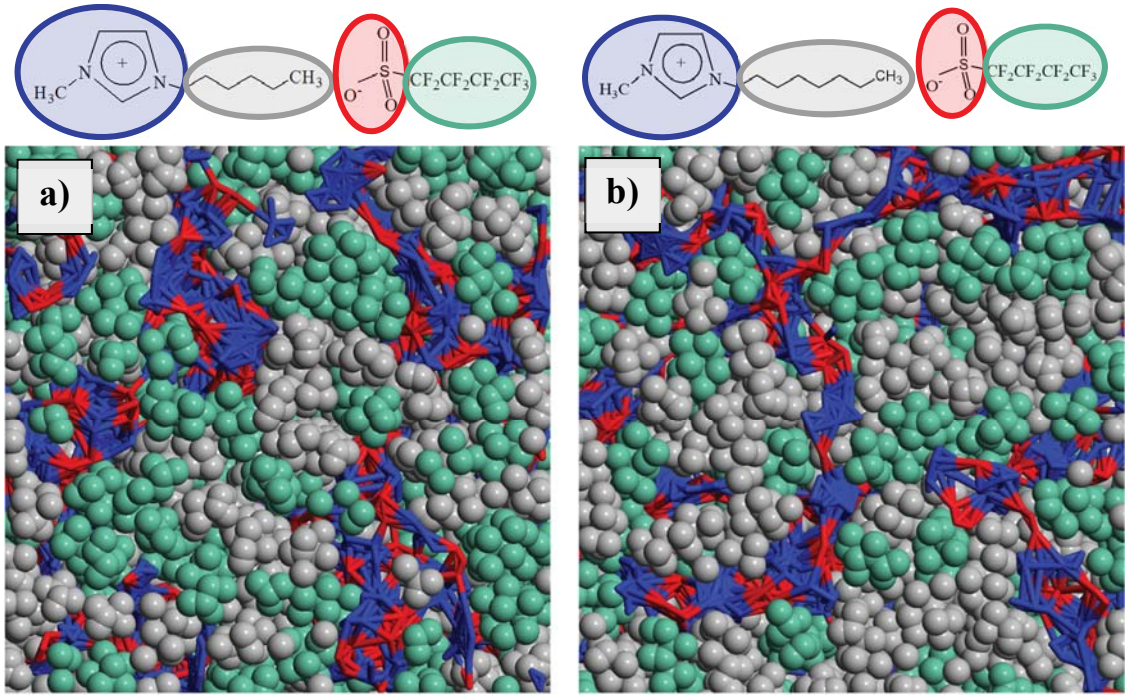

Figure 2.6. MD simulation snapshots for the FILs with different hydrogenated side chain length: (a) $[C_6C_1Im][C_4F_9SO_3]$, (b) $[C_8C_1Im][C_4F_9SO_3]$. Red (negative charges) and blue (positive charges) segments represent the interactions from the polar network of the two ions, gray space-filled areas represent the domains caused by the hydrogenated side chains while the groups of green spheres illustrate the perfluoroalkyl apolar domains. They are also represented in the structures of each ionic liquid with the corresponded colour.

2.4.2 Influence of the cation type in the nanostructure of Fluorinated Ionic Liquids

The study of the influence of the cation type in the thermal and structural behaviour of FILs was performed using four ionic liquids based on imidazolium, $[C_6C_1Im]^+$; ammonium, $[N_{4444}]^+$; pyridinium, $[C_2C_1py]^+$ and pyrrolidinium, $[C_4C_1pyr]^+$ cations, conjugated with the perfluorobutanesulfonate anion, $[C_4F_9SO_3]^-$.

In respect to the decomposition temperatures that are depicted in **Table 2.3**, the observed tendency has the following order: $[N_{4444}]^+ < [C_6C_1Im]^+ < [C_2C_1py]^+ < [C_4C_1pyr]^+$. The literature shows (36) that pyrrolidinium ILs are more resistant to temperature, followed by imidazolium, pyridinium and non-cyclic tetraalkyl ammonium cations, supporting the trend observed in this work.

Figure 2.7 represents the comparison of the DSC results for each ionic liquid with different cations. The $[C_6C_1Im]^+$ (**Figure 2.7.a**) was already described in the previous discussion, and it is also represented here for comparison. The $[N_{4444}]^+$ cation, illustrated in **Figure 2.7.b**, shows a glass transition at 235 K followed by the melting point at 327 K. Only one solid-solid transition at 249 K was reported for $[C_2C_1py]^+$ (see **Figure 2.7.c**), and the melting point occurs at 278 K. Finally, in the $[C_4C_1pyr]^+$ two solid-solid transitions at 274 and 323 K and the melting temperature at 364 K were observed as plotted in **Figure 2.7.d**. Summarizing the results, the increment of the melting (i) and number of solid-solid transitions (ii) were:

(i) $[C_2C_1py]^+ < [C_6C_1Im]^+ < [N_{4444}]^+ < [C_4C_1pyr]^+$;

(ii) $[N_{4444}]^+ < [C_2C_1py]^+ < [C_4C_1pyr]^+ < [C_6C_1Im]^+$.

Each fluorinated ionic liquid behaviour will be discussed below by comparing the experimental data previously described and the theoretical results obtained from the MD simulations to clarify their structural behaviour.

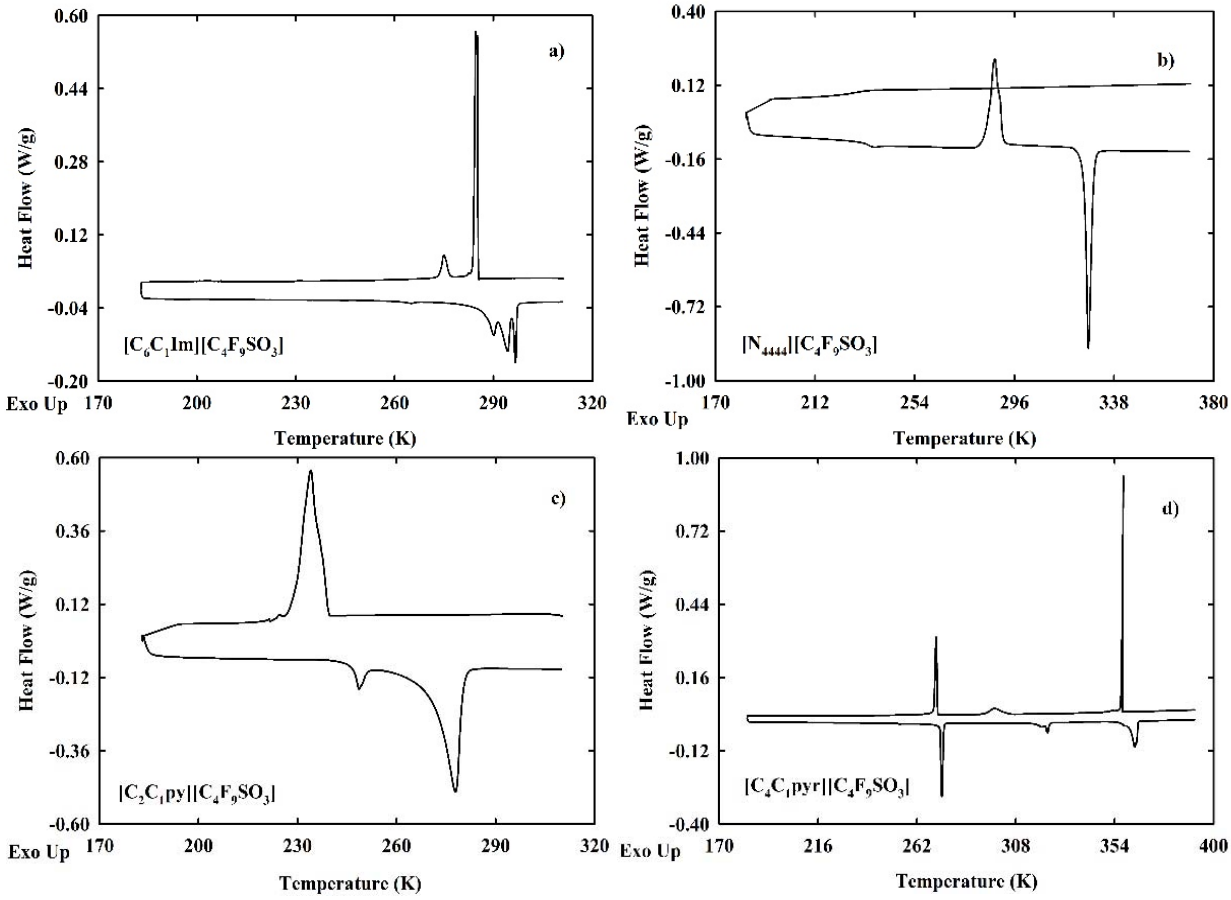

Figure 2.7. Comparison of DSC runs for FILs with different cations: (a) $[C_6C_1Im][C_4F_9SO_3]$ and (d) $[C_4C_1pyr][C_4F_9SO_3]$ at a scan rate of 1 K·min^{-1}; (b) $[N_{4444}][C_4F_9SO_3]$ and $[C_2C_1py][C_4F_9SO_3]$ at a scan rate of 5 K·min^{-1}.

The $[C_6C_1Im][C_4F_9SO_3]$ FIL showed four phase transitions being the one with the richest phase behaviour when compared to the other three types of cations (see **Table 2** and **Figure 2.7.a**). Its $S(q)$ function displays three well-defined peaks at q-values of 3.90, 9.55, 13.37 nm^{-1}(**Figure 2.8**, blue line). The effective segregation between the three domains might be the principal reason for the rich transition scenario of this FIL due to the weak interaction between the fluorinated and hydrogenated domains. The hydrogenated hexyl chain of the cation is long enough to segregate and form intermediate-sized features of hydrogenated and fluorinated domains (**Figure 2.9**) that result in proportional clusters enabling the structuration in different conformers.

The structure of $[N_{4444}][C_4F_9SO_3]$ (see **Table 1**) shows four butyl hydrogenated alkyl chains symmetric and closer to each other. The symmetry and proximity of the hydrocarbon chains may diminish the possibility of conformational changes, demonstrated by the absence of solid-solid transitions (**Figure 2.7.b**) In the $S(q)$ function of $[N_{4444}][C_4F_9SO_3]$ depicted in **Figure 2.8** (yellow line), a shoulder around 4 and 5 nm^{-1} is visible which is attached to the intermediate peak at a q-value of 7 nm^{-1} (the high q-value peak occurs at 14 nm^{-1}). In this case, the shoulder that appears at low q-value,

corresponds to the PNPP and is overlapped with the COP. As it was previously reported,(10) the polar network is encased by the hydrogenated counterparts due to their proximity, blocking the possibility of the network aggregation to occur. This is supported by the low *q*-value of the COP, meaning larger distances in the environment between the equally charged ions. However, due to the proximity of the PNPP and the COP (that show up as a peak and shoulder), it is harder to establish an unequivocal deconvolution of the S(q) function in this area. This means that the *q*-values for PNPP (4-5 nm^{-1}) and COP (7 nm^{-1}) can be affected by some degree of uncertainty. The presence of the fluorinated domain induces some level of nanosegregation between the hydrogenated clusters which contributes to the appearance of the shoulder at low *q*-values.(10) Thus, the continuous hydrogenated domain, formed by the four butyl chains (see **Figure 2.9.b**), hampers the number of crystallization options. This fact may be the possible explanation for the inexistence of solid-solid transitions in this FIL (see **Table 2.2** and **Figure 2.7.b**), since the ionic liquid is not able to rearrange in more than one conformation.

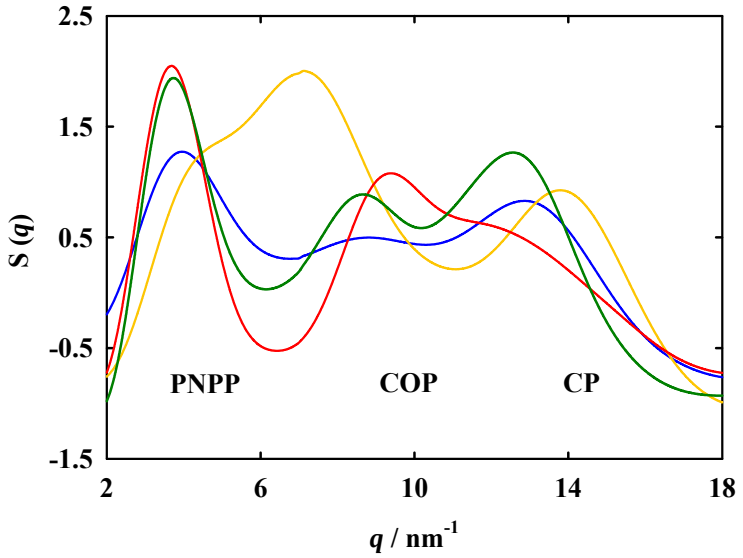

Figure 2.8. Structure factor functions, $S(q)$, of $[C_6C_1Im][C_4F_9SO_3]$ (blue line), $[N_{4444}][C_4F_9SO_3]$ (yellow line), $[C_2C_1py][C_4F_9SO_3]$ (red line) and $[C_4C_1pyr][C_4F_9SO_3]$ (green line), corresponding to FILs with different cations. The low-*q* spectra at the range of $2.0 < q / nm^{-1} < 18.0$ is depicted.

$[C_2C_1py][C_4F_9SO_3]$ shows two well defined peaks at 3.7 and 9.4 nm^{-1}. A flattened shoulder also appears at *q* distances between 11.5 and 13.5 nm^{-1} (**Figure 2.8**, red line). Since the ethyl group of the cation is too small to produce an effective segregation from the polar region,(17) the occurrence of the prominent PNPP must only result from the effective nanosegregation of the perfluoroalkyl chain from the polar moieties. The different sizes of the domains and the inexistent formation of a hydrogenated domain confers asymmetry to the ionic liquid assembling (see **Figure 2.9.c**). It may explain the lower occurrence of different conformations and the decreased melting point, as is depicted in **Table 2.2** and **Figure 2.7.c**.

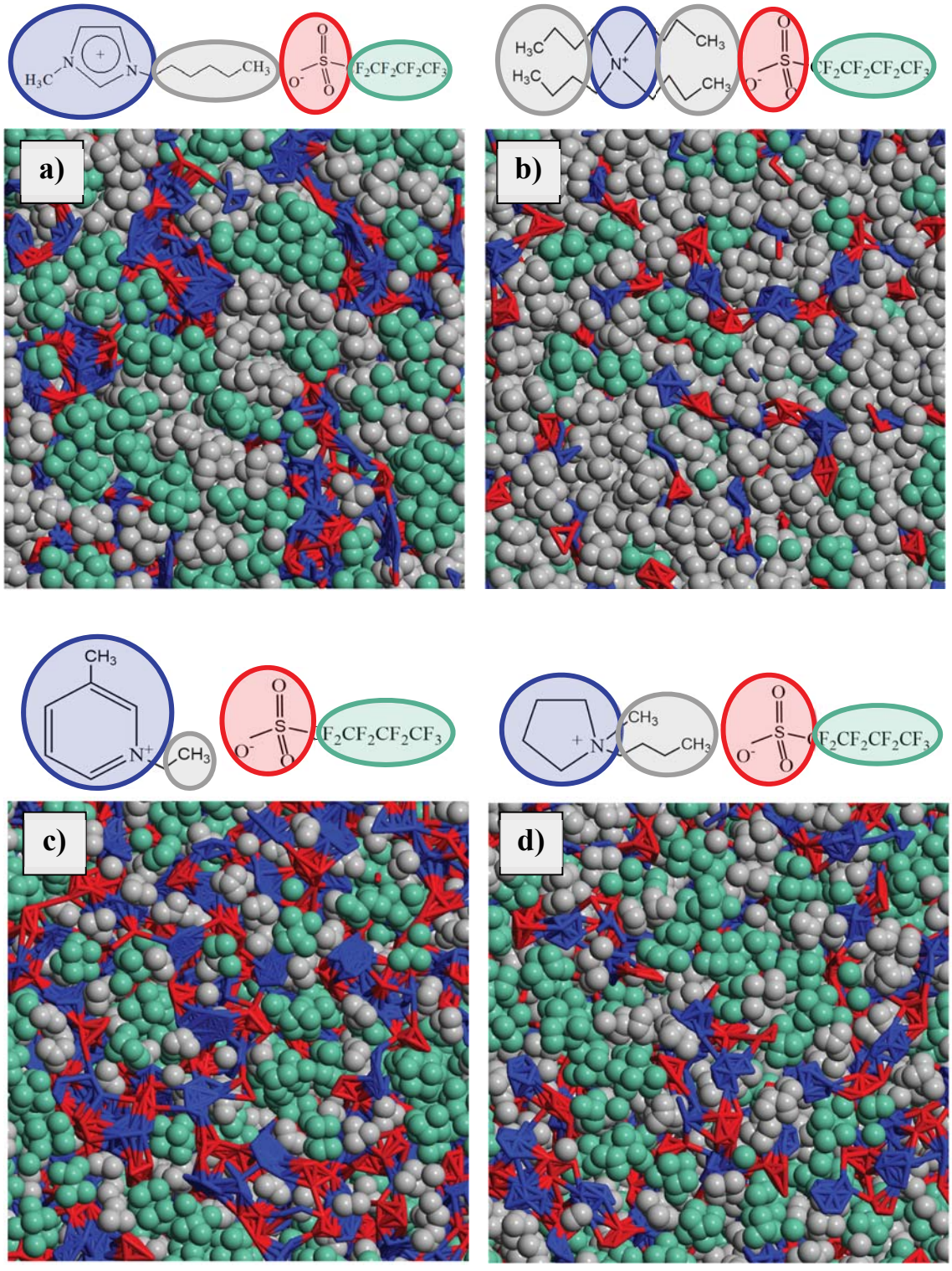

Figure 2.9. MD simulation snapshots for the FILs with different cation type: (a) $[C_6C_1Im][C_4F_9SO_3]$, (b) $[N_{4444}][C_4F_9SO_3]$, (c) $[C_2C_1py][C_4F_9SO_3]$ and (d) $[C_4C_1pyr][C_4F_9SO_3]$. Red (negative charges) and blue (positive charges) segments represent the interactions from the polar network of the two ions, gray space-filled areas represent the domains caused by the hydrogenated side chains while the groups of green spheres illustrate the perfluoroalkyl apolar domains. They are also represented in the structures of each ionic liquid with the corresponded colour.

The FIL based on pyrrolidinium cation, $[C_4C_1pyr][C_4F_9SO_3]$, exhibits three well-defined peaks at *q*-values of 3.7, 8.7 and 12.6 nm^{-1}. Herein, the same aforementioned situation is visible because the butyl chain of the cation is not long enough to yield an effective segregation from the polar cluster.(17) Therefore, the outstanding PNPP that occurs at the low *q*-value is the result of the segregated perfluoroalkyl chain of the anion. In **Figure 2.9.d**, the snapshot of this ionic liquid clearly endorses the segregation of the fluorinated counterparts and the interlocking between the hydrogenated chains and the polar moieties. The effective segregation of the fluorinated chains might contribute to the two solid-solid transitions that are observed in the thermal analysis of this compound (see **Table 2.2** and **Figure 2.7.d**).

2.4.3 Influence of the anion type in the nanostructure of Fluorinated Ionic Liquids

The anion effect on the thermal and structural behaviour of FILs was studied using the pyrrolidinium cation, $[C_4C_1pyr]^+$, combined with perfluorobutanesulfonate, $[C_4F_9SO_3]^-$, or the bis(nonafluorobutylsulfoyl)imide, $[N(C_4F_9SO_2)_2]^-$, anions. A slight increase in melting (**Table 2.2**) and decomposition (**Table 2.3**) temperatures were observed in the case of the $[N(C_4F_9SO_2)_2]^-$ anion. Similarly, the same cation combined with other fluoro-containing anions, shows an increment of the melting temperature in the following order: bis(fluorosulfonyl)imide, bis(trifluoromethanesulfoyl)imide and bis(pentafluoroethanesulfoyl)imide,(37) suggesting an influence of fluorocarbon chain length, and supporting the results. Besides, the thermal stability of the traditional fluoro-containing anions (triflate and bis(trifluoromethylsulfonyl)imide), using the same or analogous cations, is higher due to a decrease of nucleophilicity due to fluor presence.(36) Moreover, the bis(trifluoromethylsulfonyl)imide anion, with a symmetric structure, presents higher thermal stability than the asymmetric $[(FSO_2)N(SO_2C_2F_5)]^-$ anion.(36) $[N(C_4F_9SO_2)_2]^-$ also presents higher symmetry than $[C_4F_9SO_3]^-$ leading to an increased decomposition temperature.

In **Figure 2.10.a**, the ionic liquid based on $[C_4F_9SO_3]^-$ anion shows two solid-solid transitions, at 273.57 and 322.78 K, and the melting occurs at 363.49 K. In the case of the $[N(C_4F_9SO_2)_2]^-$ anion, **Figure 2.10.b** shows three different solid-solid transitions at 256, 275 and 285 K and the melting point occurs at 375 K. The structure of this anion shows symmetrical positions between the two butyl perfluoroalkyl chains while in $[C_4F_9SO_3]^-$ only one butyl fluorinated chain is present (see **Table 2.1**). The asymmetric character of ILs usually causes low melting points due to their difficulty to form crystalline structures.(15) The incorporation of another, identical butyl fluorinated alkyl chain contributes to a higher symmetry. This fact enables the existence of different crystalline conformations, slightly increasing the melting temperature and the occurrence of solid-solid transitions. The structure of bis(trifluoromethanesulfonyl)imide, $[N(CF_3SO_2)_2]^-$, has already been studied for the pyrrolidinium

cation. The flexible nature of this anion and its ability to change between the different conformers have been stated. The pyrrolidinium cation has much more limited conformational behaviour.(38)

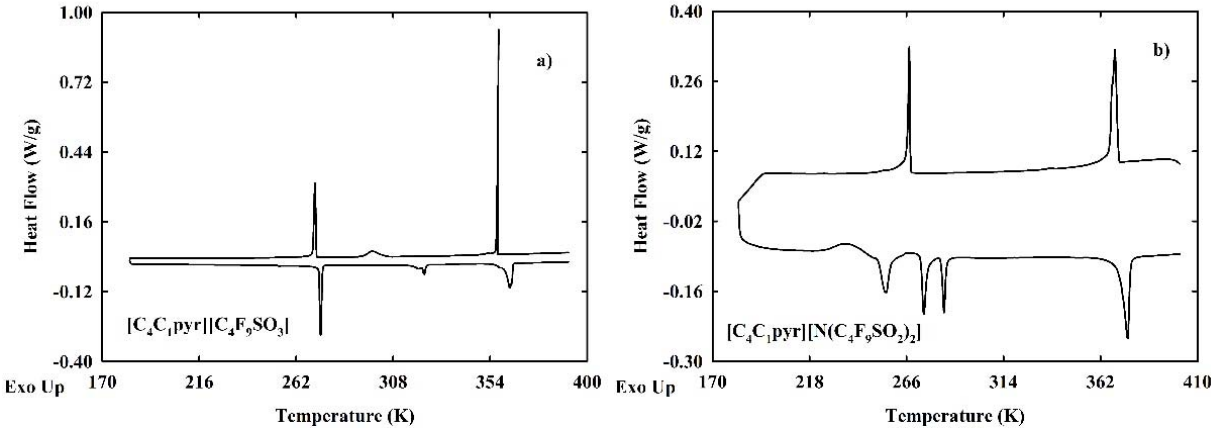

Figure 2.10. Comparison of DSC runs for FILs with different anions: (a) $[C_4C_1pyr][C_4F_9SO_3]$ at a scan rate of 1 $K \cdot min^{-1}$ and (b) $[C_4C_1pyr][N(C_4F_9SO_2)_2]$ at a scan rate of 5 $K \cdot min^{-1}$.

The global structure factors, $S(q)$, for both ionic liquids are depicted in **Figure 2.11** and show three distinct peaks at q-values of 3.7, 8.7 and 12.6 nm^{-1} for $[C_4C_1pyr][C_4F_9SO_3]$ (green line) and 4.1, 7.8 and 12.2 nm^{-1} for $[C_4C_1pyr][N(C_4F_9SO_2)_2]$ (purple line). As mentioned before, the hydrogenated side chain of the $[C_4C_1pyr]^+$ is not bulky enough to yield an efficient segregation among the polar and fluorinated clusters.(17) This means that the PNPP presented by these two FILs (**Figure 2.11**) arises from the contribution of the perfluoroalkyl side chains segregation.

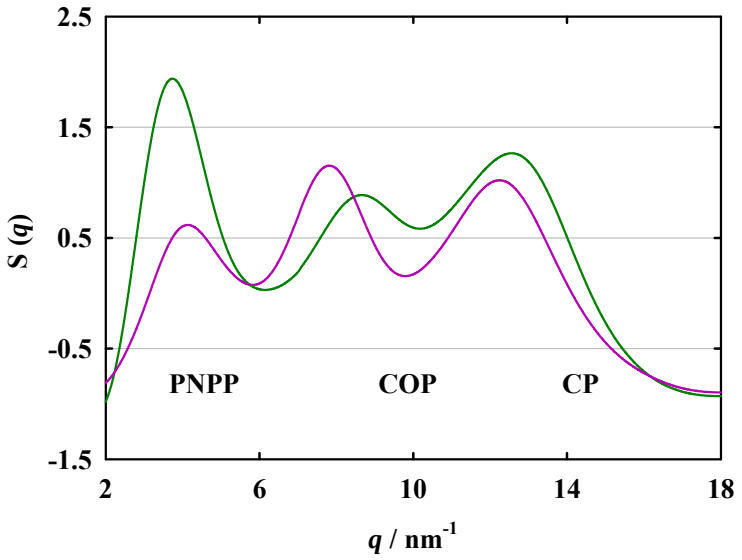

Figure 2.11. Structure factor functions, $S(q)$, $[C_4C_1pyr][C_4F_9SO_3]$ (green line) and $[C_4C_1pyr][N(C_4F_9SO_2)_2]$ (purple line), corresponding to FILs with different anions. The low-q spectra at the range of $2.0 < q / nm^{-1} < 18.0$ is depicted.

In this comparison, the discrete probability distribution functions $P(n_a)$ of apolar aggregates sizes were also obtained and represented in the **Figure 2.12**. In the case of $[C_4C_1pyr][C_4F_9SO_3]$ FIL, the size of the aggregates from the hydrogenated counterparts are very small compared with the fluorinated counterparts. They are not bulky enough to overcome the fluorinated counterparts (see **Figure 2.12.a**). The same is happening in $[C_4C_1pyr][N(C_4F_9SO_2)_2]$ (**Figure 2.12.b**). Comparing the behaviour of the two ionic liquids, two main concerns are noticed: (i) the already small hydrocarbons aggregates actually further reduce their size in the presence of the larger $[N(C_4F_9SO_2)_2]^-$ anion, demonstrating the influence of the anion fluorinated counterparts in the overall molecular organization; (ii) the apolar aggregates from the perfluoroalkyl chains in $[N(C_4F_9SO_2)_2]^-$ are larger, indicating the box percolation, since almost all anions contribute to form one single fluorinated domain. The hydrogenated and fluorinated chains of $[C_4C_1pyr][N(C_4F_9SO_2)_2]$ exhibit opposite trends in terms of clustering. Considering the aggregates in fluorinated chains, there is a continuous fluorinated apolar domain – as attested by the presence of a PNPP in the $S(q)$ functions of all systems.

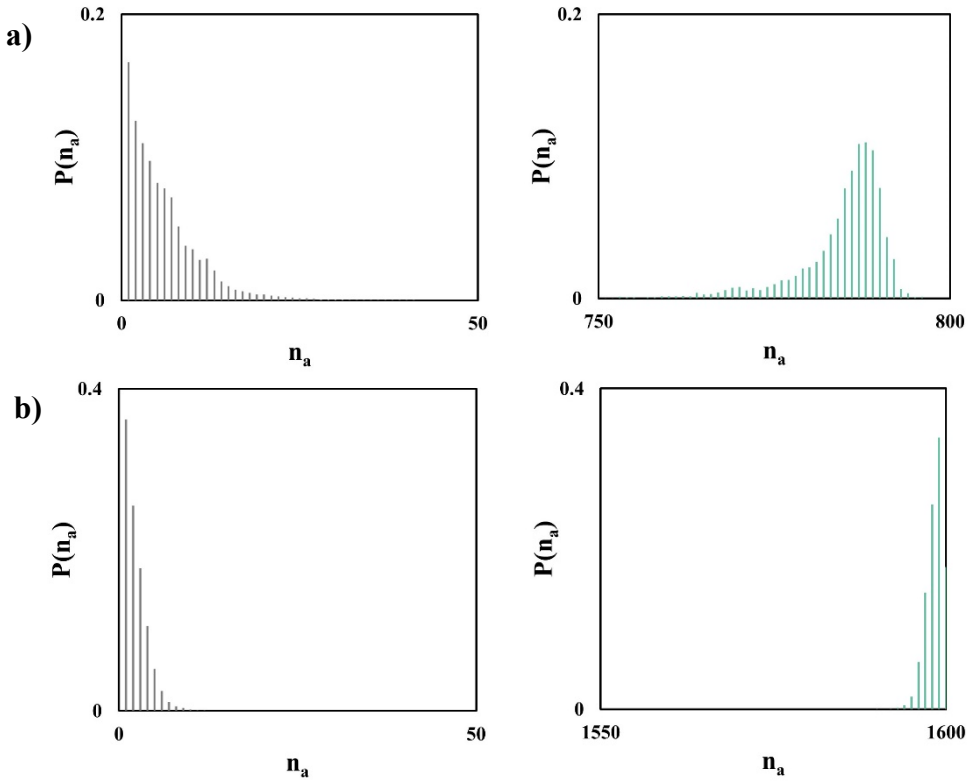

Figure 2.12. Discrete probability distribution functions of apolar aggregate sizes, $P(n_a)$, as function of aggregate size number, n_a, for (a) $[C_4C_1pyr][C_4F_9SO_3]$ and (b) $[C_4C_1pyr][N(C_4F_9SO_2)_2]$.The grey functions corresponds to the hydrocarbon aggregates and the green functions illustrate the fluorocarbon aggregates.

The snapshots of the two ionic liquids (**Figure 2.13**) corroborate the nanosegregation of the fluorinated alkyl side chains. In **Figure 2.13.b**, it is clearly visible that the fluorinated side chains start to aggregate in larger and continuous clusters for the FIL with the $[N(C_4F_9SO_2)_2]^-$ anion, which was also suggested by the cluster sizes $P(n_a)$. This fact might be one of the reasons for the increment of the melting temperature in the bis(nonafluorobutylsulfonyl)imide anion as is illustrated in **Figure 2.10.b** and **Table 2.1**. Furthermore, the outstanding symmetry characteristic of this anion might be important to explain the rich phase behaviour, increasing the number of solid-solid transitions in this FIL.

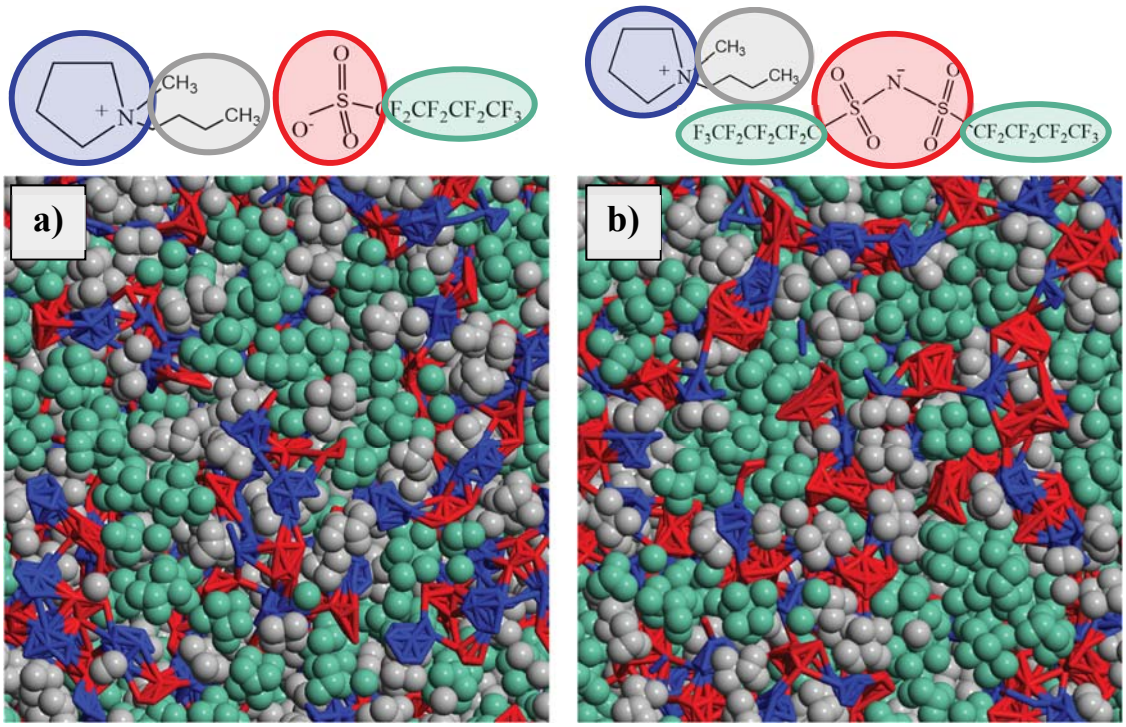

Figure 2.13. MD simulation snapshots for the FILs with different anion types: (a) $[C_4C_1pyr][C_4F_9SO_3]$ and (b) $[C_4C_1pyr][N(C_4F_9SO_2)_2]$. Red (negative charges) and blue (positive charges) segments represent the interactions from the polar network of the two ions, gray space-filled areas represent the domains caused by the hydrogenated side chains while the groups of green spheres illustrate the perfluoroalkyl apolar domains. They are also represented in the structures of each ionic liquid with the corresponded colour.

To understand this peculiar structural feature of the $[N(C_4F_9SO_2)_2]^-$ anion, a conformational analysis was included in this discussion. The structure of this anion, represented in **Figure 2.14.a**, recognizes two symmetrical dihedrals: C1-S1-N-S2 and S1-N-S2-C2, disclosed from the decomposition of the pseudo-dihedral C-S-S-C. The dihedrals are attached to a nitrogen atom that introduces an extra degree of freedom to the molecule, allowing the rotation of the dihedral angles relative to each other. Therefore, the dihedral distribution functions (**Figure 2.15**) and the potential energy surface (PES) (**Figure 2.16**) will be discussed in order to understand how this structural component might confer to the anion a remarkable flexibility. Additionally, the bis(trifluoromethanesulfonyl)imide and the

bis(fluorosulfonyl)imide anions, that were previously described,(38,39) are also used for comparison purposes.

The dihedral distribution functions for: (i) the central pseudo-dihedral angles of the bis(nonafluorobutylsulfonyl)imide, $[N(C_4F_9SO_2)_2]^-$ (**Figure 2.14.a)**; (ii) bis(trifluoromethanesulfonyl)imide, $[N(CF_3SO_2)_2]^-$ (**Figure 2.14.b**) and (iii) bis(fluorosulfonyl)imide, $[N(FSO_2)_2]^-$ (**Figure 2.14.c**), anions are shown in **Figure 2.15**. The atomic nomenclature used to define such pseudo-dihedral angles is shown in the **Figure 2.14.a to 2.14.c**. The population histogram as a function of the FSSF dihedral angle shows two peaks, one around 0º corresponding to the *cis* conformers and the other around 120º that corresponding to the *trans* conformers. In the other two anions, it is clear two main conformers around 40º and 180º that correspond to the conformers of group symmetry C1 (*gauche*) and C2 (*anti*), respectively (**Figure 2.16**).

Those results clearly show the possibility of the coexistence of the two main conformers of the $[N(FSO_2)_2]^-$ anion (*cis* and *trans* conformers) in the simulated liquid phase of $[C_2C_1Im][N(FSO_2)_2]$ and the two main conformers of the $[N(C_4F_9SO_2)_2]^-$ and $[N(CF_3SO_2)_2]^-$ anions (*anti* and *gauche*) in the simulated liquid phase of $[C_4C_1pyr][N(C_4F_9SO_2)_2]$ and $[C_4C_1Im][N(CF_3SO_2)_2]$, respectively. The $[N(FSO_2)_2]^-$ exhibits only rather different conformers (*cis* and *trans*) when compared with $[N(C_4F_9SO_2)_2]^-$ and $[N(CF_3SO_2)_2]^-$ anions (*anti* and *gauche*). The comparison between the $[N(C_4F_9SO_2)_2]^-$ anion with the $[N(CF_3SO_2)_2]^-$ anion shows that the main difference is observed around 70 and 140º where the $[N(C_4F_9SO_2)_2]^-$ distribution shows new possible conformers that are not presented in $[N(CF_3SO_2)_2]^-$ anion. Nevertheless, they still do not occur as much as the *gauche* and *anti* conformers do. It is also clear an increased probability of the *gauche* conformer in $[N(C_4F_9SO_2)_2]^-$ anion probably related to the fact that the larger C_4F_9 groups tend to be as far as possible from the charged centre of the molecule.

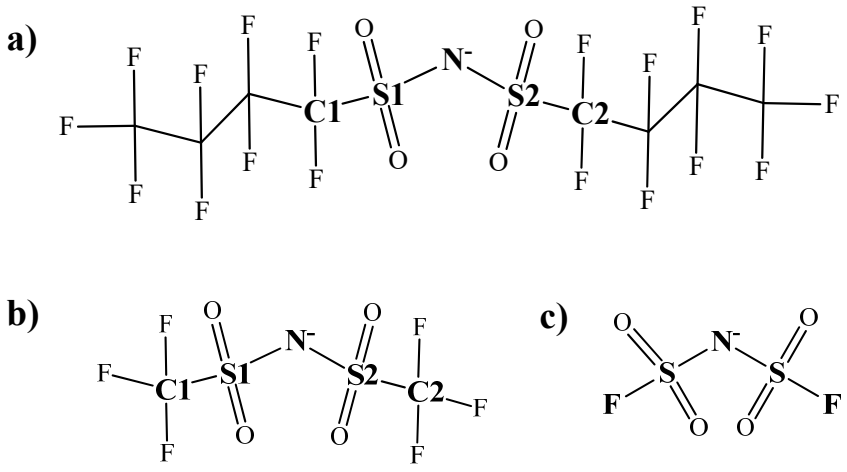

Figure 2.14. Atomic nomenclature used for the definition of pseudo-dihedral angles to a) $[N(C_4F_9SO_2)_2]^-$; b) $[N(CF_3SO_2)_2]^-$ and c) $[N[FSO_2)_2]^-$ anions. The nomenclature used for $[N(CF_3SO_2)_2]^-$ anion is the same as the use for the $[N(C_4F_9SO_2)_2]^-$ anion.

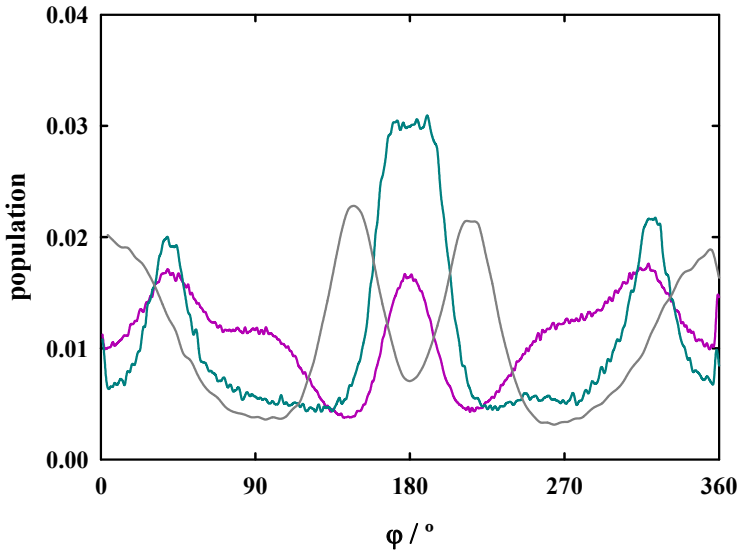

Figure 2.15. Pseudo-dihedral occurrence distribution functions for $[C_4C_1Im][N(CF_3SO_2)_2]$ (CSSC dihedral, dark cyan line); $[C_4C_1pyr][N(C_4F_9SO_2)_2]$ (CSSC dihedral, purple line) and $[C_2C_1Im][N(FSO_2)_2]$ (FSSF dihedral, grey line). All dihedral analyses were obtained from simulation data at 300 K.

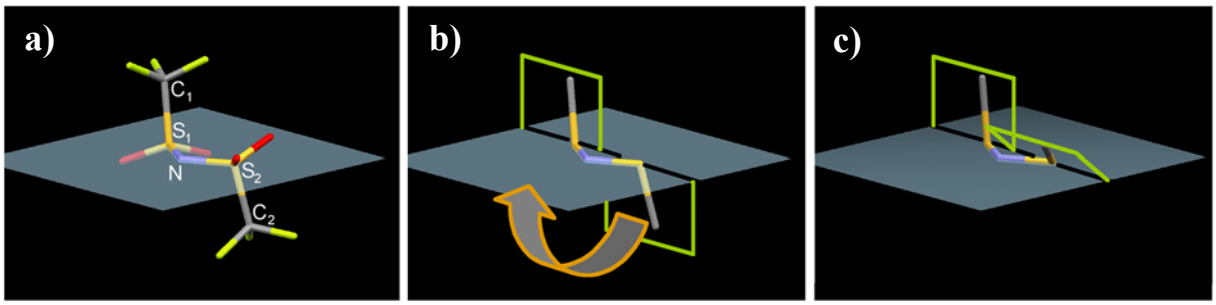

Figure 2.16. a) Representation of the CSSC pseudo-dihedral (which is shared by the $[N(C_4F_9SO_2)_2]^-$ and $[N(CF_3SO_2)_2]^-$ anions) showing the atoms and the S-N-S plane of the dihedral; b) The C1 conformer (*anti*) of the dihedral. The arrow shows the rotation of the S1-N-S2-C2 dihedral angle to yield c) C2 conformer (*gauche*). Adapted from reference (38).

If one needs to calculate the paths of interconversion between the different conformations of the $[N(C_4F_9SO_2)_2]^-$ anion, the two C1-S1-N-S2 and S1-N-S2-C2 dihedrals must be used, since that the C1-S1-S2-C2 is not a proper dihedral. The potential energy surface (PES) of the two symmetrical dihedrals is far from simple because of the extra degree of freedom introduced by the possibility of rotation of the dihedral angles relative to each other. **Figure 2.17** shows the torsion energy profile of the $[N(C_4F_9SO_2)_2]^-$ anion. It is important to note the existence of a reasonably high energy barrier (around 60 kJ/mol) as the CSNS dihedral angles approach 0º. The strong correlation between the two dihedrals makes the mapping highly dependent on the value of the second dihedral angle. The C1 and C2 conformers based on the composite dihedral angle C-S-S-C can be rationalized: (i) when the first C-S-N-S proper dihedral angles are 90º and the second 270°, one obtains the "*anti*" C1 conformer (**Figure**

2.16.b); (ii) when those one is at 90° and the other at 130° (or 270 and 230°), one obtains the "*gauche*" C2 conformer (**Figure 2.16.c**). It must be noted that, due to the presence of the nitrogen atom, each conformer has a mirror image elevating to four the number of main conformers of the molecule (two *gauche*, two *anti*). On the other hand, the 3D surface plot presents the four conformers of the anion, with each *anti* conformer (the round basin) surrounded by the *gauche* conformer (the elongated pools).

From the PES presented in **Figure 2.17,** it is observed that an energy barrier of ca. 12 kJ/mol lies between the two conformer populations, the *anti* and the *gauche*. As previously observed for bis(trifluoromethanesulfonyl)imide,(38) the conformer interconversion is possible by the rotation of the torsion angle in only one direction, corresponding to the path throughout the central island. The energetics of interconversion between the two anions present two major differences: (i) the energy barrier for the $[N(C_4F_9SO_2)_2]^-$ anion is higher than that for bis(trifluoromethanesulfonyl)imide (8 kJ/mol); and (ii) for the $[N(C_4F_9SO_2)_2]^-$ anion a wider torsion angle distribution around the *gauche* conformer was found.

To sum up, the presence of the two main conformers in the liquid phase are almost in the same proportion and the other conformers gives to the $[N(C_4F_9SO_2)_2]^-$ anion higher flexibility. This means that, during the crystallization process, the molecules are able to adopt the conformation that best fits the crystal structure. These evidences, herein discussed, possibly justify the high number of phase transitions shown in the thermal analysis (see **Figure 2.10.b** and **Table 2.1**) because the enhanced flexibility of this anion permits its rearrangement in different conformations when the FIL crystallizes.

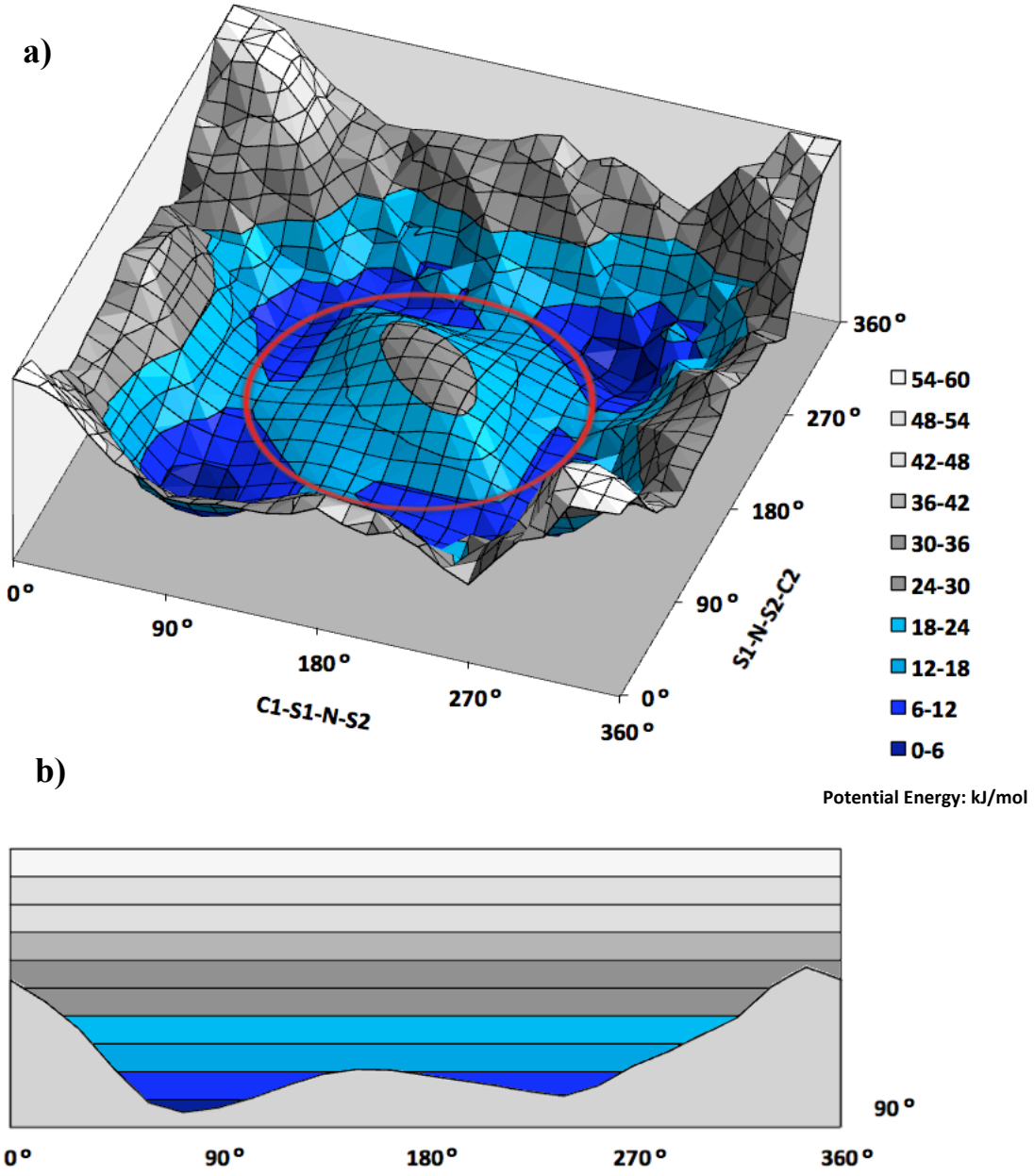

Figure 2.17. a) Potential energy profile (PES) (kJ/mol) of $[N(C_4F_9SO_2)_2]^-$ as a function of the two SNSC dihedral angles. b) PES of $[N(C_4F_9SO_2)_2]^-$ with one of the dihedral set to 90º. The areas shaded in dark blue represent the location of the two main conformers (basins), *gauche* and *anti* conformers and the light blue the interconversion path between them.

2.5 Conclusions

In this chapter, a complete thermodynamic characterization of several FILs was carried out. A combined study of the thermal properties (melting, solid-solid transitions and decomposition temperatures) and structural features (structure factors, aggregation and dihedral analysis) of the fluorinated ionic liquids were achieved. The FILs studied in this work show rich phase transition scenario and suggest that the formation of a third nanosegregated domain enhances the formation of multiple types of crystals, classifying them as highly nanostructured compounds. It was shown that the interplay between the three domains is highly influenced by varying the hydrogenated alkyl side chain length, cation and anion type. These facts allow the fluorinated ionic liquids to assume different conformations, making them flexible, adaptable and thermal stable molecules. Otherwise, the relationship between the two apolar domains segregation (fluorinated and hydrogenated) is the most variable structural feature that affects the nanostructured nature of these compounds.

In conclusion, the FIL with the best thermal and structural properties, to be used in the biomedical application herein studied, is the $[C_2C_1py][C_4F_9SO_3]$. This FIL presents the highest thermal stability with a melting point below the human body temperature average. However, $[C_2C_1py][C_4F_9SO_3]$ is not one of the most nanostructured ionic liquids.

The highly nanostructure nature of these compounds, that is improved by the addition of the fluorinated counterpart, can be responsible to enhance the accommodation of solutes such as respiratory gases or biomolecules. The strong tendency to self-assemble forming continuous and supramolecular structures and the versatility to rearrange in several conformational features may permit the built of stable micelles, vesicles, tubules and other colloidal systems. This fact makes them great candidates to form emulsions and microemulsions to use in biomedical applications such as respiratory gas carriers.

As mentioned before, it is essential to perform a global and complete study of all the possible structural features to understand the behaviour of this type of compounds. Therefore, this work can be considered a screening on the phase and structural behaviour of these novel FILs in order to find out and develop the best compounds to apply not only in the biomedical research but also in other fields where the FILs are suitable and advantageous.

This overall structural characterization turned out to be incredibly advantageous to make possible the design of novel compounds. This information increases the biocompatibility properties of these compounds due to the knowledge herein obtained about some of the possible combinations of anions and cations. For that, is still necessary to study the biological aspects, such as the biocompatibility and biodegradation of these FILs, to make the appropriated choices regarding the physicochemical and biological criteria for *in vivo* artificial oxygen carrier.

2.6 References

(1) Krafft, M. P. Fluorocarbons and Fluorinated Amphililes in Drug Delivery and Biomedical. *Adv Drug Deliv Rev*. **2001**, 47, 209-288.

(2) Triolo, A.; Russina, O.; Bleif H.-J.; Di Cola, E. Nanoscale Segregation in Room Temperature Ionic Liquids. *J Phys Chem B*. **2007**, 111, 4641-4644.

(3) Shimizu, K.; Costa Gomes, M. F.; Pádua, A. A. H.; Rebelo, L. P. N.; Canongia Lopes, J. N. Three Commentaries on The Nano-Segregated Structure of Ionic Liquids. *THEOCHEM*, **2010**, 946, 70-76.

(4) Greaves, T. L.; Kennedy, D. F.; Mudie, S. T.; Drummond, C. J. Diversity Observed in the Nanostructure of Protic Ionic Liquids. *J Phys Chem B*. **2010**, 114, 10022-10031.

(5) Canongia Lopes, J. N.; Pádua, A. A. H. Nanostructural Organization in Ionic Liquids. *J Phys Chem B*. **2006**, 110, 3330-3335.

(6) Hayes, R.; Warr, G. G.; Atkin, R. Structure and Nanostructure in Ionic Liquids. *Chem Rev*. **2015**, 115, 6357-6426.

(7) Freitas, A. A.; Shimizu, K.; Canongia Lopes, J. N. Complex Structure of Ionic Liquids. Molecular Dynamics Studies with Different Cation–Anion Combinations. *J Chem Eng Data*. **2014**, 59, 3120-3129.

(8) Shen, Y.; Kennedy, D. F.; Greaves, T. L.; Weerawardena, A.; Mulder, R. J.; Kirby, N.; Song, G.; Drummond, C. J. Protic Ionic Liquids with Fluorous Anions: Physicochemical Properties and Self-Assembly Nanostructure. *Phys Chem Chem Phys*. **2012**,14, 7981-7992

(9) Almantariotis, D.; Gefflaut, T.; Pádua, A. A. H.; Coxam J.-Y., Gomes M. F. C. Effect of Fluorination and Size of The Alkyl Side-Chain on the Solubility of Carbon Dioxide in 1-Alkyl-3-Methylimidazolium Bis(trifluoromethylsulfonyl)amide Ionic Liquids. *J Phys Chem B.* **2010**, 114, 3608-3617.

(10) Pereiro, A. B.; Pastoriza-Gallego, M. J.; Shimizu, K.; Marrucho, I. M.; Lopes, J. N. C.; Piñeiro, M. M.; Rebelo, L. P. N. On the Formation of a Third, Nanostructured Domain in Ionic Liquids. *J Phys Chem B*. **2013**, 117, 10826-10833.

(11) Castiglione, F.; Moreno, M.; Raos, G.; Famulari, A.; Mele, A.; Appetecchi, G. B.; Passerini, S. Structural Organization and Transport Properties of Novel Pyrrolidinium-Based Ionic Liquids with Perfluoroalkyl Sulfonylimide Anions. *J Phys Chem B*. **2009**, 113, 10750-10759.

(12) Hollóczki, O.; Macchiagodena, M.; Weber, H.; Thomas, M.; Brehm, M.; Stark, A.; Russina, O.; Triolo, A.; Kirchner, B. Triphilic Ionic-Liquid Mixtures: Fluorinated and Non-Fluorinated Aprotic Ionic-Liquid Mixtures. *ChemPhysChem*. **2015**, 16, 3325-3333.

(13) Russina, O.; Lo Celso, F.; Di Michiel, M.; Passerini, S.; Appetecchi, G. B.; Castiglione, F.; Mele, A.; Caminiti, R.; Triolo, A. Mesoscopic Structural Organization in Triphilic Room Temperature Ionic Liquids. *Faraday Discuss*. **2013**, 167, 499-513.

(14) Shimizu, K.; Freitas A. A.; Canongia Lopes, J. N. Structural Characterization of the $[C_nC_1im][C_4F_9SO_3]$ Ionic Liquid Series: Alkyl versus Perfluoroalkyl Side Chains. *J Mol Liq*. **2016**, http://dx.doi.org/10.1016/j.molliq.2016.08.014

(15) Luczak, J.; Paszkiewicz, M.; Krukowska, A.; Malankowska, A.; Zaleska-Medynska, A. Ionic Lquids for Nano- and Microstructures Preparation. Part 1: Properties and Multifunctional Role. *Adv Colloid Interface Sci*. **2016**, 230, 13-28.

(16) Pereiro, A. B.; Araújo, J. M. M.; Martinho, S.; Alves, F.; Nunes, S.; Matias, A.; Duarte, C. M. M.; Rebelo, L. P. N.; Marrucho, I. M. Fluorinated Ionic Liquids: Properties and Applications. *ACS Sustainable Chem. Eng.* **2013**, 1, 427-439.

(17) Vieira, N. S. M.; Reis, P. M.; Shimizu, K.; Cortes, O. A.; Marrucho, I. M.; Araújo, J. M. M.; Esperança, J. M. S. S.; Canongia Lopes, J. N.; Pereiro, A. B.; Rebelo, L. P. N. A Thermophysical and Structural Characterization of Ionic Liquids with Alkyl and Perfluoroalkyl Side Chains. *RSC Adv*. **2015**, 5, 65337-65350.

(18) Aguirre, C. L.; Cisternas, L. A.; Valderrama, J. O. Melting-Point Estimation of Ionic Liquids by a Group Contribution Method. *Int J Thermophys*. **2012**; 33, 34-46.

(19) Wasserscheid, P.; Welton, T. Electrodeposition in Ionic Liquids Green Chemistry and Catalysis Microwaves in Organic Synthesis Second, Completely Revised and Enlarged Edition. *Weinheim: Wiley-Vch.* **2008**

(20) Canongia Lopes, J. N.; Deschamps, J.; Pádua, A. A. H. Modeling Ionic Liquids Using a Systematic All-Atom Force Field. *J Phys Chem B*. **2004**, 108, 2038-2047.

(21) Lopes, J. N. C.; Pádua, A. A. H. Molecular Force Field for Ionic Liquids Composed of Triflate or Bistriflylimide Anions. *J Phys Chem B*. **2004**; 108, 16893-16898.

(22) Canongia Lopes, J. N.; Pádua, A. A. H. A Generic and Systematic Force Field for Ionic Liquids Modeling. *Theor Chem Acc*. **2012**, 131, 1-11.

(23) Jorgensen, W. L.; Maxwell, D. S.; Tirado-Rives, J. Development and Testing of the OLPS All-Atom Force Field on Conformational Energetics and Properties of Organic Liquids. *J Am Chem Soc*. **1996**, 118, 11225-11236.

(24) Todorov, I.; Smith, W.; Cheshire, U. The DL POLY 4 User Manual. *STFC Daresbury*. **2011**

(25) Shimizu, K.; Bernardes, C. A. S.; Triolo, A.; Canongia Lopes, J. N. Nano-segregation in Ionic Liquids: Scorpions and Vanishing Chains. *Phys Chem Chem Phys*. **2013**, 15, 16256-16262.

(26) Brown, P. J.; Fox, A. G.; Maslen, E. N.; O'Keefe, M. A.; Willis, T. M. International Tables for Crystallography, Ed. E. Prince, *International Union of Crystallography: Dordrecht*, **2004**, C, 554-595.

(27) Lorch, E. *J. Phys. C: Solid State Phys*., **1969**, 2, 229-237.

(28) Shimizu, K.; Bernardes, C. E. S.; Canongia Lopes, J. N. Structure and Aggregation in the 1-Alkyl-3-Methylimidazolium Bis(trifluoromethylsulfonyl)imide Ionic Liquid Homologous Series. *J. Phys. Chem. B*. **2014**, 118, 567-576.

(29) Bernardes, C. E. S.; Minas Da Piedade, M. E.; Canongia Lopes, J. N. The Structure of Aqueous Solutions of a Hydrophilic Ionic Liquid: The Full Concentration Range of 1-Ethyl-3-Methylimidazolium Ethylsulfate and Water. *J Phys Chem B*, **2011**, 115, 2067-2074.

(30) Becke, A. D. Density-Functional Thermochemistry. III. The Role of Exact Exchange. *J Chem Phys* **1993**, 98, 5648-5652.

(31) Frisch, M. J.; Trucks, G. W.; Schlegel, H. B.; Scuseria, G. E.; Robb, M. A.; Cheeseman, J. A.; Montgomery, J. A.; Vreven, T.; Kudin, K. N.; Burant, J. C. et al. Gaussian 03, Revision B.04. *Pittsburgh PA: Gaussian*, *Inc*. **2003**.

(32) Vieira, N. S. M.; Luís, A.; Reis, P. M.; Carvalho, P. J.; Lopes-Da-Silva, J. A.; Esperança, J. M. S. S.; Araújo, J. M. M.; Rebelo, L. P. N.; Freire, M. G.; Pereiro, A. B. Fluorination Effects on the Thermodynamic, Thermophysical and Surface Properties of Ionic Liquids. *J Chem Thermodyn.* **2016**; 97, 354-361.

(33) Hughes, T. J.; Syed, T.; Graham, B. F.; Marsh, K. N.; May, E. F. Heat Capacities and Low Temperature Thermal Transitions of 1-Hexyl and 1-Octyl-3-methylimidazolium bis(trifluoromethylsulfonyl)amide. *J. Chem. Eng. Data.* **2011**, 56, 2153-2159.

(34) Verevkin, S. P.; Zaitsau, D. H.; Emel, V. N.; Ralys, R. V.; Yermalayeu, A. V.; Schick, C. Does Alkyl Chain Length Really Matter? Structure – Property Relationships in Thermochemistry of Ionic Liquids. *Thermochim Acta*. **2013**; 562, 84-95

(35) Papaiconomou, N.; Yakelis, N.; Salminen, J.; Bergman, R.; Prausnitz, J. M. Synthesis and Properties of Seven Ionic Liquids Containing 1-Methyl-3-Octylimidazolium or 1-Butyl-4-Methylpyridinium Cations. *J Chem Eng Data*. **2006**; 51, 1389-1393.

(36) Maton, C.; De Vos, N.; Stevens, C. V. Ionic Liquid Thermal Stabilities: Decomposition Mechanisms and Analysis Tools. *Chem Soc Rev.* **2013**, 42, 5963-5977.

(37) Kunze, M.; Jeong, S.; Paillard, E.; Winter, M.; Passerini, S. Melting Behavior of Pyrrolidinium-Based Ionic Liquids and Their Binary Mixtures. *J Phys Chem C*. **2010**, 114, 12364-12369.

(38) Canongia Lopes, J. N.; Shimizu, K.; Pádua, A. A. H; Umebayashi, Y.; Fukoda, S.; Fujii, K.; Ishiguro, S.-I. A Tale of Two Ions: The Conformational Landscapes of Bis(trifluoromethanesulfonyl)amide and N,N-dialkylpyrrolidinium. *J Phys Chem B*. **2008**, 112, 1465-1472.

(39) Canongia Lopes, J. N.; Shimizu, K.; Pádua, A. A. H.; Umebayashi, Y.; Fukuda, S.; Fujii K.; Ishiguro, S.-I. Potential Energy Landscape of Bis(fluorosulfonyl)amide. *J Phys Chem B*. **2008**, 112, 9449-9455.

3. Solubility of Respiratory Gases in Fluorinated Ionic Liquids

3.1 Introduction

The constant requirement to understand the physico-chemical properties and thermodynamic behaviour of ILs is one of the major limitations of the investigation concerning these compounds, hindering their use in a wide range of applications. Furthermore, the huge possibilities to combine different cations and anions amplifies this lack of information, making urgent the development of reliable, faster and economical methods to expand the available data.

Models using empirical (methods derived through regressions) and theoretical (methods based on predictive calculations) approaches have been developed to characterize the thermodynamic properties of ionic liquids in a systematic way.(1–3) However, it is necessary to evaluate which it is the best applicable and reliable method to characterize specific properties.

The implementation of equations of state (EoS) as a modelling method has been revealed as an outstanding tool. However, more complex theoretical approaches, such as molecular simulations, have an important role in the study of ionic liquids thermodynamic properties.(4–6) The complexity of these molecules limits the predictive capabilities of the theoretical approaches, while molecular simulations are time-consuming.

The Statistical Associating Fluid Theory (SAFT) (7–9) is an EoS developed by Chapman *at al* which has received considerable attention because it is able to predict and reproduce experimental data to describe the thermophysical properties of pure ILs and their mixtures.(10–15) This well-known theory was developed based on the Wertheim's perturbation theory for associating fluids. The different contributions to the free energy can be explicitly separated in the thermodynamic potential functions. In this sense, it is straightforward to obtain the different microscopic contributions and relate them to the macroscopic properties of the fluid. This is means that the SAFT model not only describes the molecules as simpler, hard-sphere monomers but also takes into account the molecular shape and molecular association.(16–19) The SAFT approach has become a very useful tool to describe the behaviour of complex systems and for designing purposes. Several refined versions have appeared since its development, (7,9) most of them differing in the term used for the reference fluid.

In this chapter, the Soft Statistical Associating Fluid Theory Equation of State (soft-SAFT EoS), (20,21) which is an accurate version of SAFT, was used to obtain insights into the solubility of respiratory gases in the selected FILs. This approach is characterized by the relatively simple models for the estimation and prediction of the thermophysical properties and phase behaviour of ionic liquids and their mixtures. It has been providing several reliable results, using a minimum amount of experimental information and a high degree of accuracy and transferability. It can describe pure ILs

density, transport, interfacial and derivative properties and phase equilibria of their mixtures with water, gases, and also with other ILs.(10,22–26). The soft-SAFT EoS methodology and the molecular models are further described.

3.2 Soft Statistical Associating Fluid Theory Equation of State (soft-SAFT EoS)

3.2.1. Theory

The soft-SAFT EoS (20,21) is an accurate version of SAFT equation.(7,8) This version is characterized by use of a Lennard-Jones (LJ) intermolecular potential as the reference term where the repulsive and dispersive contributions of the monomers that constitute the chain are taken into account simultaneously. This equation of state, as all other versions of SAFT, is based on the first order thermodynamic perturbation theory (TPT1) of Wertheim.(16–19) It is written in terms of the residual Helmholtz free energy where the total free energy of the system is the sum of different microscopic contributions:

$$a^{\mathrm{res}} = a - a^{\mathrm{id}} = a^{\mathrm{ref}} + a^{\mathrm{chain}} + a^{\mathrm{assoc}} + a^{\mathrm{polar}} \quad \textbf{(1)}$$

where a^{res} is the residual Helmholtz free energy and a^{id} corresponds to the ideal contribution. Subsequently, a^{ref} is used as reference, a^{chain} as chain, a^{assoc} as association and a^{polar} as polar terms which refer to the residual contributions to the free energy due to the monomer-monomer repulsive and attractive (dispersion) interactions, to the formation of chains, to site-site intermolecular association, and to the polar interactions, respectively.

In the soft-SAFT EoS, the reference term is a Lennard Jones (LJ) spherical fluid which takes into account the repulsive and attractive interactions of the monomers that constitute the chain. The reference/LJ term includes two molecular parameters that identify the monomer: the segment diameter, $\sigma_{ii} = \sigma$, and the dispersive energy between segments, $\varepsilon_{ii}/k_B = \varepsilon/k_B$. The accurate EoS of Johnson *et al*.(27) is used here to calculate the contribution of the reference term.

The extension of the equation to mixtures is performed by applying the van der Waals one-fluid theory with the modified Lorentz-Berthelot combining rules:

$$\sigma_{ij} = \eta_{ij}\left(\frac{\sigma_{ii} + \sigma_{jj}}{2}\right) \quad \textbf{(2)}$$

$$\varepsilon_{ij} = \xi_{ij} \left(\varepsilon_{ii}\varepsilon_{jj}\right)^{1/2} \quad \textbf{(3)}$$

where η_{ij} and ξ_{ij} are the size and energy binary parameters, respectively, accounting for size and energy asymmetries between the different compounds in the mixture. These values become unity when the equation is used in a predictive approach, from pure component parameters. However, ξ_{ij} is fitted, when necessary, to phase equilibrium binary data.

Regarding the chain and association terms of the equation, they derive directly from the Weirthem's first-order thermodynamic perturbation theory (TPT1):

$$a^{\text{chain}} = \rho k_B T \sum_i x_i (1 - m_i) \ln g_{LJ} \quad \textbf{(4)}$$

$$a^{\text{assoc}} = \rho k_B T \sum_i x_i \sum_\alpha \left(\ln X_i^\alpha - \frac{X_i^\alpha}{2} \right) + \frac{M_i}{2} \quad \textbf{(5)}$$

where ρ is the molecular density of the system, k_B the Boltzmann constant, T the temperature, x_i the molar fraction of component i, and $m_i$the chain length. The function was fitted to computer simulation data using $g_{LJ}^{ii}(\sigma_{ii})$ as a function of density and temperature, provided by Johnson *et al*.(28) X_i^α is the fraction of pure component i not bonded at sites of type α and M_i is the number of association sites of type α on component i. X_i^α is given by:

$$X_i^\alpha = \frac{1}{1 + N_{\text{avog}} \rho \sum_j x_j \sum_\beta X_j^\beta \Delta_{\alpha\beta,ij}} \quad \textbf{(6)}$$

The specific site-site function, $\Delta_{\alpha\beta,ij}$, can be described as:(9)

$$\Delta_{\alpha\beta,ij} = K_{\alpha\beta,ij} f_{\alpha\beta,ij} g_{LJ}^{ij} \quad \textbf{(7)}$$

where $K_{\alpha\beta,ij}$ is related to the site-site bonding volume of association and the Mayer f-function:

$$f_{\alpha\beta,ij} = \left[\exp\left(\frac{\varepsilon_{\alpha\beta,ij}^{HB}}{k_B T} \right) - 1 \right] \quad \textbf{(8)}$$

The Mayer function includes the site-site association energy parameter, $\varepsilon_{\alpha\beta,ij}^{HB}/k_B$.

The multipolar term for fluids of linear symmetrical molecules, such as CO_2 and N_2, is of interest for this work and accounts for the quadrupole−quadrupole interactions. This term is obtained using an extension of the theory of Gubbins and Twu (29) (originally developed for spherical molecules) to chain fluids, following the ideas of Jog *et al.*(30) This methodology is based on a perturbative approach of the Helmholtz free energy density due to the polarity effects. The free energy is expanded in a series of terms, written with the Padé approximation:(31)

$$a^{qq} = a_2^{qq}\left(1 - \frac{a_3^{qq}}{a_2^{qq}}\right)^{-1} \quad \textbf{(9)}$$

where $a_2^{qq}$is the second-order term in the perturbation expansion, and $a_3^{qq}$is the third-order term. Expressions for a_2^{qq} and a_3^{qq} were obtained for an arbitrary intermolecular reference potential and involve state variables, molecular parameters, and the integral *J* for the reference fluid.(29) The previous expressions include the quadrupole moment, Q_i, of the molecule. Moreover, the extension to chain fluids assumes that the polar moments are well-localized on certain segments of the chain.(30) As a consequence, a fraction x_{pi} is defined as the fraction of the molecule affected by the quadrupole.

The calculation of interfacial properties has been performed by coupling the soft-SAFT equation with the density gradient theory (DGT) originally proposed by van der Waals (32) and rediscovered by Cahn and Hilliard.(33) The expression for the Helmholtz energy of the system is given by:

$$A = \int \left[a_0(\rho) + \sum_i \sum_j \frac{1}{2} c_{ij} \nabla\rho_i \nabla\rho_j \right] d^3r \quad \textbf{(10)}$$

where $a_0(\rho)$ is the Helmholtz free energy density of the homogeneous fluid at the local density ρ and ρ_i is the molar density of component *i*. The parameter c_{ij} for the components *i* and *j* is known as the influence parameter which is assumed to be temperature independent. Its value is normally obtained by fitting to interfacial tension experimental data.

Considering a planar interface and assuming that the density dependence of the influence parameter can be neglected, an expression that relates the interfacial tension to the square of the density gradient can be derived:(34)

$$\gamma = \sum_i \sum_j \int_{-\infty}^{\infty} c_{ij} \frac{d\rho_i}{dz}\frac{d\rho_j}{dz} dz = 2\int_{-\infty}^{\infty} \left[a_0(\rho) - \sum_i \rho_i \mu_{0i} - p_0 \right] dz \quad \textbf{(11)}$$

where μ_{0i} and p_0 are the equilibrium chemical potential and pressure, respectively, and *z* is the direction perpendicular to the interface.

The viscosity is reproduced using the Free-Volume Theory (FVT) approach of Allal and co-workers (35,36) coupled to soft-SAFT EoS.(37,38) This approach expresses the viscosity η (mPa s) of a system as a sum of a dilute gas term, η_0 (where the intermolecular effects are neglected), and a dense-state correction term, $\Delta\eta$ (related to the density and the microstructure of the fluid). The dilute gas term is obtained using a modification of the Chapman-Enskog kinetic theory proposed by Chung *et al.*:(39)

$$\eta_0 = 40.785 \cdot 10^{-2} \frac{\sqrt{M_w T}}{{v_c}^{2/3} \Omega^*(T^*)} F_c \quad \textbf{(12)}$$

where M_w is the molecular weight (g/mol), v_c is the critical volume (L/mol) and Ω^* is a reduced collision integral, whose expression was calculated for a LJ potential by Neufeld *et al.*(40) Finally, F_c is an empirical factor introduced by Chung *et al.* (39) that includes three different factors accounting for non-sphericity (ω), polarity (μ_r) and hydrogen bonding (κ), respectively.

The dense-state term $\Delta\eta$ is obtained through an expression that relates the viscosity to the microstructure of the fluid. In parallel, this expression is also related to the free space among the molecules, defined as a free-volume fraction through an exponential relation originally proposed by Doolittle.(41) Then, the final expression is:

$$\Delta\eta = L_v(0.1P + 10^{-4}\alpha\rho^2 M_w)\sqrt{\frac{10^{-3}M_w}{3Nk_BT}} \quad \textbf{(13)}$$

$$\times \exp\left[B\left(\frac{10^3 P + \alpha\rho^2 M_w}{\rho N k_B T}\right)^{3/2}\right] \quad \textbf{(14)}$$

The approach includes three parameters related to the structural and energetic properties of the fluid: α (J m^3/mol kg) that describes the proportionality between the energy barrier and the density; B that corresponds to the free-volume overlap; and L_v (Å) that is a length parameter related to the structure of the molecules and the characteristic relaxation time. These parameters are fitted to available experimental viscosity data and related to the molecular weight of members of the same chemical family. The thermodynamic variables, such as the pressure P (MPa), the temperature T (K) and the density ρ (mol/L), are obtained from soft-SAFT.

3.2.2. Molecular Models

In order to have an accurate prediction of the thermodynamic properties from a molecular-based EoS, the selection of a reliable and appropriated model that can represent the physical features of the compounds is imperative. In Soft-SAFT EoS, it is necessary to pre-select a molecular model for pure compounds. Non-associating molecules are defined only for three molecular parameters: the chain length, m; the segment diameter, σ and the dispersive energy between the segments, ε/k_B. Linear symmetrical molecules involve two additional molecular parameters: the quadrupolar moment, Q, and the fraction of segments in the chain that contains the quadrupole, x_p. In the case of associating molecules, two more parameters are included to consider the associating interactions in the model: the site-site association energy, $\varepsilon^{\mathrm{HB}}/k_B$; and the site-site bonding-volume of association, K^{HB}.

3.2.2.1. Non-Associating Molecules

In this work, the molecular models of carbon dioxide (CO_2) (42), nitrogen (N_2) (43) and oxygen (O_2) (44) (considered as non-associating molecules) were used. These molecules had been already modeled in the literature with the soft-SAFT EoS.(42–44)

The CO_2 and N_2 were modelled as a LJ chains. Quadrupolar interactions were taken into account with the molecular parameter x_p fixed to 1/3 for CO_2 and 1/2 for N_2 which represents the number of segments in those molecules that may momentarily contain the quadrupole. In the case of O_2 model, the quadrupole moment is not considered.(44) In **Figure 3.1** is represented the schematic representation of the respiratory gases using soft-SAFT molecular models. The values of Q and the respective molecular parameters for the three respiratory gases are summarized in **Table 3.1**.(42–44)

Table 3.1. Molecular weight and molecular parameters of carbon dioxide,(42) nitrogen,(43) oxygen(44) and water(45) used in this work.

	M_w (g/mol)	m	σ (Å)	ε/k_B (K)	ε^{HB}/k_B (K)	K^{HB} (Å^3)	Q (C m^2)	x_p
CO_2	44.01	1.571	3.184	160.2	-	-	4.4×10^{-40}	⅓
N_2	28.01	1.205	3.384	89.16	-	-	1.2×10^{-40}	½
O_2	32.00	1.168	3.198	111.5	-	-	-	-
H_2O	18.01	1.000	3.154	365.0	2388	2932	-	-

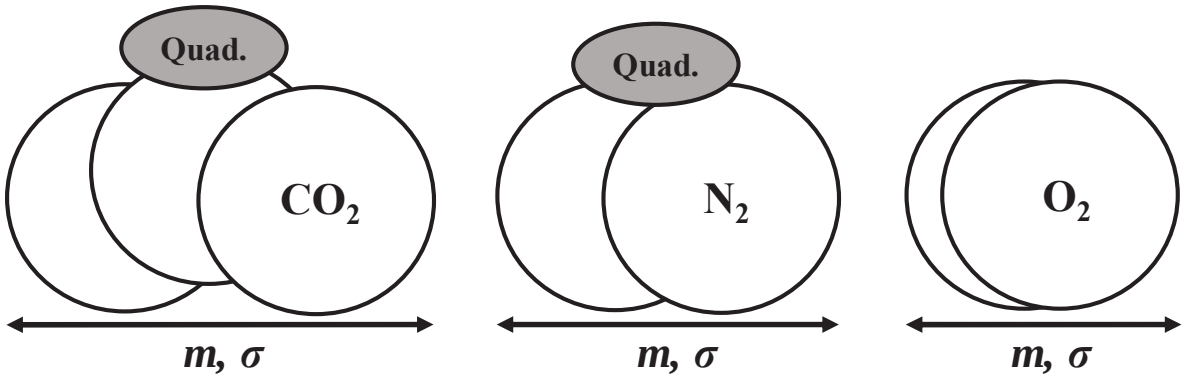

Figure 3.1. Soft-SAFT molecular models of respiratory gases studied in this work.

3.2.2.2. Associating Molecules

The choice of an appropriate association scheme, which represents the main physical short-range interactions, is vital for an accurate description of its thermodynamic properties for an associating compound. In previous efforts to model ILs with soft-SAFT EoS,(10,22–26,46) the anions and cations are considered to be together as ion pairs. Besides, specific associating sites can be used to represent the interactions between the IL counterions and their interactions with other associating molecules.

In a previous step of the ongoing project of which this thesis is part, a molecular model of the $[C_nC_1Im][C_4F_9SO_3]$ FILs family was developed. To achieve this model, the density gradient theory (DGT) was coupled with the soft-SAFT equation to compute interfacial properties. The modelling results have not been published yet. Consequently, a brief explanation of the developed molecular model is given to contextualize the results herein achieved.

The $[C_nC_1Im][C_4F_9SO_3]$ homologous series have been modelled as a homonuclear chainlike molecule with three associating sites which represent the strong interactions between the anion and cation. This model considers that the cation and anion are forming a unique chain. This assumption is sustained by results obtained from molecular dynamics simulations which show the continuous formation of ionic pairs or ionic clusters of these systems.(47,48) Results previously obtained from contributions using other IL families also supported it.(22,49) The number of the associating sites was chosen based on the charge distribution of the molecule, since the delocalization of the anion electric charge is due to the presence of the fluorine atoms in the anion, enhancing the possibility of interaction with the surrounding cations. This feature can be observed from preliminary computational chemistry calculations carried out by our group (not published yet) where the charge distribution in this molecule is shown (see **Figure 3.2**).

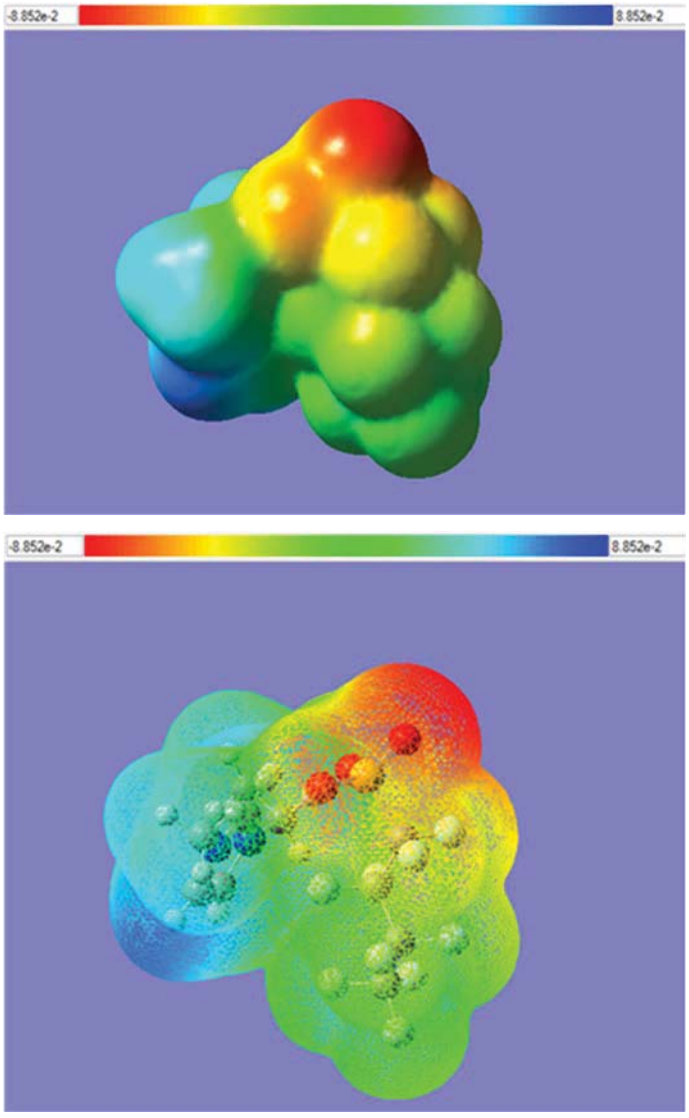

Figure 3.2. Electrostatic surface potential (ESP) of the $[C_2C_1Im][C_4F_9SO_3]$ ionic liquid.

In **Figure 3.2** the highly negative charged area (red zone) is delocalized. Based on this study, several options, including multiple association sites, are possible. One associating site, *A* type, represents the main interactions of the fluorine atom with the cation, while one or two *B* sites may represent the delocalized charge due the surrounding fluorine atoms and the oxygens of the anion. Only *A*-*B* interactions between different FIL molecules are allowed. Considering the complexity of the molecule and the amount of molecular interactions described through molecular dynamics calculations,(50) it is preferable to increase the degrees of freedom of the molecule and consider a 3-site model. Furthermore, a similar approach was utilized in a previous contribution for the $[C_nC_1Im][N(CF_3SO_2)_2]$ IL family, obtaining very successful results.(22) A sketch of the model with soft-SAFT is presented in **Figure 3.3**.

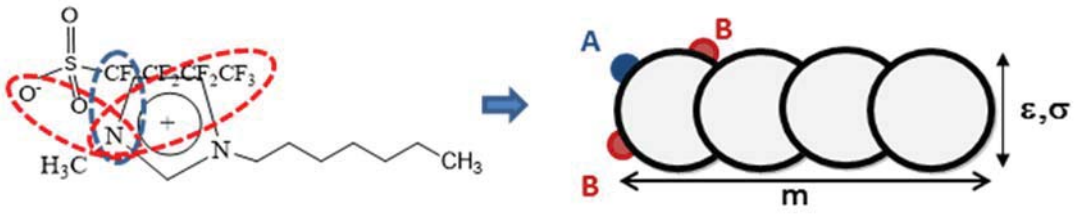

Figure 3.3. Soft-SAFT molecular model of $[C_nC_1Im][C_4F_9SO_3]$ fluorinated ionic liquids family.

The set of molecular parameter values is found by fitting to the temperature-density experimental data provided by the literature. In order to reduce the parameters degeneracy and increase the transferability between compounds, several assumptions have been made. The most important restriction affects the parameters describing the strength and volume of association, which have been fixed to constant values. An excellent agreement between the measurements and the theory were achieved.

In order to verify the adequacy of the optimization approach used in this thesis, the systems of FILs with water were also considered. The model of $[C_nC_1Im][C_4F_9SO_3]$ with water has not been published yet, following a succinct explanation. Water was already modelled in a previous work,(45) as a single spherical Lennard-Jones monomer ($m_{H_2O} = 1$) with a segment diameter, σ, and energy of interaction between the monomers, ε, and with four association sites, two *e* sites (negative, corresponding to the lone pairs of electrons of the oxygen) and two *H* type sites (positive, corresponding to the hydrogen atoms. Only *e*-*H* bonding is allowed. These four association sites preserve the tetrahedral geometry of the compound. The molecular parameters of water are descripted in **Table 3.1**.

Regarding the binary system (FIL + water), cross-association interactions between the water and FIL molecules were explicitly considered. **Figure 3.4** illustrates the schematic representation of the water interaction within the FIL family. The association parameters of the binary system, are calculated using the following combining rules:

$$K_{\alpha\beta,ij} = \left(\frac{\sqrt[3]{K_{\alpha\beta,ii}} + \sqrt[3]{K_{\alpha\beta,jj}}}{2} \right)^3 \quad \textbf{(15)}$$

$$\varepsilon^{HB}_{\alpha\beta,ij} = \left(\varepsilon^{HB}_{\alpha\beta,ii} \varepsilon^{HB}_{\alpha\beta,jj} \right)^{1/2} \quad \textbf{(16)}$$

where $K_{\alpha\beta,ij}$ is the association volume and $\varepsilon^{HB}_{\alpha\beta,ij}$ represents the cross-association energy between the binary system. As represented in **Figure 3.4,** only the *A-H* and *B-e* bonding types, between the ionic liquids and water, are allowed.

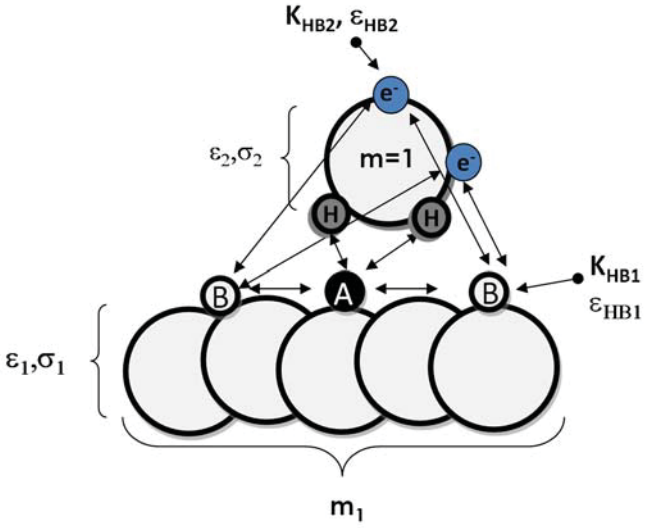

Figure 3.4. Schematic representation of soft-SAFT molecular model for the mixtures of [C_nC_1Im][$C_4F_9SO_3$] fluorinated ionic liquids family with water.

3.3 Results and Discussion

The results discussed in this chapter belong to an ongoing project performed in our lab with the collaboration of Prof. Fèlix Llovell (Ramon Llull University, Barcelona, Spain) and Prof. Lourdes Vega (the Petroleum Institute, Abu Dhabi, United Arab Emirates). The aim of this project is to design and characterize the best FILs to use in biomedical applications. In this case, the achieved results were specifically focused on the application of FILs as artificial oxygen carriers. With this goal in mind, the study of respiratory gases solubility in the fluorinated ionic liquids was accomplished by using a combined theoretical-experimental approach. Furthermore, calculations of thermodynamic properties such as density, viscosity and surface tension were also considered in this work, in order to guarantee the accuracy of the modelling approach allowing the verification of the calculated data with the experimental data.(51-54)

3.3.1. Molecular Parameters Optimization

The molecular model of $[C_nC_1Im][C_4F_9SO_3]$ FILs family, previously described in section **3.2.2.2** of this chapter, was used to optimize and predict the molecular parameters of four distinct FILs: 1-ethyl-3-methylimidazolium perfluorobutanesulfonate, $[C_2C_1Im][C_4F_9SO_3]$; 1-ethyl-3-methypyridinium perfluorobutanesulfonate, $[C_2C_1py][C_4F_9SO_3]$; 1-ethyl-3-methylimidazolium perfluoropentanoate, $[C_2C_1Im][C_4F_9CO_2]$; 1-ethyl-3-methylpyridinium perfluoropentanoate, $[C_2C_1py][C_4F_9CO_2]$. These FILs were chosen based on preliminary toxicology results available in our lab. These preliminary studies prove the low toxicity of these four compounds which it is crucial for biomedical applications. These results have not been published yet. The chemical structure and respective acronyms for FILs studied in this work are represented in **Table 3.2.**

Table 3.2. Chemical structure and respective acronyms of the studied fluorinated ionic liquids.

FIL Designation	Chemical Structure
1-Ethyl-3-methylimidazolium perfluorobutanesulfonate **$[C_2C_1Im][C_4F_9SO_3]$**	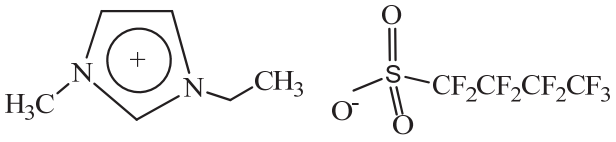
1-Ethyl-3-methylpyridinium perfluorobutanesulfonate **$[C_2C_1py][C_4F_9SO_3]$**	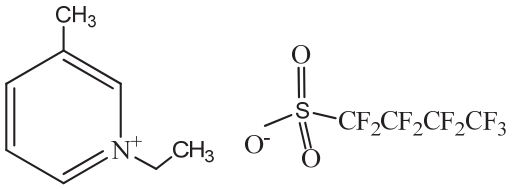
1-Ethyl-3-methylimidazolium perfluoropentanoate **$[C_2C_1Im][C_4F_9CO_2]$**	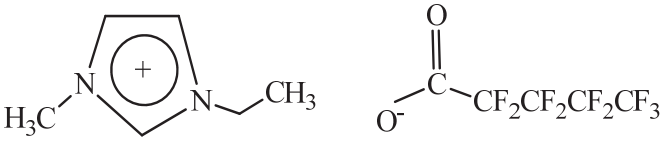
1-Ethyl-3-methylpyridinium perfluoropentanoate **$[C_2C_1py][C_4F_9CO_2]$**	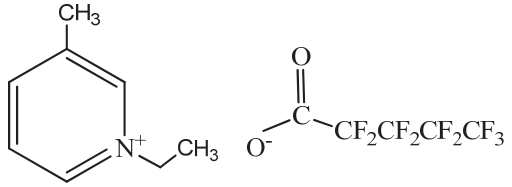

The molecular parameters optimization of the four FILs was attained through several steps, in order to predict the best molecular parameters to study the solubility of the respiratory gases in this compounds. The optimization procedure for each FIL is bellow described.

First, the molecular parameters of $[C_2C_1Im][C_4F_9SO_3]$ FIL, already determined from the modelling approach previously described, were used to optimize a new set of molecular and association parameters to describe the $[C_2C_1py][C_4F_9SO_3]$ FIL. This approach was accomplished by fitting temperature-density experimental data of the pure ionic liquid. Through this optimization, a potential set of molecular and association parameters were obtained.

Table 3.3 reports the molecular parameters calculated and optimized for all FILs using the following procedure. These molecular parameters were used to study the solubility of the respiratory gases in the fluorinated ionic liquids.

Table 3.3. Molecular weight, optimized molecular parameters and absolute average deviation (AAD) for the densities of the fluorinated ionic liquids.

	M_w (g/mol)	m	σ (Å)	ε/k_B (K)	ε^{HB}/k_B (K)	K^{HB} (Å^3)	AAD%
$[C_2C_1Im][C_4F_9SO_3]$	410.26	7.949	3.967	363.4	3450	5250	-
$[C_2C_1py][C_4F_9SO_3]$	421.28	5.949	4.163	352.1	3856	5250	0.013
$[C_2C_1Im][C_4F_9CO_2]$	374.21	7.949	3.642	334.5	6082	5250	0.003
$[C_2C_1py][C_4F_9CO_2]$	385.23	5.949	4.087	339.9	3938	5250	0.004

In order to support and verify the accuracy of the predicted parameters, the viscosity and surface tension were also calculated for the pure ionic liquid and compared with experimental data.(51-54) Afterwards, to ensure that the optimized parameters were the best to describe $[C_2C_1py][C_4F_9SO_3]$, a sensibility test was accomplished. The most variable parameter, when a model is transferred from one molecule to another, is the length of the molecular structure, *m*. In this case, the descriptor *m* is the only structural difference between the imidazolium and pyridinium FILs is the cation. To verify whether this structural feature can influence the molecular parameters, optimizations increasing and decreasing the *m* value were accomplished and compared with experimental data. This optimization shows that a lower *m* yielded values much closer to the experimental data. **Figure 3.5** depicts the temperature-density diagram which shows a good fit between the calculated results and the experimental data (51-53) for both FILs conjugated with perfluorobutanesulfonate anion.

In order to achieve an accurate model for $[C_2C_1Im][C_4F_9CO_2]$ and $[C_2C_1py][C_4F_9CO_2]$, an optimization of the molecular and association parameters was also carried out using the previous parameters for $[C_2C_1Im][C_4F_9SO_3]$ and $[C_2C_1py][C_4F_9SO_3]$. The temperature-density experimental data (51-53) of each FIL were fitted to achieve a new set of molecular parameters for each FIL based on perfluoropentanoate anion (**Figure 3.5**). In these two FILs, a model with 3 association sites, such as in $[C_nC_1Im][C_4F_9SO_3]$ IL family, was also considered. The optimized parameters were also compared with the experimental data of viscosity and surface tension.(51-54)

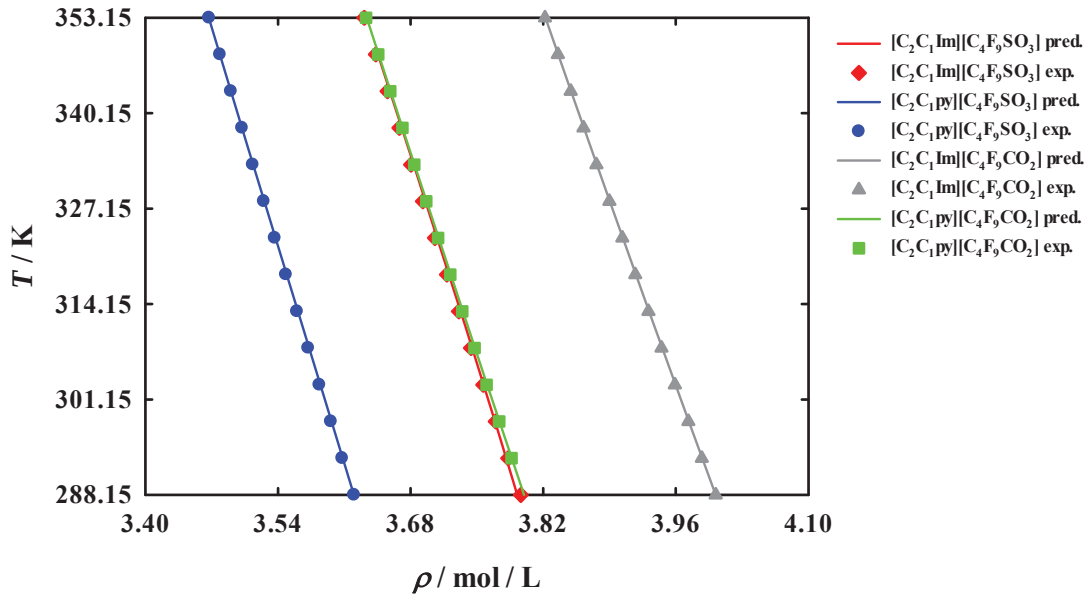

Figure 3.5. Temperature-density diagrams using soft-SAFT calculations (solid lines) together the corresponding experimental data (symbols), taken from references: (51) to $[C_2C_1Im][C_4F_9SO_3]$ (♦) and $[C_2C_1Im][C_4F_9CO_2]$ (▲); (52) to $[C_2C_1py][C_4F_9SO_3]$ (●); (53) to $[C_2C_1py][C_4F_9CO_2]$ (■).

As previously disclosed, the viscosity and surface tension were calculated with the molecular parameters calculated for all FILs. Afterwards, they were compared with the experimental data available in order to confirm the accuracy of these models.

In order to calculate the viscosity of the FILs, the soft-SAFT EoS is coupled to the Free-Volume Theory (FVT) approach. This methodology describes each system through three parameters: α, that describes the proportionality between the energy barrier and the density; B, that corresponds to the free-volume overlap, and L_v, which is a length parameter related to the structure of the molecules and the characteristic relaxation time.(36) These parameters are fitted, when possible, to the experimental viscosity data available. The viscosity parameters optimized for each FIL are described in **Table 3.4**.

Table 3.4. Optimized characteristic parameters of the free-volume theory for the fluorinated ionic liquids studied in this work. The absolute average deviation (AAD) is also included.

FILs	α (J·m^3/mol·Kg)	$B \cdot 10^3$	L_v(Å)	AAD%
$[C_2C_1Im][C_4F_9SO_3]$	226.4	5.983	0.1202	3.01
$[C_2C_1py][C_4F_9SO_3]$	226.4	5.496	0.04282	5.79
$[C_2C_1Im][C_4F_9CO_2]$	226.4	4.642	0.07444	4.16
$[C_2C_1py][C_4F_9CO_2]$	226.4	5.309	0.04982	5.39

Once the parametrization was concluded, the viscosity-temperature diagram was calculated considering the molecular parameters of these FILs. The results obtained show a significant approximation to the experimental data,(51-53) supporting the molecular parameters chosen to describe these FILs (**Figure 3.6**).

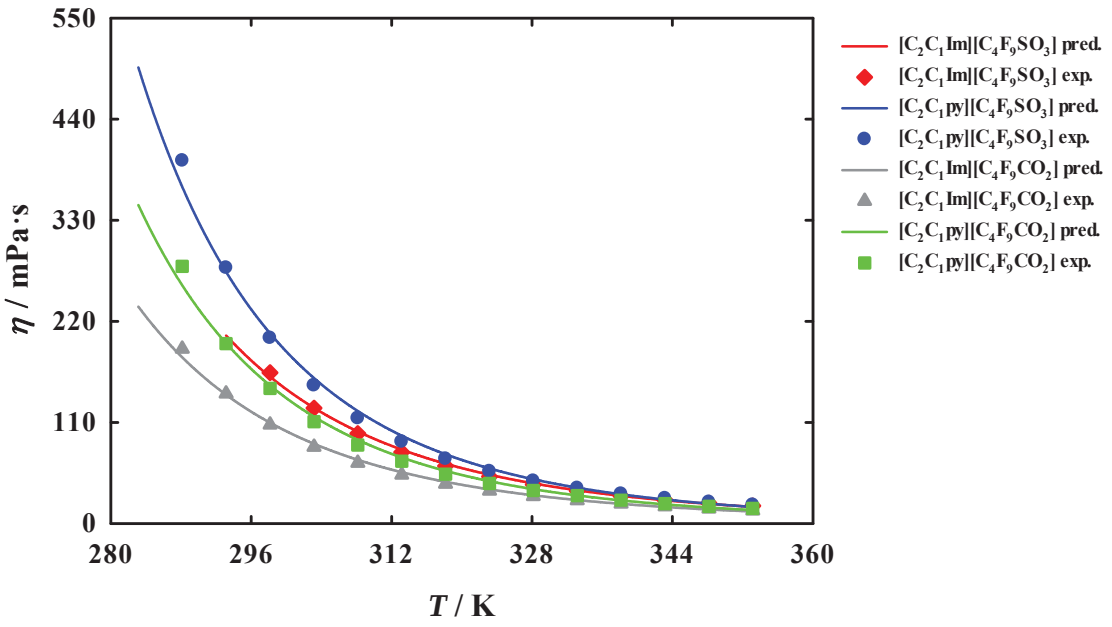

Figure 3.6. Temperature-viscosity diagrams using soft-SAFT calculations (solid lines) and the comparison with experimental data (symbols), taken from references: (51) to $[C_2C_1Im][C_4F_9SO_3]$ (♦) and $[C_2C_1Im][C_4F_9CO_2]$ (▲); (52) to $[C_2C_1py][C_4F_9SO_3]$ (●); and (53) to $[C_2C_1py][C_4F_9CO_2]$ (■).

In order to validate the calculated molecular parameters, the interfacial properties of the pure ionic liquids were also studied. For that, surface tension experimental data of the pure compounds are necessary. In this case the experimental surface tension data for $[C_2C_1Im][C_4F_9CO_2]$ are not available.

The density gradient theory (DGT) was coupled with the soft-SAFT equation to compute interfacial properties. Once the set of molecular parameters were established, the influence parameter *c* (adjustable temperature independent parameter) was fitted to the experimental data, when available, for each compound, reaching good agreement in all cases. After optimization of this parameter, it is valuable to use it as a predictive tool in the calculations of interfacial properties for other FILs.(55,56) A summary of the influence parameter values and the global average deviations for the soft-SAFT + DGT results is shown in **Table 3.5**.

Table 3.5. Optimized influence parameter for the studied FILs and modelling results for surface tension.[a]

FILs	10^{19} *c* ($J \cdot m^5/mol^2$)	AAD%
$[C_2C_1Im][C_4F_9SO_3]$(54)	12.66	0.16
$[C_2C_1py][C_4F_9SO_3]$(53)	12.11	0.86
$[C_2C_1py][C_4F_9CO_2]$(53)	11.47	0.72

[a] References include the sources of experimental data.

Afterwards, the interfacial properties were calculated with the optimized *c* parameter for each case. The results obtained showed a good approximation between the calculated data and those experimental ones, as is illustrated in **Figure 3.7**.

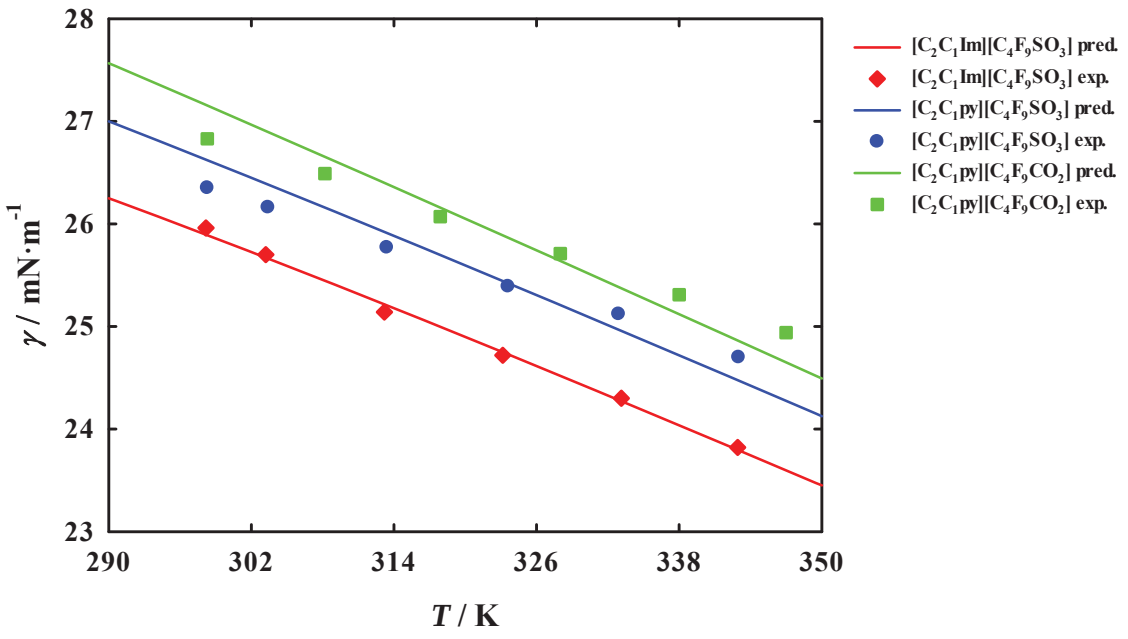

Figure 3.7. Surface tension as function of temperature for the selected FILs. Solid lines represent the calculated values using soft-SAFT. The experimental data are represented by the symbols and were taken from references: (54) to $[C_2C_1Im][C_4F_9SO_3]$ (♦); and (53) to $[C_2C_1py][C_4F_9SO_3]$ (●) and $[C_2C_1py][C_4F_9CO_2]$ (■).

The phase equilibrium of FIL + water binary systems were also calculated. In this case, the model descripted in section **3.2.2.2.** was used. As reported, the volume and energy of association of the systems FIL + water must be calculated using the Lorentz-Berthelot combining rules due to cross-association interactions between the water and the ionic liquids. These calculations were performed at 298.15 K, since this temperature corresponds to the experimental data available.(57) The binary parameter ξ, important for deviations of the cross-dispersive energy of the mixture (ε/k_B parameter), is fitted to experimental data of the binary mixtures. In this case, this parameter was adjusted to $\xi = 1.15$ for all FILs. Then, the density of the binary mixture was calculated for the FILs based on perfluorobutanesulfonate because there are only experimental data available for these compounds. The results are shown in **Figure 3.8** and good approximations to experimental data were achieved.

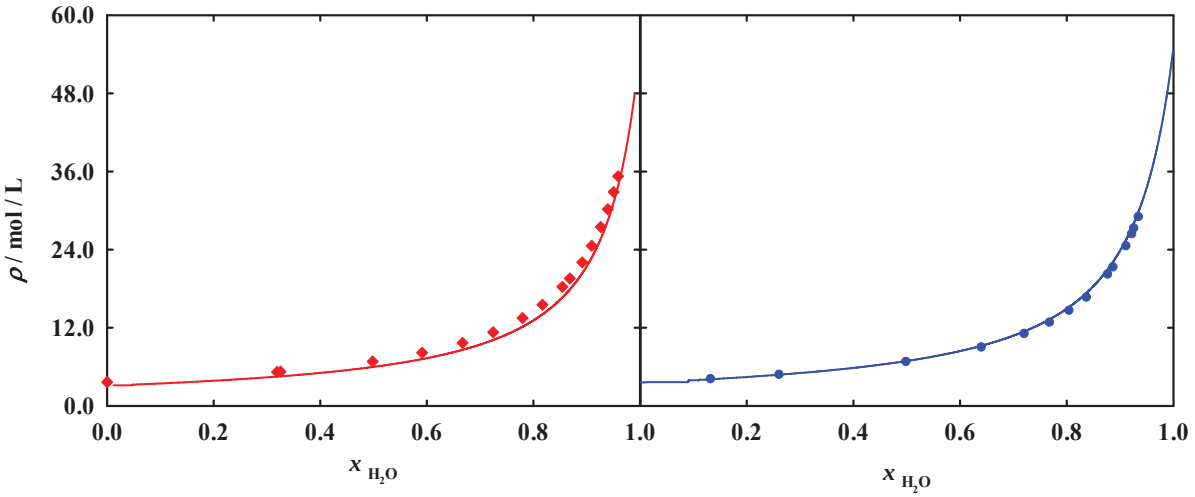

Figure 3.8. Density as function of water composition of the binary systems of FILs + water at 298.15 K. The solid lines represent the soft-SAFT calculations (red, $[C_2C_1Im][C_4F_9SO_3]$ and blue, $[C_2C_1py][C_4F_9SO_3]$) while the symbols represent the experimental data (57) (♦, $[C_2C_1Im][C_4F_9SO_3]$ and ●, $[C_2C_1py][C_4F_9SO_3]$). The results are plotted in different graphs to better visualization.

As a second step, the liquid-liquid equilibria for all FILs was calculated. This approach was used, since these ionic liquids are totally miscible in water. Thus, in the diagram of pressure versus water composition, (**Figure 3.9**), the curve of the water composition must reach one. This value means that the FIL solubilize 100% of water composition. In all these FILs, this event is visible when the calculations are carried out using soft-SAFT approach. These results support the molecular parameters obtained.

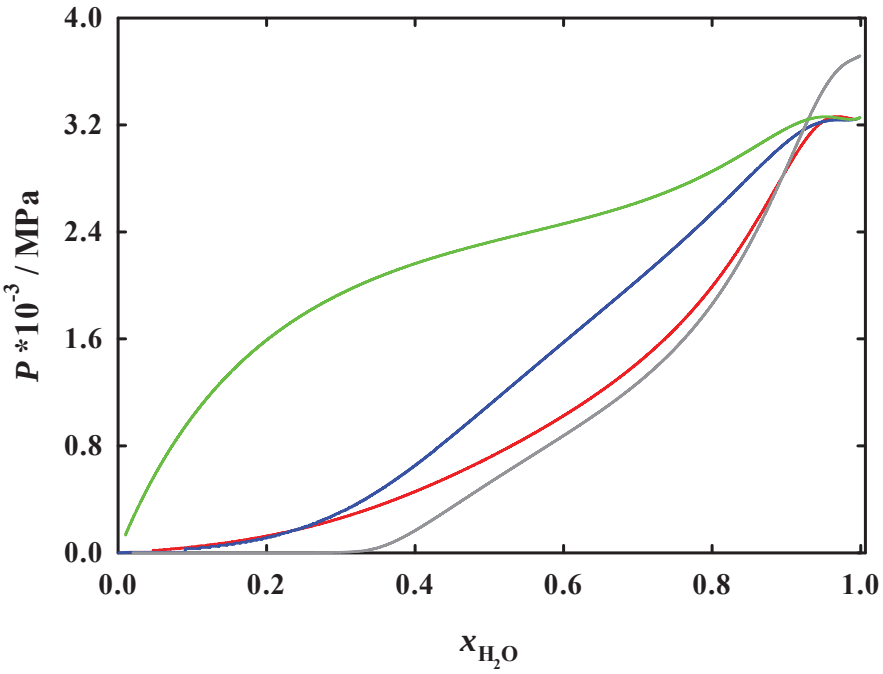

Figure 3.9. Liquid-liquid equilibrium for the binary systems FILs + water at 298.15 K: red line, $[C_2C_1Im][C_4F_9SO_3]$; blue line, $[C_2C_1py][C_4F_9SO_3]$; gray line, $[C_2C_1Im][C_4F_9CO_2]$; green line, $[C_2C_1py][C_4F_9CO_2]$.

3.3.2. Solubility of Respiratory Gases in Fluorinated Ionic Liquids

The main goal of this work is to study the solubility of the respiratory gases in the selected FILs. As was previously described, the molecular parameters for the FILs were calculated and optimized in order to study the binary systems FIL + respiratory gases.

With this goal in mind, the vapour-liquid equilibria (VLE) were calculated at fixed temperatures. The chosen temperatures were: 294.00 K, because the experimental data available were determined at this temperature; 298.15 K as representative of the room temperature; 310.15 K which corresponds to the human body average temperature; and finally, 333.15 K because this theoretical procedure usually starts the calculations at higher temperatures and reduces it gradually in order to stabilize and allow calculations with lower temperatures.

The only experimental data available for these mixtures were the Henry constants (H_c) for the binary system $[C_2C_1py][C_4F_9SO_3]$ + respiratory gases.(58) As described by Henry's law, the H_c can be calculated through the diagram of the pressure (that is applied to the system) as function of gas composition. In these calculations using soft-SAFT approach, it is necessary calculate the VLE at low pressures and compositions (infinite dilution), considering the ideal behaviour of the gases. Since the H_c

is the slope of the pressure as a function of the gas composition, the slope of the VLE at a range of 0.001 to 0.01 gas composition corresponds to the H_c calculated. With this information, the binary parameter ξ of the systems $[C_2C_1py][C_4F_9SO_3]$ + respiratory gases can be fitted to the experimental data and transferred to the other ionic liquids. The optimization of the ξ parameter was accomplished by fitting the value of the H_c value. The results are presented in **Table 3.6**. However, these H_c values do not represent the H_c for each FIL, but the most approximated value to the experimental data that could be obtained by optimizing the binary parameter ξ.

In this optimization process, the binary parameter was fitted before and after the sensibility test of the molecular and association parameters. However, since the first optimization is closer to the initial model of FIL based on $[C_2C_1Im][C_4F_9SO_3]$, the first binary parameter was transferred to $[C_2C_1Im][C_4F_9SO_3]$ and $[C_2C_1Im][C_4F_9CO_2]$. In the second optimization done after the sensibility test (where the molecular and association parameters were better fitted to the experimental data of the pure ionic liquid $[C_2C_1py][C_4F_9SO_3]$), the value of ξ was transferred for $[C_2C_1py][C_4F_9CO_2]$. The Henry constants were compared with the experimental values. The optimized binary parameter used is depicted in **Table 3.6**.

Table 3.6. Adjusted binary parameter ξ for the solubility of respiratory gases using the experimental H_c obtained at 294 K.

Systems	CO_2		N_2		O_2	
	ξ	H_c (MPa)	ξ	H_c (MPa)	ξ	H_c (MPa)
experimental data for $[C_2C_1py][C_4F_9SO_3]$[a]		2.63		131.42		73.76
$[C_2C_1Im][C_4F_9SO_3]$ **$[C_2C_1Im][C_4F_9CO_2]$**	1.062	2.64[b]	0.983	131.38[b]	0.875	73.58[b]
$[C_2C_1py][C_4F_9SO_3]$ **$[C_2C_1py][C_4F_9CO_2]$**	0.996	2.62[b]	0.806	131.49[b]	0.723	73.72[b]

[a] experimental data from reference (58)
[b] Note that these values do not correspond to the H_c of each FIL but to the H_c value calculated using the fitted ξ parameter.

Until now, the molecular, association and binary parameters of the mixtures FILs + respiratory gases were optimized and calculated. Then, the conditions to amplify the insights in the solubility of the respiratory gases in the selected FILs are reunited. These conditions are discussed below in two different

ways: varying the cation and preserving the anion; and changing the anion and maintaining the cation. The best FIL to use as gas carrier in artificial blood substitutes will be selected using the soft-SAFT EoS calculations.

3.3.2.1 Effect of the cation in the solubility of respiratory gases

In order to study the effect of the cation in the solubility of respiratory gases, two distinct comparisons were studied. First, the effect of the cation in FILs based on perfluorobutanesulfonate anion and FILs based on perfluoropentanoate anion were studied. This comparison was carried out using the vapour-liquid equilibria of the systems FILs + respiratory gases. **Figures 3.10-3.12** illustrate the VLE of these systems FILs + respiratory gases.

Figure 3.10 shows the VLE of the mixture FIL + carbon dioxide. In the case of FILs based on $[C_4F_9SO_3]^-$ (**Figure 3.10.a),** the results show that the solubility of CO_2 is higher when the temperature is diminished in both FILs (it is necessary to apply less pressure to reach the same gas composition absorbed by the FIL). Furthermore, the FIL based on $[C_2C_1Im]^+$ cation has a higher capacity to absorb CO_2, at the four temperatures, than the $[C_2C_1py]^+$cation. In **Figure 3.10.b**, the opposite behaviour is observed when the same cations are conjugated with the $[C_4F_9CO_2]^-$ anion. $[C_2C_1py][C_4F_9CO_2]$ has a slightly increased capacity to absorb CO_2 and the solubility is also increased at lower temperatures. This behaviour was also found in mixtures PFCs + respiratory gases where the solubility is higher with the decrease of the temperature.(59)

Regarding the absorption of N_2 in FILs based on $[C_4F_9SO_3]^-$ anion (**Figure 3.11.a**), imidazolium cation provides a higher capacity to solubilize N_2. However, the $[C_2C_1Im][C_4F_9SO_3]$ increases the absorption of N_2 when the temperature is increased. This behaviour is also noticed in FILs based on $[C_4F_9CO_2]^-$ anion **(Figure 3.11.b)**. The results show that $[C_2C_1py][C_4F_9CO_2]$ presents a better absorption of N_2.

In the case of FILs + O_2 systems, **Figure 3.12.a** shows that $[C_2C_1Im][C_4F_9SO_3]$ have more capability to absorb this gas. However, both FILs present a change in the absorption behaviour at lower compositions. The gas solubility increases when the temperature decreases at low gas composition but the opposite behaviour is verified at higher gas compositions. The same change of behaviour is noticed for FILs based on $[C_4F_9CO_2]^-$ anion (**Figure 3.12.b)**. $[C_2C_1py][C_4F_9CO_2]$ obtain the highest solubility of O_2.

Briefly, the comparison between $[C_2C_1Im]^+$ and $[C_2C_1py]^+$ cations show that they have a completely different behaviour regarding the capacity to absorb respiratory gases. Then, the soft-SAFT

approach reveals that $[C_2C_1Im][C_4F_9SO_3]$ and $[C_2C_1py][C_4F_9CO_2]$ are the most promising gases to use as respiratory gas carriers.

3.3.2.2 Effect of the anion in the solubility of respiratory gases

The anion effect was also studied in this work. The same approach, previously used, was applied to verify which anion, $[C_4F_9SO_3]^-$ or $[C_4F_9CO_2]^-$, has an higher capacity to solubilize respiratory gases.

Figure 3.13.a illustrates the comparison of the solubility of carbon dioxide for FILs based on imidazolium cation. The higher absorption of carbon dioxide is clearly in $[C_2C_1Im][C_4F_9SO_3]$ FIL. In both ILs, the capacity for gas absorption increases when the temperature decreases. In the case of FILs based on pyridinium cation (**Figure 3.13.b)**, the same tendency with the temperature is shown. Then, the most promising FIL for solubilize CO_2 is $[C_2C_1py]$ $[C_4F_9SO_3]$.

The study of the systems FILs + N_2 is depicted in **Figure 3.14**. The **Figure 3.14.a** shows the behaviour of FILs based on imidazolium cation, where the $[C_2C_1Im][C_4F_9SO_3]$ has higher ability to solubilize N_2 than $[C_2C_1Im][C_4F_9CO_2]$. In the case of FIL based on $[C_4F_9CO_2]^-$ anion, the absorption of this gas is increased with the increment of the temperature, and on opposite behaviour is observed in FIL based on $[C_4F_9SO_3]^-$ anion. **Figure 3.14.b** depicts the behaviour of FILs based on pyridinium cation. Both FILs show the same behaviour regarding the temperature, being N_2 more solubilize at higher temperatures. The best FIL to be used in this biomedical application is $[C_2C_1py][C_4F_9SO_3]$.

In the case of O_2 gas, FILs based on perfluoropentanoate anion show again a behaviour that depends of the gas composition (**Figure 3.15**). These FILs solubilize more O_2 gas at lower temperatures when the gas composition is small. However, the increment of gas composition shows a higher solubilisation with the increase of the temperature (see **Figure 3.15**). Finally, both studies show that the FILs conjugated with $[C_4F_9SO_3]^-$ anion have a higher ability to solubilize oxygen.

The effect of the anion in the solubility of respiratory gases in all cases show that FILs based on $[C_4F_9SO_3]^-$ anion have the best capacity to solubilize respiratory gases, CO_2, N_2 and O_2.

In conclusion, the influence of the cation and anion was studied in this section. The results show that the most reliable ionic liquids to use as gas carrier may be $[C_2C_1Im][C_4F_9SO_3]$ and $[C_2C_1py][C_4F_9SO_3]$. However, the imidazolium cation demonstrated higher solubility of respiratory gases. Therefore, the $[C_2C_1Im][C_4F_9SO_3]$ FIL show a great potential to be used as an artificial gas carrier.

It is important to emphasize that the results herein obtained are predictions using a reliable theoretical tool. Soft-SAFT EoS allow to characterize the thermodynamic properties of these FILs and

their mixtures. However, it is important to obtain more experimental data for the binary mixtures FILs + gases to ensure the accuracy of the calculations herein obtain and transferred the models to other ILs families, extending the power of this tool.

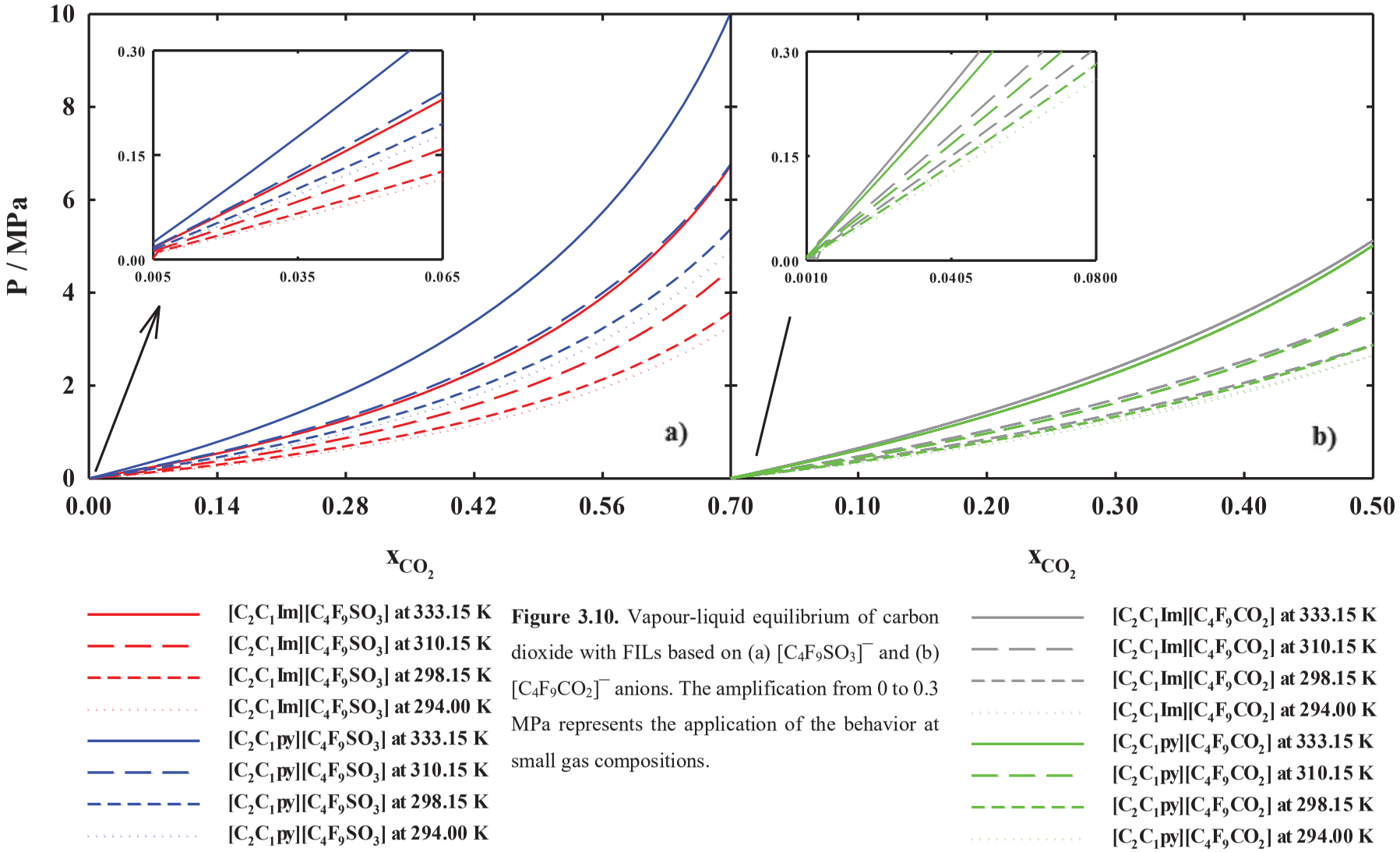

Figure 3.10. Vapour-liquid equilibrium of carbon dioxide with FILs based on (a) $[C_4F_9SO_3]^-$ and (b) $[C_4F_9CO_2]^-$ anions. The amplification from 0 to 0.3 MPa represents the application of the behavior at small gas compositions.

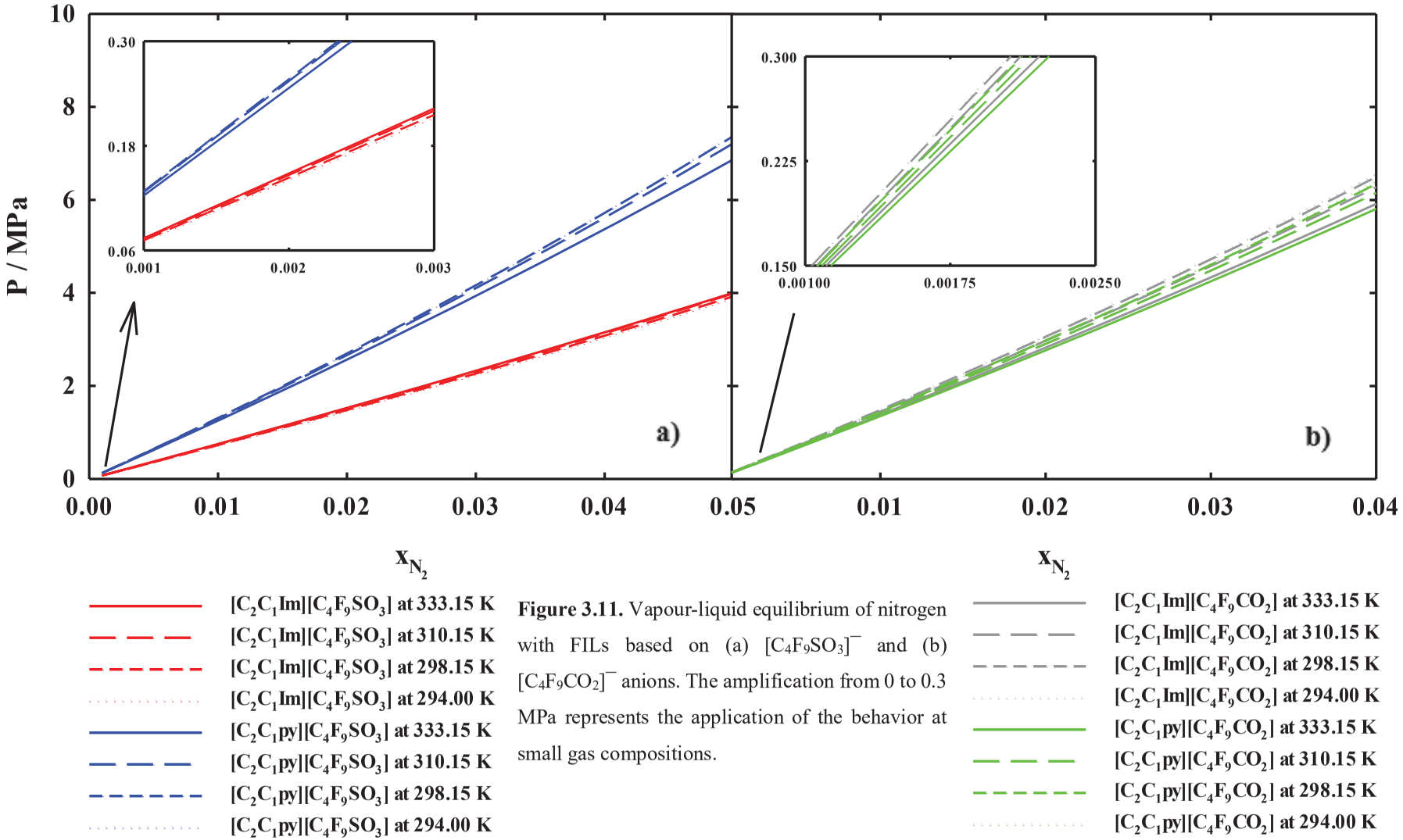

Figure 3.11. Vapour-liquid equilibrium of nitrogen with FILs based on (a) $[C_4F_9SO_3]^-$ and (b) $[C_4F_9CO_2]^-$ anions. The amplification from 0 to 0.3 MPa represents the application of the behavior at small gas compositions.

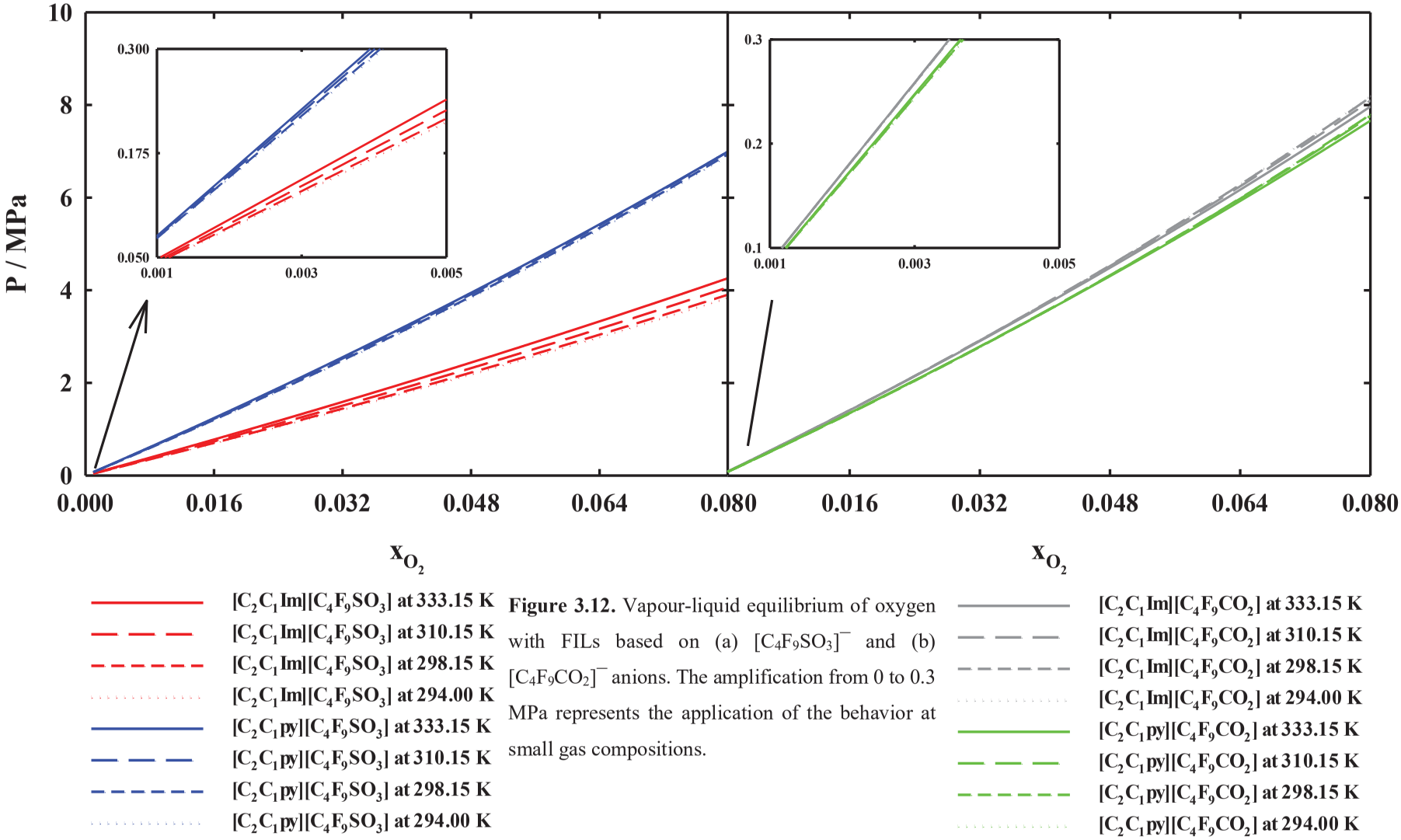

Figure 3.12. Vapour-liquid equilibrium of oxygen with FILs based on (a) $[C_4F_9SO_3]^-$ and (b) $[C_4F_9CO_2]^-$ anions. The amplification from 0 to 0.3 MPa represents the application of the behavior at small gas compositions.

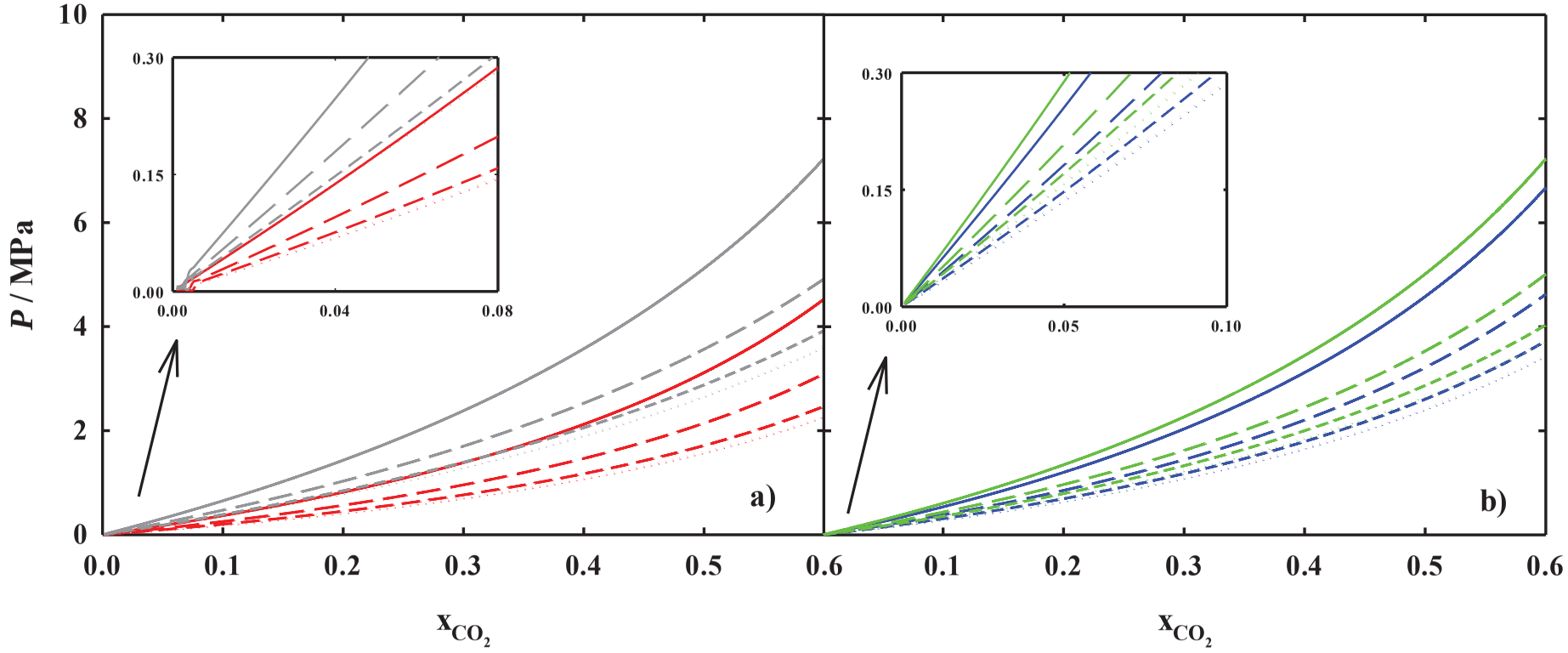

Figure 3.13. Vapour-liquid equilibrium of carbon dioxide with FILs based on (a) $[C_2C_1Im]^+$ and (b) $[C_2C_1py]^+$ cations. The amplification from 0 to 0.3 MPa represents the application of the behavior at small gas compositions.

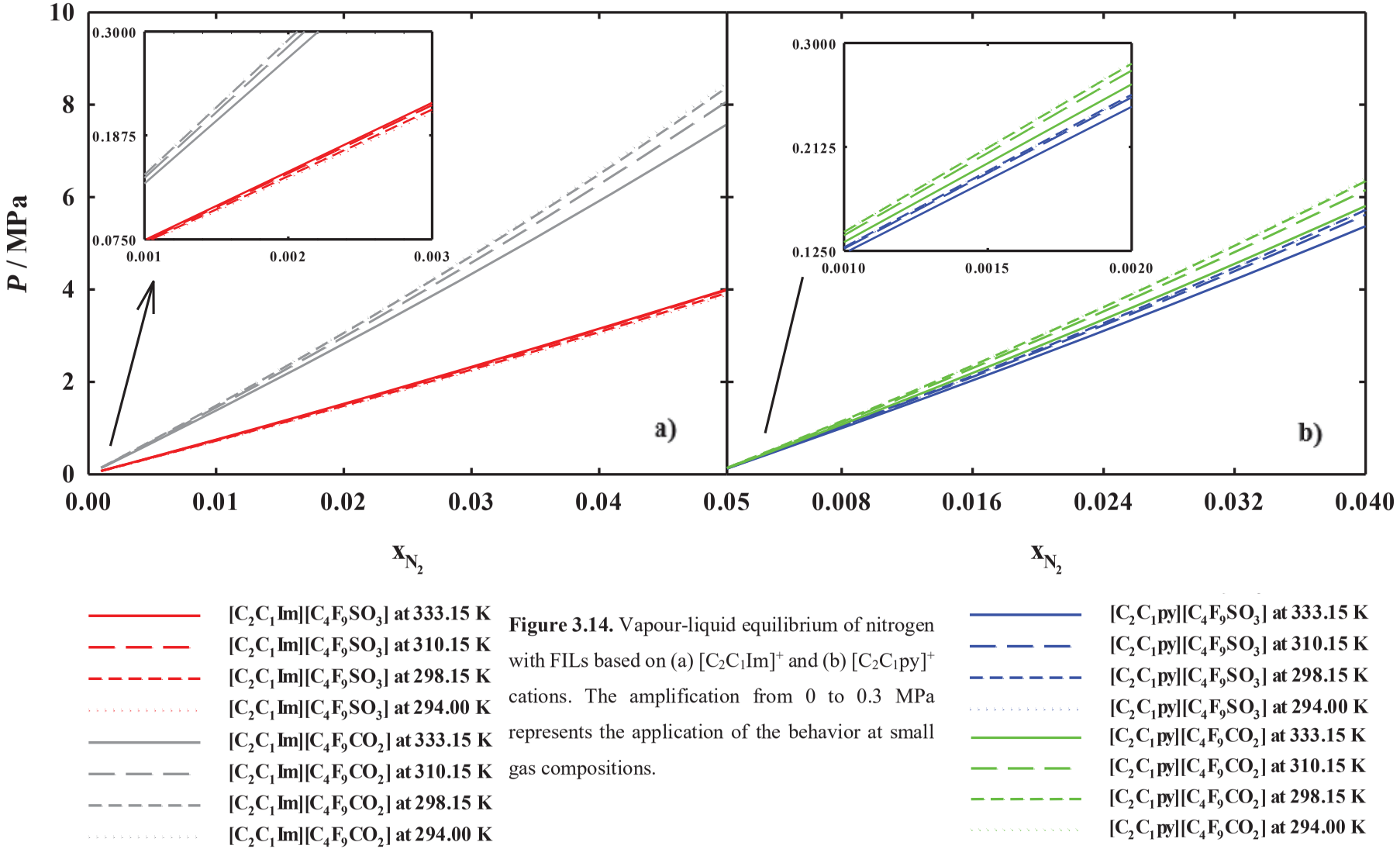

Figure 3.14. Vapour-liquid equilibrium of nitrogen with FILs based on (a) $[C_2C_1Im]^+$ and (b) $[C_2C_1py]^+$ cations. The amplification from 0 to 0.3 MPa represents the application of the behavior at small gas compositions.

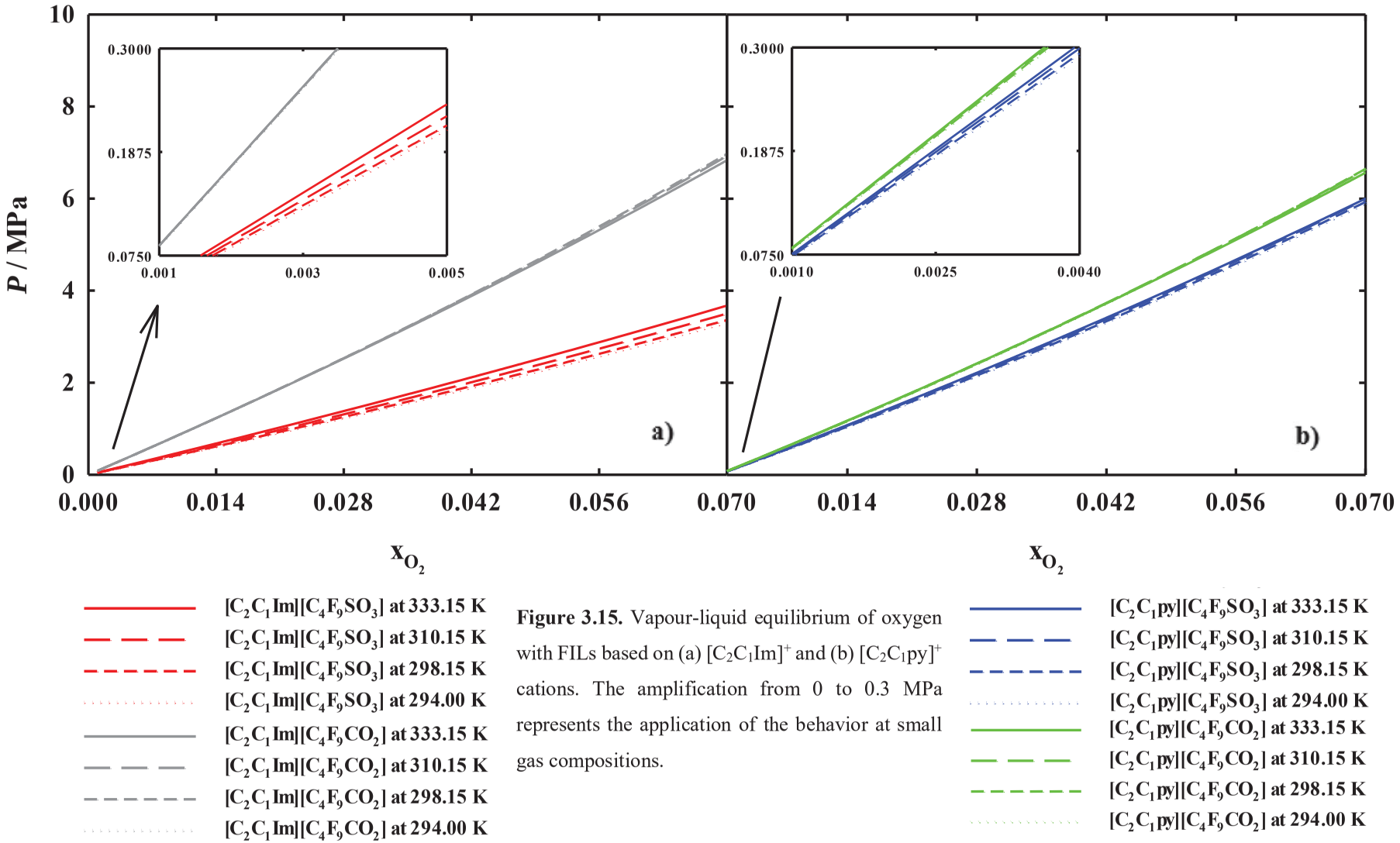

Figure 3.15. Vapour-liquid equilibrium of oxygen with FILs based on (a) $[C_2C_1Im]^+$ and (b) $[C_2C_1py]^+$ cations. The amplification from 0 to 0.3 MPa represents the application of the behavior at small gas compositions.

3.4 Conclusions

In this chapter, a theoretical approach was used as a tool to obtain insights in the solubility of respiratory gases in fluorinated ionic liquids. In this study, experimental data were used to fit and calculate molecular, association and binary parameters using soft-SAFT EoS. The molecular parameters were transferred to other FILs families to understand the vapour-liquid equilibrium behaviour in the binary mixtures of FILs with respiratory gases.

Taking all studies into consideration, the FIL with the best capability to solubilize the respiratory gases is the $[C_2C_1Im][C_4F_9SO_3]$. At all temperatures, this FIL shows a greater power to absorb CO_2, N_2 and O_2. The effect of the cation and anion in the solubility of respiratory gases show that this $[C_2C_1Im][C_4F_9SO_3]$ FIL can be consider the best candidate to use as a gas carrier in the biomedical application herein studied.

However, it is essential to obtain more experimental data with the aim to evaluate the results of the absorption of respiratory gases in these FILs. This experimental information allows us to validate the models herein proposed. Therefore, the transferability to other FILs families may be possible. This fact increases the power of this theoretical approach as an accurate tool to obtain results in a faster and simplified way allowing the study of FILs as potential candidates to replace, partially or totally, the use of perfluorocarbons as artificial oxygen carriers

3.5 References

(1) Coutinho, J. A. P.; Carvalho, P. J.; Oliveira, N. M. C. Predictive Methods for the Estimation of Thermophysical Properties of Ionic Liquids. *RSC Adv* **2012**, 2, 7322-7346

(2) Aparicio, S.; Atilhan, M.; Karadas, F. Thermophysical Properties of Pure Ionic Liquids: Review of Present Situation. *Eng Chem Res*. **2010**, 49, 9580–9595

(3) Mu, T.; Han, B. Structures and Thermodynamic Properties of Ionic Liquids. *Springer Berlin Heidelberg*. **2014**, 151, 107-139

(4) Alavianmehr, M. M.; Taghizadehfard, M.; Hosseini, S. M. Development of a Perturbed Hard-Sphere Equation of State for Pure and Mixture of Ionic Liquids. *Ionics,* **2016**, 22, 649–660.

(5) Lei, Z.; Dai, C.; Chen, B. Gas Solubility in Ionic Liquids. *Chem Rev.* **2014***,* 114, 1289−1326.

(6) Gubbins, K. E. Perturbation Theories of the Thermodynamics of Polar and Associating Liquids: A Historical Perspective. *Fluid Phase Equilib*. **2015**, 1–15.

(7) Chapman, W. G.; Gubbins, K. E.; Jackson, G.; Radosz, M. SAFT: Equation-of-State Solution Model for Associating Fluids. *Fluid Phase Equilib.* **1989**, 52, 31–38.

(8) Chapman, W. G.; Gubbins, K. E.; Jackson, G.; Radosz, M. New Reference Equation of State for Associating Liquids. *Ind Eng Chem Res*. **1990**, 29, 1709–1721.

(9) Huang, S. H.; Radosz, M. Equation of State for Small, Large, Polydisperse and Associating Molecules. *Ind Eng Chem Res*. **1990**, 29, 2284–2294.

(10) Andreu, J. S.; Vega, L. F. Capturing the Solubility Behavior of CO_2 in Ionic Liquids by a Simple Model. *J Phys Chem C.* **2007**, 111, 16028–16034.

(11) Ji, X.; Adidharma, H. Thermodynamic Modeling of Ionic Liquid Density with Heterosegmented Statistical Associating Fluid Theory. *Chem Eng Sci*. **2009**, 64, 1985–1992.

(12) Ji, X.; Adidharma, H. Thermodynamic Modeling of CO_2 Solubility in Ionic Liquid with Heterosegmented Statistical Associating Fluid Theory. *Fluid Phase Equilib*. **2010**, 293, 141–150

(13) Karakatsani, E. K.; Economou, I. G.; Kroon, M. C.; Peters, C. J.; Witkamp, G. J. tPC-PSAFT Modeling of Gas Solubility in Imidazolium-based Ionic Liquids. *J Phys Chem C.*, **2007**, 111, 15487–15492.

(14) Karakatsani, E. K.; Economou, I. G.; Kroon, M. C.; Bermejo, M. D.; Peters, C. J.; Witkamp, G.-J. Equation of State Modeling of the Phase Equilibria of Ionic Liquid Mixtures at Low and High Pressure. *Phys Chem Chem Phys*, **2008**, 10, 6160–6168

(15) Kroon, M. C.; Karakatsani, E. K.; Economou, I. G.; Witkamp, G.-J.; Peters, C. J. Modeling of the Carbon Dioxide Solubility in Imidazolium-Based Ionic Liquids with the tPC-SAFT Equation of State. *J Phys Chem B.* **2006**, 110, 9262–9269.

(16) Wertheim, M. S. Fluids with Highly Directional Attractive Forces.1. Statistical Thermodynamics. *J Stat Phys.* **1984**, 35, 19–34.

(17) Wertheim, M. S. Fluids with Highly Directional Attractive Forces. II. Thermodynamic Perturbation Theory and Integral Equations. *J Stat Phys.* **1984**, 35, 35–47.

(18) Wertheim, M. S. Fluids with Highly Directional Attractive Forces. III. Multiple Attraction Sites. *J Stat Phys.* **1986**, 42, 459–476.

(19) Wertheim, M. S. Fluids with Highly Directional Attractive Forces. IV. Equilibrium Polymerization. *J Stat Phys.* **1986**, 42, 477–492.

(20) Blas, F. J.; Vega, L. F. Thermodynamic Behaviour of Homonuclear and Heteronuclear Lennard-Jones Chains with Association Sites from Simulation and Theory. *Mol Phys*. **1997**, 92, 135–150.

(21) Blas, F. J.; Vega, L. F. Prediction of Binary and Ternary Diagrams Using the Statistical Associating Fluid Theory (SAFT) Equation of State. *Ind Eng Chem Res*. **1998**, 37, 660–674.

(22) Llovell, F.; Valente, E.; Vilaseca, O.; Vega, L. F. Modeling Complex Associating Mixtures with [$C_n$mim][Tf2N] Ionic Liquids: Predictions from the Soft-SAFT Equation. *J Phys Chem B.* **2011**, 115, 4387–4398.

(23) Pereira, L. M. C.; Oliveira, M. B.; Llovell, F.; Vega, L. F.; Coutinho, J. A. P. Assessing the N_2O/CO_2 High Pressure Separation Using Ionic Liquids with the Soft-SAFT Eos. *J Supercrit Fluids*. **2014**, 92, 231–241.

(24) Oliveira, M. B.; Llovell, F.; Coutinho, J. A. P.; Vega, L. F. Modeling the [NTf2] Pyridinium Ionic Liquids Family and Their Mixtures with the Soft Statistical Associating Fluid Theory Equation of State. *J Phys Chem B*. **2012**, 116, 9089–9100.

(25) Vega, L. F.; Vilaseca, O.; Llovell, F.; Andreu, J. S. Modeling Ionic Liquids and the Solubility of Gases in them: Recent Advances and Perspectives. *Fluid Phase Equilib*. **2010**, 294, 15–30.

(26) Vega, L. F.; Llovell, F. Review and New Insights into the Application of Molecular-Based Equations of State to Water and Aqueous Solutions. *Fluid Phase Equilib.* **2016**, 416, 150–173

(27) Johnson, J. K.; Zollweg, J. A.; Gubbins, K. E. Molecular Physics: An International Journal at the Interface Between Chemistry and Physics the Structure of Ambient Water. *Molecular Physics*. **1993**, 78, 591-618.

(28) Johnson, J. K.; Zollweg, J. A.; Gubbins, K. E. Equation of State for Lennard-Jones Chains. *J Phys Chem*. **1994**, 98, 6413–6419.

(29) Gubbins, K. E.; Twu, C. H. Thermodynamics of Polyatomic Fluid Mixtures-I Theory. *Chem Eng Sci*. **1978**, 33, 863–878.

(30) Jog, P. K.; Sauer, S. G.; Blaesing, J.; Chapman, W. G. Application of Dipolar Chain Theory to the Phase Behavior of Polar Fluids and Mixtures. *Ind Eng Chem Res*. **2001**, 40, 4641–4648.

(31) Stell, G.; Rasaiah, J. C; Narang, H. Thermodynamic Perturbation Theory for Simple Polar Fluids. II. *Mol Phys.* **1974**, 27, 1393–1414.

(32) Waals, J. D. Translation of JD Van der Waals "The Thermodynamic Theory of Capillarity under the Hypothesis of a Continuous Variation of Density." *J Stat Phys*. **1979**, 20, 200–244

(33) Cahn J. W.; Hilliard, J. E. Free Energy of a Nonuniform System. I. Interfacial Free Energy. *J Chem Phys*. **1958**, 28, 258–267.

(34) Bongiorno, V.; Scriven, L.; Davis, H. Molecular Theory of Fluid Interfaces. *J Colloid Interface Sci* **1976**, 57, 462–475.

(35) Allal, A.; Moha-ouchane, M,; Boned, C. A New Free Volume Model for Dynamic Viscosity and Density of Dense Fluids Versus Pressure and Temperature. *Physics and Chemistry of Liquids.* **2001**, 39, 1-30.

(36) Allal, A. Boned, C. Baylaucq, A. Free-Volume Viscosity Model for Fluids in the Dense and Gaseous States. *Phys Rev E*. **2001**, 64, 11203.

(37) Llovell, F.; Marcos, R. M.; Vega, L. F. Free-Volume-Theory Coupled with soft-SAFT for Viscosity Calculations: Comparison with Molecular Simulation and Experimental Data. *J Phys Chem B*, **2013**, 117, 8159-8171.

(38) Llovell. F.; Marcos, R. M.; Vega, L. F. Transport Properties of Mixtures by the Soft-SAFT + Free-Volume Theory: Application to Mixtures of n -Alkanes and Hydrofluorocarbons. *J Phys Chem B,* **2013**, 117(17):5195–205.

(39) Chung, T. H.; Ajlan, M.; Lee, L. L.; Starling, K. E. Generalized Multiparameter Correlation for Nonpolar and Polar Fluid Transport Properties. *Ind Eng Chem Res.* **1988**, 27, 671–679.

(40) Wachter, P.; Schreiner, C.; Schweiger, H.-G.; Gores, H. J. Determination of Phase Transition Points of Ionic Liquids by Combination of Thermal Analysis and Conductivity Measurements at Very Low Heating and Cooling Rates. *J Chem Thermodyn* **2010**, 42, 900–903

(41) Doolittle, A. K. Studies in Newtonian Flow. II. The Dependence of the Viscosity of Liquids on Free-Space. *J Appl Phys.* **1951**, 22, 1471–1475.

(42) Dias, A. M. A; Carrier, H.; Daridon, J. L.; Pámies, J. C.; Vega, L. F.; Coutinho, J. A. P; Marrucho, I. M. Vapor - Liquid Equilibrium of Carbon Dioxide - Perfluoroalkane Mixtures: Experimental Data and SAFT Modeling. *Ind Eng Chem Res*. **2006**, 45, 2341–2350.

(43) Pedrosa, N.; Pámies, J. C.; Coutinho, J. A. P.; Marrucho, I. M.; Vega, L. F. Phase Equilibria of Ethylene Glycol Oligomers and their Mixtures. *Ind Eng Chem Res.* **2005**;44(17):7027–37.

(44) Dias, A. M. A.; Pámies, J. C.; Marrucho, I. M.; Vega, L. F. Modeling of the Solubility of Gases in Perfluoroalkanes. *J Phys Chem B.* **2004**, 108, 1450–1457.

(45) Vega, L. F.; Llovell, F.; Blas, F. J. Capturing the Solubility Minima of N-alkanes in Water by Soft-SAFT. *J Phys Chem B*. **2009**, 113, 7621–7630.

(46) Llovell, F.; Vega, L. F. Assessing Ionic Liquids Experimental Data Using Molecular Modeling: The [$C_n$mim][BF_4] Case Study. *J Chem Eng Data*. **2014**, 416, 1898–1911

(47) Urahata, S. M.; Ribeiro, M. C. C. Single Particle Dynamics in Ionic Liquids of 1-Alkyl-3-Methylimidazolium Cations. *J Chem Phys*. **2005**, 122, 024511.

(48) Del Pópolo, M. G.; Voth, G. A. On the Structure and Dynamics of Ionic Liquids. *J Phys Chem B*. **2004**, 108, 1744–1752.

(49) Llovell, F.; Marcos, R. M.; MacDowell, N.; Vega, L. F. Modeling the Absorption of Weak Electrolytes and Acid Gases with Ionic Liquids Using the Soft-SAFT Approach. *J Phys Chem B.* **2012**, 116, 7709–7718.

(50) Pereiro, A. B.; Pastoriza-Gallego, M. J.; Shimizu, K.; Marrucho, I. M.; Lopes, J. N. C.; Piñeiro, M. M.; Rebelo, L. P. N. On the Formation of a Third, Nanostructured Domain in Ionic Liquids. *J Phys Chem B*. **2013**, 117, 10826-10833.

(51) Vieira, N. S. M.; Reis, P. M.; Shimizu, K.; Cortes, O. A.; Marrucho, I. M.; Araújo, J. M. M.; Esperança, J. M. S. S.; Canongia Lopes, J. N.; Pereiro, A. B.; Rebelo, L. P. N. A Thermophysical and Structural Characterization of Ionic Liquids with Alkyl and Perfluoroalkyl Side Chains. *RSC Adv*. **2015**, 5, 65337-65350.

(52) Pereiro, A. B.; Araújo, J. M. M.; Martinho, S.; Alves, F.; Nunes, S.; Matias, A.; Duarte, C. M. M.; Rebelo, L. P. N.; Marrucho, I. M. Fluorinated Ionic Liquids: Properties and Applications. *ACS Sustainable Chem. Eng.* **2013**, 1, 427-439.

(53) Vieira, N. S. M.; Luís, A.; Reis, P. M.; Carvalho, P. J.; Lopes-Da-Silva, J. A.; Esperança, J. M. S. S.; Araújo, J. M. M.; Rebelo, L. P. N.; Freire, M. G.; Pereiro, A. B. Fluorination Effects on the

Thermodynamic, Thermophysical and Surface Properties of Ionic Liquids. *J Chem Thermodyn*. 2016; 97, 354-361.

(54) Luís, A.; Shimizu, K.; Araújo, J. M. M.; Carvalho, P. J.; Lopes-da-Silva, J. A.; Canongia Lopes, J. N.; Rebelo, L. P. N.; Coutinho, J. A. P.; Freire, M. G., Pereiro, A. B. Influence of Nanosegregation on the Surface Tension of Fluorinated Ionic Liquids. *Langmuir*. **2016**, 32, 6130-6139.

(55) Dias, A. M. A.; Llovell, F.; Coutinho, J. A. P.; Marrucho, I. M.; Vega, L. F. Thermodynamic Characterization of Pure Perfluoroalkanes, Including Interfacial and Second Order Derivative Properties, Using the Crossover Soft-Saft EoS. *Fluid Phase Equilib*. **2009**, 286, 134–143.

(56) Vilaseca, O.; Vega, L. F. Direct Calculation of Interfacial Properties of Fluids Close to the Critical Region by a Molecular-Based Equation of State. *Fluid Phase Equilib*. **2011**, 306, 4–14

(57) Pereiro, A. B.; Araújo, J. M. M.; Teixeira, F. S.; Marrucho, I. M.; Piñeiro, M. M.; Rebelo, L. P. N. Aggregation Behavior and Total Miscibility of Fluorinated Ionic Liquids in Water. *Langmuir*. **2015**, 31, 1283-1295.

(58) Pereiro, A. B.; Tomé, L. C.; Martinho, S.; Rebelo, L. P. N.; Marrucho, I. M. Gas Permeation Properties of Fluorinated Ionic Liquids. *Ind Eng Chem Res,* **2013**, 52, 4994–5001.

(59) Spiess, B. D. Perfluorocarbon Emulsions as a Promising Technology: A Review of Tissue and Vascular Gas Dynamics. *J Appl Physiol*. **2009**, 106, 1444–1452.

4. Final Remarks

4.1. General Conclusion

This work is integrated in an ongoing project whose global objective is the development and improved generation of artificial oxygen carriers containing fluorinated ionic liquids. The overall aim of this thesis was to evaluate the influence of the nanostructural features in the phase behaviour of pure FILs and study the solubility of respiratory gases in the FILs.

In the first chapter of this thesis, the highly nanostructured of FILs was evidenced. This behaviour was enhanced by the addition of the fluorinated domains, characteristic of these compounds. In this study, it was concluded that the FIL with best promising properties to replace PFCs was $[C_2C_1py][C_4F_9SO_3]$.

In the second part of this thesis, the solubility of respiratory gases in FILs was studied using a theoretical approach. These results show that the $[C_2C_1Im][C_4F_9SO_3]$ has a higher potential to solubilize respiratory gases, being the best candidate to use as a gas carrier.

The overall study herein presented, provides information about the strong tendency to these compounds to self-assemble. It has vital importance to understand the accommodation of respiratory gases molecules and build stable emulsions used as AOCs. The widely range of FILs studied in this work was selected with the aim to understand their complete structural behaviour. This information allows the design of novel FILs with more biocompatibility. The knowledge of the thermal and structured properties enables the choice of the best FILs to increase their solubilisation power. Then, FILs with higher absorption of respiratory gases can be developed. Furthermore, theoretical models, such as the Soft Statistical Associating Fluid Theory Equation of State (soft-SAFT EoS), produce accurate results, allowing the study of a large range of compounds in a cheaper and faster way.

4.2. Future Work

The increased number of applications inherent to ionic liquids make this area very attractive. Then, research in different fields and future work will always be innovative.

As a future work, the following steps can be accomplished in order to continue the study of the respiratory gases solubility in FILs:

(i) The study of toxicity should be performed in order to find the most biocompatible FILs.

(ii) The self-aggregation behaviour of FILs in mixtures: with gas molecules, aqueous solutions or biological fluids can be accomplished using Molecular Dynamics Simulations tools. Then, it will be possible to understand the behaviour of these systems with the aim to formulate new emulsions to improve AOCs.

(iii) The solubility of respiratory gases in FILs should be determined experimentally in order to support the theoretical models herein achieved. A continuous optimization of the soft-SAFT EoS models will allow finding the most accurate models that will open a window to transfer these molecular models to other FILs families. Consequently, the calculations can be as much accurate as experimental data and are attained faster.

The future work will allow the total characterization of these complex systems. Afterwards, it will be possible to formulate new emulsions to obtain a feasible, effective and biocompatible artificial gas carrier.

4.3. Scientific Publications

Papers

1. Accepted to publication in *The Journal of Physical Chemistry C*, September 2016

"The Influence of Nanosegregation on the Phase Behavior of Fluorinated Ionic Liquids"

Margarida L. Ferreira, María J. Pastoriza-Gallego, João M. M. Araújo, José N. Canongia Lopes, Luís Paulo N. Rebelo, Manuel M. Piñeiro, Karina Shimizu, Ana B. Pereiro

2. In preparation to submit in *Separation and Purification Technology*

"Solubility of Respiratory Gases in Fluorinated Ionic Liquids"

Margarida L. Ferreira, João M. M. Araújo, Luís Paulo N. Rebelo, Lourdes F. Vega, Félix Llovell, Ana B. Pereiro

Posters in Scientific Meetings

1. "The Influence of Fluorinated Domains in Ionic Liquids Nanosegregation"

Margarida L. Ferreira, María J. Pastoriza-Gallego, João M. M. Araújo, José N. Canongia Lopes, Luís Paulo N. Rebelo, Manuel M. Piñeiro, Karina Shimizu, Ana B. Pereiro.

5th Portuguese Young Chemists Meeting (5th PYCheM) and 1st European Young Chemists Meeting (1st EYCheM), April 2016, Guimarães, Portugal.

2. "Solubility of Respiratory Gases in Fluorinated Ionic Liquids"

Ana B. Pereiro, Margarida L. Ferreira, João M. M. Araújo, Luís Paulo N. Rebelo, Lourdes F. Vega and Fèlix Llovell.

26th EUCHEM Conference on Molten Salts and Ionic Liquids, July 2016, Vienna, Austria.

3. "Physico-Chemical Characterization of Fluorinated Ionic Liquids for Their Use as Blood Substitutes"

Margarida L. Ferreira, Fèlix Llovell, Ana B. Pereiro, João M. M. Araújo, Manuel Piñeiro, Luís P. N. Rebelo and Lourdes F. Vega.

2016 AIChE Annual Meeting, November 2016, San Francisco, USA.

Appendix

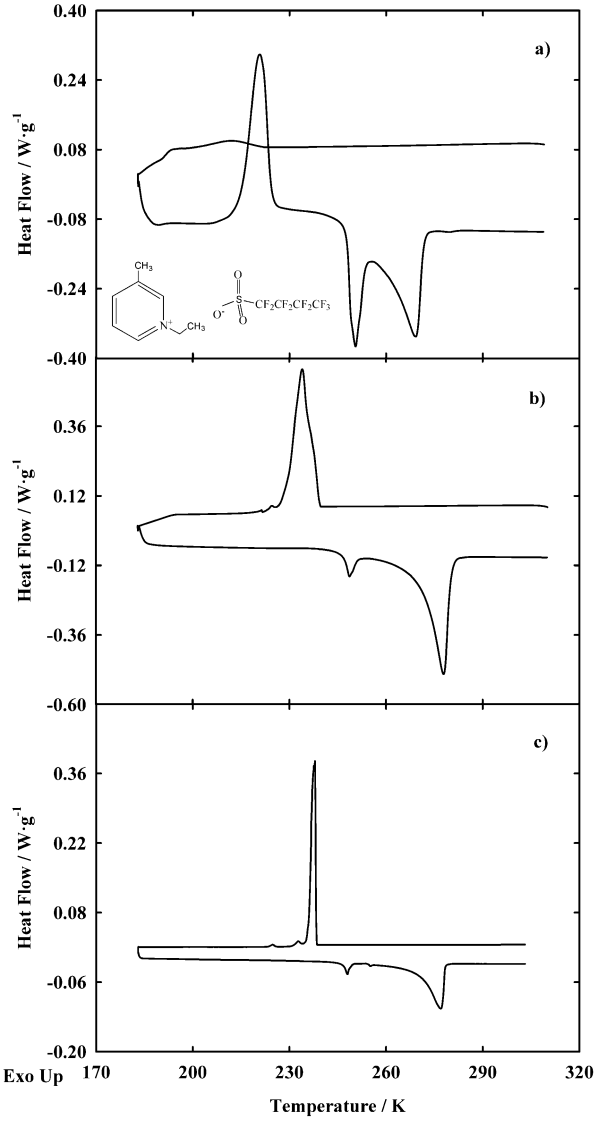

Figure A.1. DSC runs for $[C_2C_1py][C_4F_9SO_3]$ at a scan rate of : **(**a) 10 K·min^{-1}; (b) 5 K·min^{-1}; (c) 1 K·min^{-1}.

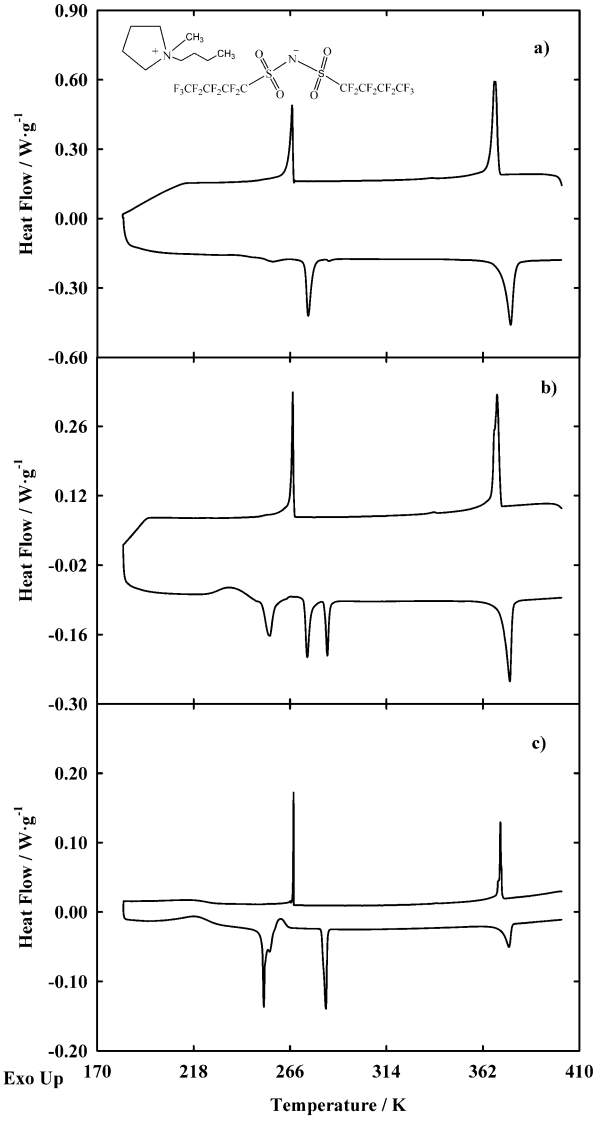

Figure A.2. DSC runs for $[C_4C_1pyr][N(C_4F_9SO_2)_2]$ at a scan rate of : **(**a) 10 K·min^{-1}; (b) 5 K·min^{-1}; (c) 1 K·min^{-1}.

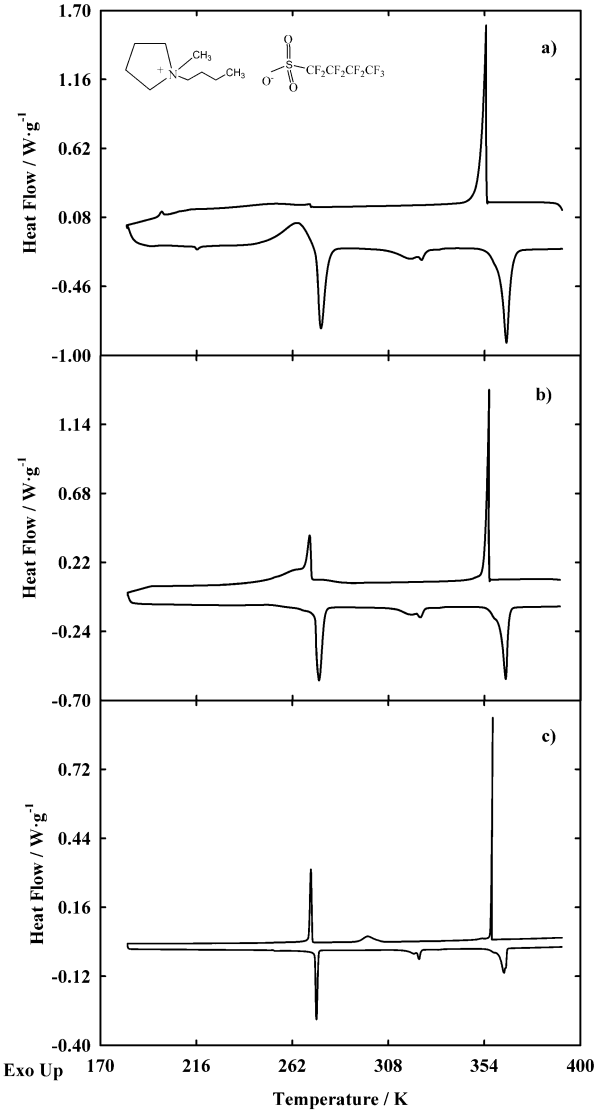

Figure A.3. DSC runs for $[C_4C_1pyr][C_4F_9SO_3]$ at a scan rate of : **(**a) 10 K·min^{-1}; (b) 5 K·min^{-1}; (c) 1 K·min^{-1}.

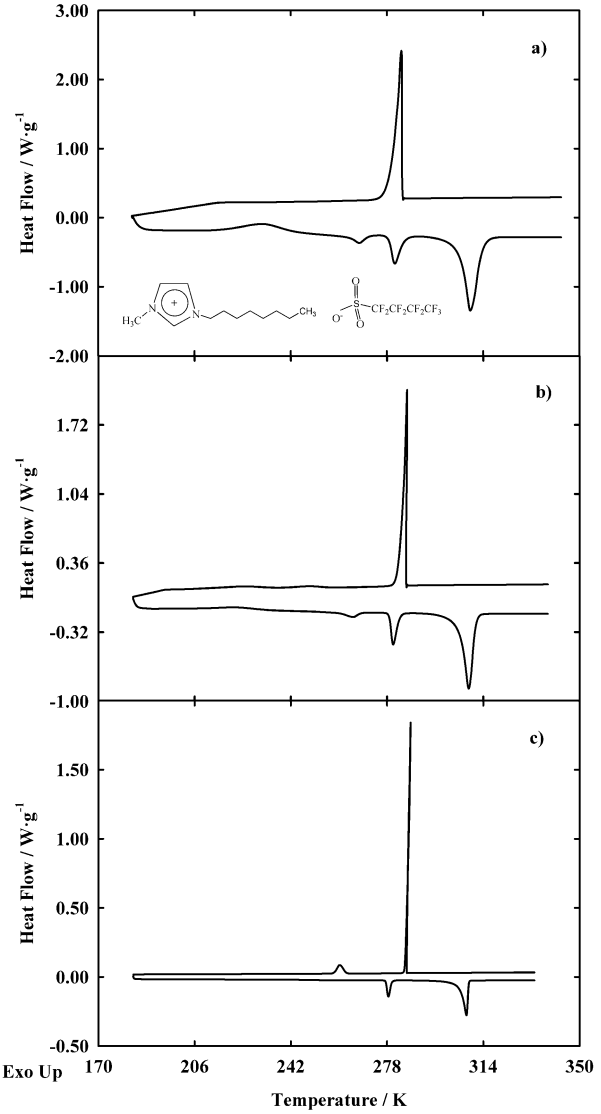

Figure A.4. DSC runs for $[C_8C_1Im][C_4F_9SO_3]$ at a scan rate of : **(**a) 10 K·min^{-1}; (b) 5 K·min^{-1}; (c) 1 K·min^{-1}.

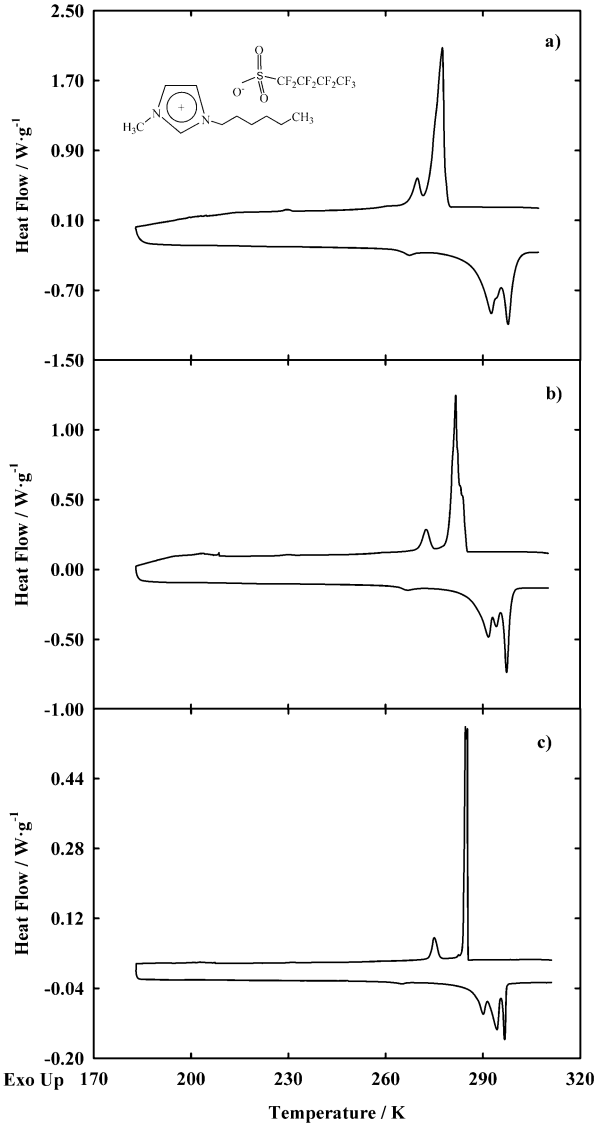

Figure A.5. DSC runs for $[C_6C_1Im][C_4F_9SO_3]$ at a scan rate of : **(**a) 10 K·min^{-1}; (b) 5 K·min^{-1}; (c) 1 K·min^{-1}

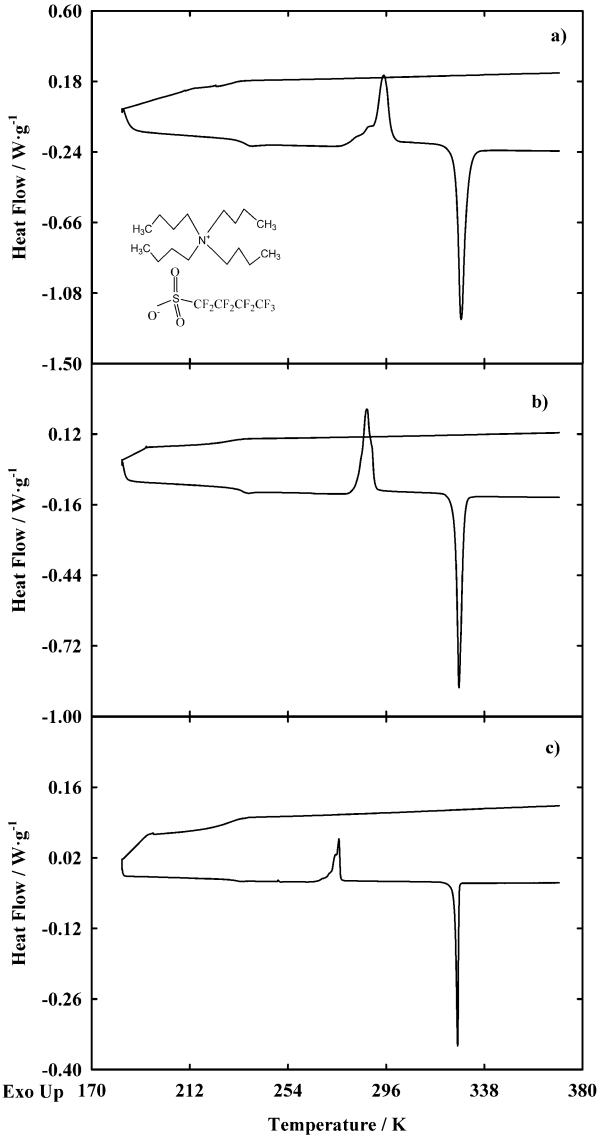

Figure A.6. DSC runs for $[N_{4444}][C_4F_9SO_3]$ at a scan rate of : **(**a) 10 K·min^{-1}; (b) 5 K·min^{-1}; (c) 1 K·min^{-1}

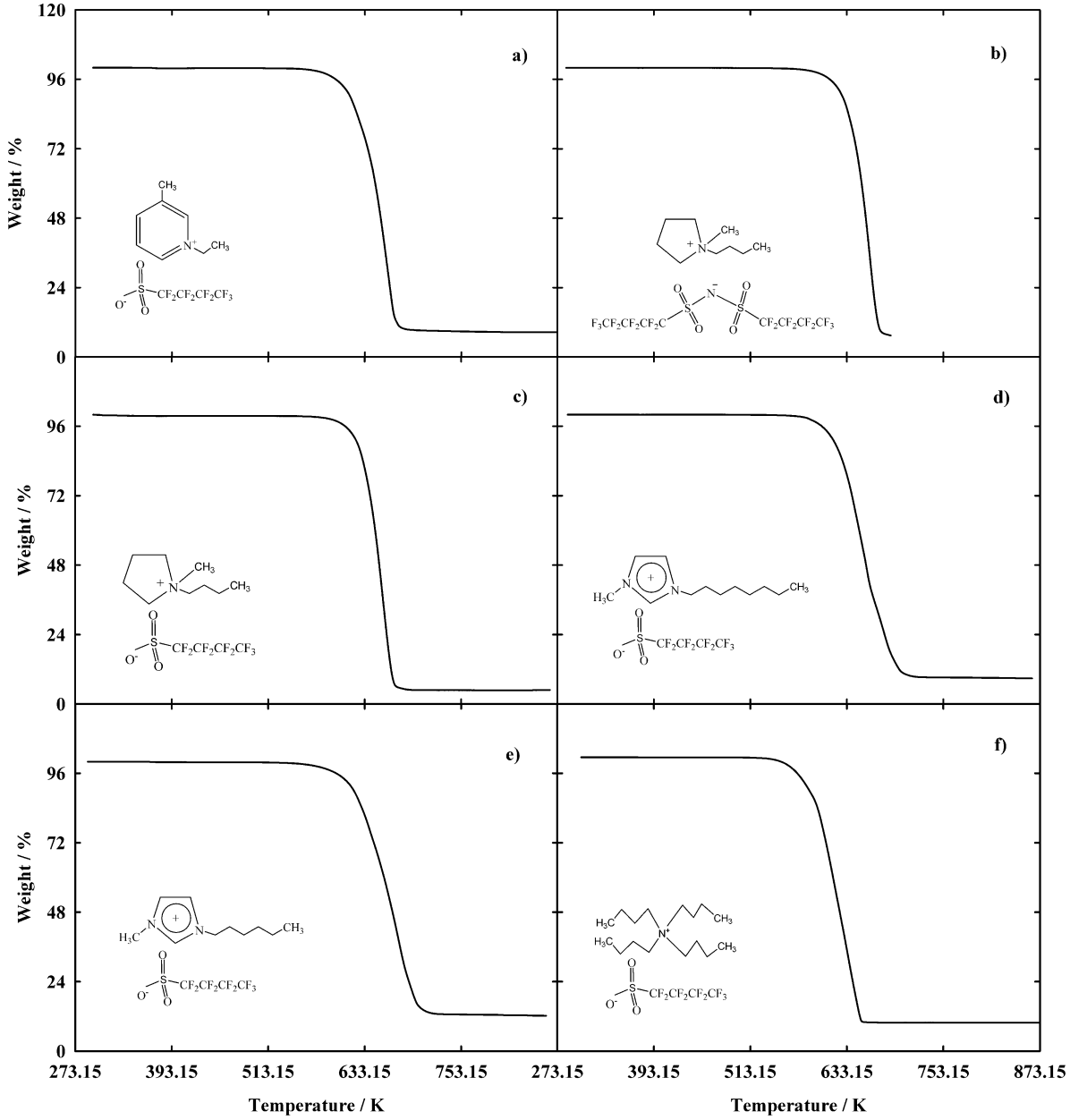

Figure A.7. TGA runs at a scan rate of 1 K·min^{-1}: (a) [C_2C_1py][$C_4F_9SO_3$]; (b) [C_4C_1pyr][N($C_4F_9SO_2$)$_2$]; (c) [C_4C_1pyr][$C_4F_9SO_3$]; (d) [C_8C_1Im][$C_4F_9SO_3$]; (e) [C_6C_1Im][$C_4F_9SO_3$]; (f) [N_{4444}][$C_4F_9SO_3$].

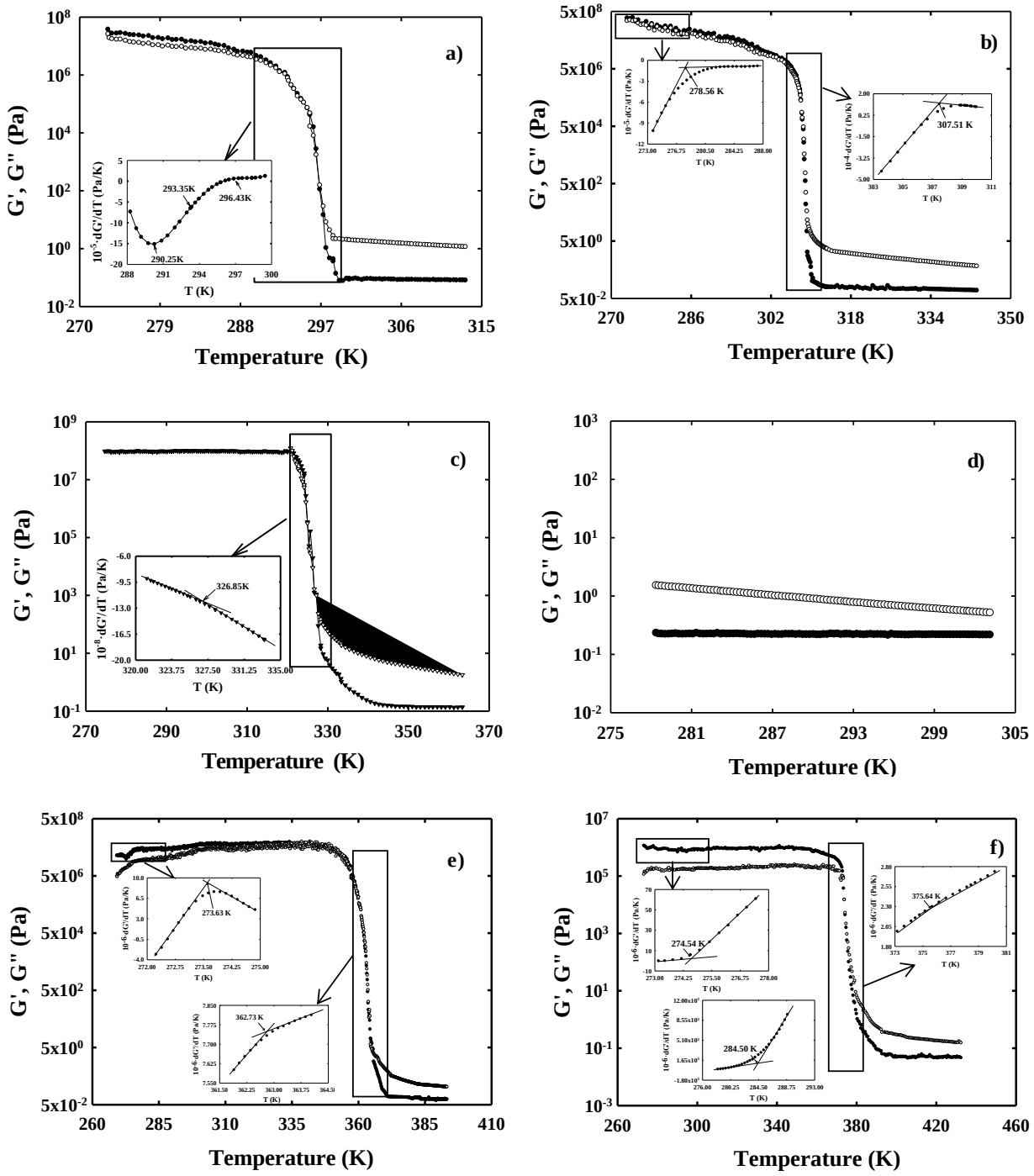

Figure A.8. Store (G', black symbols) and loss (G", empty symbols) moduli versus temperature measured at a fixed angular frequency = 10 rad·s^{-1}, and strains varying between 0.0005% and 20% (ensuring its location within the LVR) of (a) $[C_6C_1Im][C_4F_9SO_3]$, (b) $[C_8C_1Im][C_4F_9SO_3]$ and (e) $[C_4C_1pyr][C_4F_9SO_3]$ at a scan rate of 1 K·min^{-1}; (c) $[N_{4444}][C_4F_9SO_3]$, (d) $[C_2C_1py][C_4F_9SO_3]$ and (f) $[C_4C_1pyr][N(C_4F_9SO_2)_2]$ at a scan rate of 5 K·min^{-1}.